

Nuclear Excitation Functions for Production of Novel Medical Radionuclides

Andrew S. Voyles

03 August 2017 – PhD Oral Qualifying Exam

Overview

- Background & History of Nuclear Medicine
- ^{64}Cu and ^{47}Sc (n,p) Cross-Section Measurements
- Stacked-target charged particle excitation functions

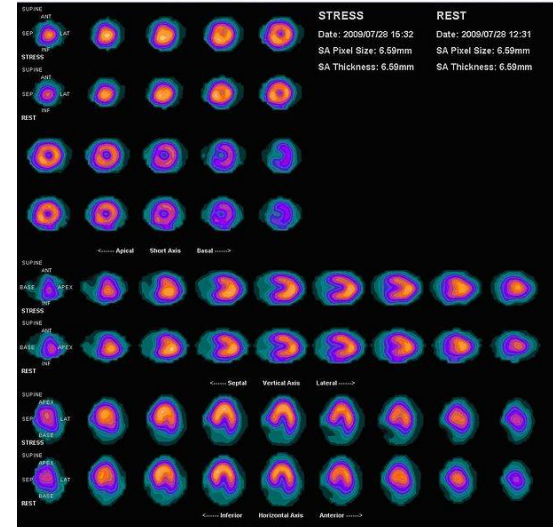
Background & History of Nuclear Medicine

Nuclear Medicine in the U.S.

- Dates back to 1946 – ^{14}C production at ORNL Graphite Reactor¹
- Per the US Society of Nuclear Medicine & Molecular Imaging, approximately 17 million nuclear medicine (diagnostic and therapeutic, on top of another ~130M of radiology) procedures are performed in the US annually
 - Nearly 1 in 20 people!
 - Annual industry estimated at \$2.4 B

Nuclear Medicine in the U.S.

- Major isotopes in modern clinical nuclear medicine:
 - ^{99m}Tc
 - Diagnostic isotope for cardiac, renal, lung function, tumor imaging
 - Produced as fission product in thermal reactors
 - Costs per 10-mCi dose ranges \$20-40¹

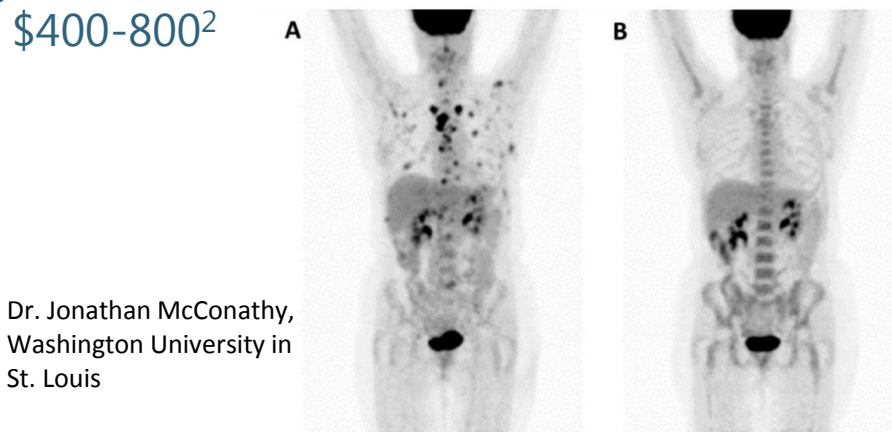


Wikimedia Commons

- [1] C. Whipple and S. Larson, *Medical Isotope Production Without Highly Enriched Uranium*, 2009.
- [2] United States Government Accountability Office and U.S. General Accounting Office, *Report GAO-08-452*, 2008.
- [3] A. N. Khalid, *et al*, *Arch. Otolaryngol. Neck Surg.*, vol. 132, no. 3, pp. 244–250, 2006.

Nuclear Medicine in the U.S.

- Major isotopes in modern clinical nuclear medicine:
 - ^{99m}Tc
 - Diagnostic isotope for cardiac, renal, lung function, tumor imaging
 - Produced as fission product in thermal reactors
 - Costs per 10-mCi dose ranges \$20-40¹
 - ^{18}F
 - PET isotope used for metabolic tumor & metastasis imaging
 - Produced by K~15 medical cyclotrons via $^{18}\text{O}(\text{p},\text{n})^{18}\text{F}$
 - Costs per 5-mCi dose ranges \$400-800²



Dr. Jonathan McConathy,
Washington University in
St. Louis

Nuclear Medicine in the U.S.

- Major isotopes in modern clinical nuclear medicine:
 - ^{99m}Tc
 - Diagnostic isotope for cardiac, renal, lung function, tumor imaging
 - Produced as fission product in thermal reactors
 - Costs per 10-mCi dose ranges \$20-40¹
 - ^{18}F
 - PET isotope used for metabolic tumor & metastasis imaging
 - Produced by K~15 medical cyclotrons via $^{18}\text{O}(\text{p},\text{n})^{18}\text{F}$
 - Costs per 5-mCi dose ranges \$400-800²
 - ^{131}I
 - β -therapy isotope used for treatment of cancers, including thyroid and neuroendocrine
 - Produced as fission product in thermal reactors
 - Costs per 200-mCi dose approximately \$200³

Nuclear Medicine in the U.S.

- Established medical radioisotopes face several challenges:
 - Non-ideal decay properties for desired application
 - Extra dose
 - Extra range
 - Curtailment of production facilities (^{99m}Tc)
 - Thermal reactor issues
 - Low yield
 - Difficult radiochemical purification
 - Feasibility & deployability

Why do we keep doing this?

How can we improve this?

Nuclear Medicine in the U.S.

- Established medical radioisotopes face several challenges:
 - Non-ideal properties
 - Extraneous isotopes
 - Extraneous radionuclides
 - Curtailment of production facilities (^{99m}Tc)
 - Thermal neutron capture
 - Low yields
 - Difficult to separate
 - Feasibility & deployability

Novel isotopes...

**...and new paradigms for
isotope production!**

Why do we keep doing this?

How can we improve this?

Some perspective

Nuclear Data Needs and Capabilities for Applications

May 27-29, 2015

Lawrence Berkeley National Laboratory,
Berkeley, CA USA



Some perspective

Isotope Production Needs

1. Charged-particle reactions for the production of medical isotopes at low energies ($E < 30$ MeV):
 - o $^{45}\text{Sc}(\text{p},\text{n})^{45}\text{Ti}$; $^{52}\text{Cr}(\text{p},\text{n})^{52}\text{Mn}$; $^{54}\text{Fe}(\text{d},\text{n})^{55}\text{Co}$; $^{67}\text{Zn}(\text{p},\alpha)^{64}\text{Cu}$; $^{72}\text{Ge}(\text{p},\text{n})^{72}\text{As}$, $^{74}\text{Se}(\text{d},\text{n})^{75}\text{Br}$;
 - o $^{88}\text{Sr}(\text{p},\text{n})^{88}\text{Y}$; $^{120}\text{Te}(\text{p},\text{n})^{120}\text{I}$
2. Nuclear data needed for Super Heavy Element (SHE) target
 - o $^{90}\text{Co}(\text{p},3\text{n})^{87}\text{Ni}$, $^{75}\text{As}(\text{p},3\text{n})^{75}\text{Se}$, $^{122}\text{Sb}(\text{p},3\text{n})^{119}\text{Te}/^{119}\text{Sb}$, $^{132}\text{Cs}(\text{p},3\text{n})^{129}\text{Ba}$
 - o $^{95}\text{Mn}(\text{p},4\text{n})^{92}\text{Fe}$, $^{71}\text{Ga}(\text{p},4\text{n})^{68}\text{Ge}$, $^{133}\text{Cs}(\text{p},5\text{n})^{128}\text{Ba}$
 - o $^{127}\text{I}(\text{p},6\text{n})^{122}\text{Xe}$
 - o $^{nat}\text{Br}(\text{p},\text{x})^{72}\text{Se}$, $^{nat}\text{In}(\text{p},\text{x})^{110}\text{Sn}$, ^{122}T
 - o $^{nat}\text{Sb}(\text{p},\text{xn})^{119}\text{Te}/^{119}\text{Sb}$, $^{nat}\text{La}(\text{p},\text{xn})^{119}\text{Ce}$
 - o $^{68}\text{Zn}(\text{p},\text{xn})^{64}\text{Cu}$
 - o $^{89}\text{Zn}(\text{p},2\text{p})^{82}\text{Cu}$, $^{124}\text{Xe}(\text{p},2\text{p})^{123}\text{I}$
 - o $^{120}\text{Xe}(\text{p},\text{pn})^{123}\text{Xe}$
 - o (p,x) reaction on $^{84-90}\text{Mo}$ for impurity
 - o $^{107}\text{Ag}(\text{p},\text{xn})^{107}\text{Pd}$
 - o $^{115}\text{Cd}(\text{a},3\text{n})^{117m}\text{Sn}$; $^{192}\text{Os}(\text{a},3\text{n})^{193}$
3. Nuclear data needed for radionuclides produced via fission neutrons:
 - o $^{20}\text{Si}(\text{n},\text{x})^{20}\text{Si}$
 - o $^{nat}\text{Cl}(\text{n},\text{x})^{32}\text{Si}$, $^{37}\text{Cl}(\text{n},\text{x})^{32}\text{Si}$
 - o $^{nat}\text{Zn}(\text{n},\text{x})^{65}\text{Cu}$, $^{nat}\text{Zn}(\text{n},\text{x})^{67}\text{Cu}$, ^{70}Z
 - o $^{220}\text{Ra}(\text{n},2\text{n})^{222}\text{Ra}$
 - o $^{222}\text{Th}(\text{n},\text{x})^{223}\text{Ac}$, $^{222}\text{Th}(\text{n},\text{x})^{227}\text{Ac}$
 - o $^{22}\text{Si}(\text{n},\text{x})^{20}\text{P}$, $^{47}\text{Ti}(\text{n},\text{p})^{47}\text{Ca}$, $^{67}\text{Zn}(\text{n},\text{x})^{65}\text{Cu}$, $^{149}\text{Sm}(\text{n},\text{p})^{149}\text{Pm}$, $^{153}\text{Eu}(\text{n},\text{p})^{153}\text{Sm}$, $^{158}\text{Tb}(\text{n},\text{p})^{158}\text{Gd}$, $^{161}\text{Dy}(\text{n},\text{p})^{161}\text{Tb}$, $^{166}\text{Er}(\text{n},\text{p})^{166}\text{Ho}$, $^{169}\text{Tm}(\text{n},\text{p})^{169}\text{Er}$, $^{175}\text{Lu}(\text{n},\text{p})^{175}\text{Yb}$; $^{177}\text{Lu}(\text{n},\text{p})^{177}\text{Yb}$
4. High-energy photon-induced reactions
 - o $^{20}\text{Zn}(\text{y},\text{p})^{20}\text{Cu}$; $^{100}\text{Moly},\text{n})^{99}\text{Mo}$; 10
5. Nuclear data needs for inertial confinement fusion
 - o $^{238}\text{U}(\text{n},\text{y})^{238}\text{U}$
 - o $^{100}\text{Mo}(\text{p},\text{pn})$ - data on long-lived
6. Need small uncertainties on all dosimetry reactions
 - o In standard benchmark neutron field: $^{31}\text{P}(\text{n},\text{p})$, $^{10}\text{B}(\text{n},\text{X})\text{a}$, $^{54}\text{Fe}(\text{n},\text{a})$, $^{23}\text{Na}(\text{n},2\text{n})$, $^{180}\text{W}(\text{n},\text{y})$, $^{56}\text{Sc}(\text{n},\text{y})$, and $^{60}\text{Zn}(\text{n},\text{p})$
 - o In room return: $^{240}\text{Pu}(\text{n},\text{y})$, $^{238}\text{U}(\text{n},\text{y})$ and $^{239}\text{U}(\text{n},\text{2n})$
7. Nuclear data needed for Super Heavy Element (SHE) target
 - o $^{248}\text{Cm}(\text{n},\text{y})$ low energy resonances
 - o $^{240}\text{Bk}(\text{n},\text{y})$
8. IRMM Exploratory Study of Validation Data in ^{252}Cf Standard Neutron Benchmark Field
 - o Issues with existing $^{197}\text{Au}(\text{n},\text{y})$ due to room return
 - o Issues with existing $^{90}\text{Zr}(\text{n},2\text{n})$ due to Th contamination
 - o Issue with existing $^{90}\text{Zr}(\text{n},2\text{n})$ due to $^{94}\text{Zr}(\text{n},\text{y})$ contribution
9. Test and improve decay chains
10. Gamma Emission Probabilities
 - o $^{100m}\text{Rh} \rightarrow \text{X-ray emission}$
11. Xe dopants to probe ablation front instabilities
12. Br(d,2n)Kr to probe ablator/cold fuel and ablator/hot core mix.
13. Alpha particle induced reactions to probe hot core mix: ^{6}Li , ^{10}Be , ^{10}B (best one), ^{12}C , ^{14}N , ^{16}O , ^{18}F , ^{20}Ne , ^{23}Na , ^{24}Mg , ^{27}Al .
14. Gamma-ray diagnostics for performance and ablator/fuel instabilities.
 - o Total yield from d-t fusion γ branching ratio at 17.6 MeV.
 - o $^{12}\text{C}(\text{n},\text{n}'\gamma)$ 4.4 MeV time-integrated emission provides hydrocarbon areal densities (remaining mass). Cross section at 14 MeV must be accurate.
 - o Does $^{13}\text{C}(\text{n},\text{n}'\gamma)$ have strong emission near 4 MeV? If not, then a useful mix diagnostic is possible.
15. Solid Radiochemistry Diagnostic (SRC) is currently an NIF diagnostic complementary to $^{12}\text{C}-\text{y}$ GRH detection (CH pr).
 - o Ratio of $^{198}\text{Au}/^{196}\text{Au}$ from the activated hohlraum.
 - o $(\text{n},\text{y})/(\text{n},2\text{n})$: low energy neutrons/14 MeV neutrons.

Highlight from WTTC 2016: $^{54}\text{Fe}(\text{p},\alpha)^{51}\text{Mn}$

1. $^{117}\text{Sn}(\text{n},\text{n}')$, covering energy response 0.3 – 3.0 MeV
2. Data to support new evaluations
 - o $^{23}\text{Na}(\text{n},\text{y})$, discrepant in fast neutron region, > 100 keV
 - o $^{23}\text{Na}(\text{n},2\text{n})$
 - o $^{27}\text{Al}(\text{n},2\text{n})$
3. Address discrepancies:

4. Need small uncertainties on all dosimetry reactions

10. Gamma Emission Probabilities
 - o $^{100m}\text{Rh} \rightarrow \text{X-ray emission}$
11. Cs^{+} , Cl^{-} , K^{+} , Ca^{2+} , Mg^{2+}
12. Uncertainty in recoil spectrum
 - o Recoil spectrum char:
 - o ^{60}Ga , ^{71}Ga , ^{75}As
 - o Fe isotopes
 - o Validate/test use of ce

4. Gamma-ray diagnostics for performance and ablator/fuel instabilities.
 - o Total yield from d-t fusion γ branching ratio at 17.6 MeV.
 - o $^{12}\text{C}(\text{n},\text{n}'\gamma)$ 4.4 MeV time-integrated emission provides hydrocarbon areal densities (remaining mass). Cross section at 14 MeV must be accurate.
 - o Does $^{13}\text{C}(\text{n},\text{n}'\gamma)$ have strong emission near 4 MeV? If not, then a useful mix diagnostic is possible.
5. Solid Radiochemistry Diagnostic (SRC) is currently an NIF diagnostic complementary to $^{12}\text{C}-\text{y}$ GRH detection (CH pr).
 - o Ratio of $^{198}\text{Au}/^{196}\text{Au}$ from the activated hohlraum.
 - o $(\text{n},\text{y})/(\text{n},2\text{n})$: low energy neutrons/14 MeV neutrons.

Some perspective



Contents lists available at ScienceDirect

Nuclear Medicine and Biology

journal homepage: www.elsevier.com/locate/nucmedbio

Nuclear data for production and medical application of radionuclides:
Present status and future needs[☆]

Syed M. Qaim *

Institut für Neurowissenschaften und Medizin, INM-5 (Nuklearchemie), Forschungszentrum Jülich, D-52425 Jülich, Germany

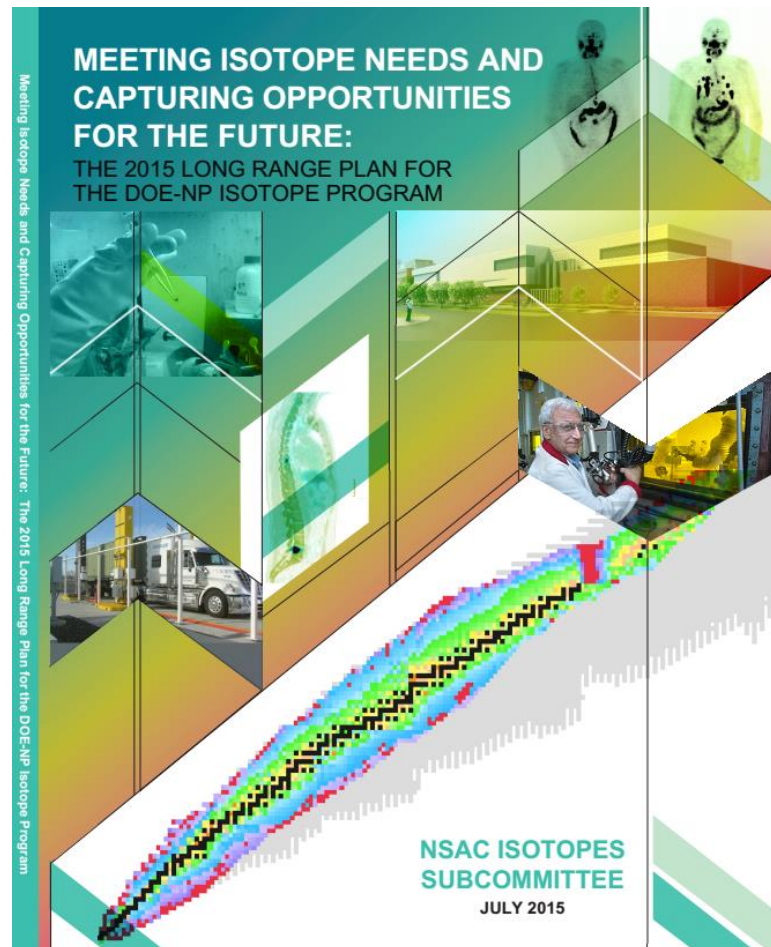
ARTICLE INFO

Article history:

Received 28 July 2016

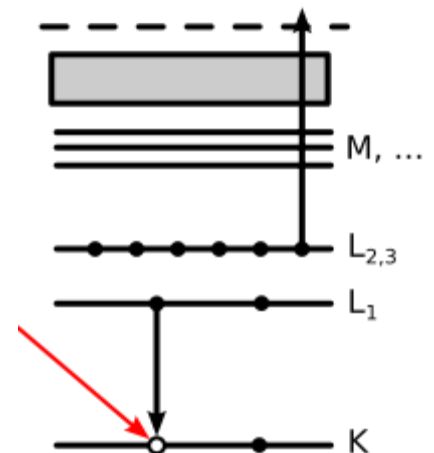
Received in revised form 22 August 2016

Accepted 23 August 2016



Some perspective

- Emerging trends for next-generation (targeted & personalized) nuclear medicine:
 - Targeted alpha therapy (5-10 MeV)
 - 40-80 μm range \rightarrow single cell
 - Targeted Auger therapy (20 eV – 1 keV)
 - 1 nm – 2 μm \rightarrow cellular nucleus
 - Theranostic medicine
 - Simultaneous imaging and therapy



Overview

- Ongoing targeted experimental campaign to address these needs:
 - (n,p) production cross sections – UCB
 - Stacked-target charged particle excitation functions
 - Low energy – LBNL
 - Moderate energy – LANL
 - Bonus – spin distribution of excited nuclear states

^{64}Cu and ^{47}Sc (n,p) Cross-Section Measurements

Medical Applications

- Emerging medical radionuclides
 - ^{64}Cu ($t_{1/2} = 12.7$ hr) – 61% β^+ to ^{64}Ni , 39% β^- to ^{64}Zn
 - ^{47}Sc ($t_{1/2} = 3.35$ d) – β^- to ^{47}Ti , with 159-keV γ

Promising Prospects for ^{44}Sc -/ ^{47}Sc -Based Theragnostics: Application of ^{47}Sc for Radionuclide Tumor Therapy in Mice

Cristina Müller¹, Maruta Bunka^{2,3}, Stephanie Haller¹, Ulli Köster⁴, Viola Groehn⁵, Peter Bernhardt^{6,7},
Nicholas van der Meulen², Andreas Türler^{2,3}, and Roger Schibli^{1,8}

¹Center for Radiopharmaceutical Sciences ETH-PSI-USZ, Paul Scherrer Institute, Villigen-PSI, Switzerland; ²Laboratory of Radiochemistry and Environmental Chemistry, Paul Scherrer Institute, Villigen-PSI, Switzerland; ³Laboratory of Radiochemistry and Environmental Chemistry, Department of Chemistry and Biochemistry University of Bern, Bern, Switzerland; ⁴Institut Laue-Langevin, Grenoble, France; ⁵Merck and Cie, Schaffhausen, Switzerland; ⁶Department of Radiation Physics, The Sahlgrenska Academy, University of Gothenburg, Gothenburg, Sweden; ⁷Department of Medical Physics and Medical Bioengineering, University Hospital, Gothenburg, Sweden; and ⁸Department of Chemistry and Applied Biosciences, ETH Zurich

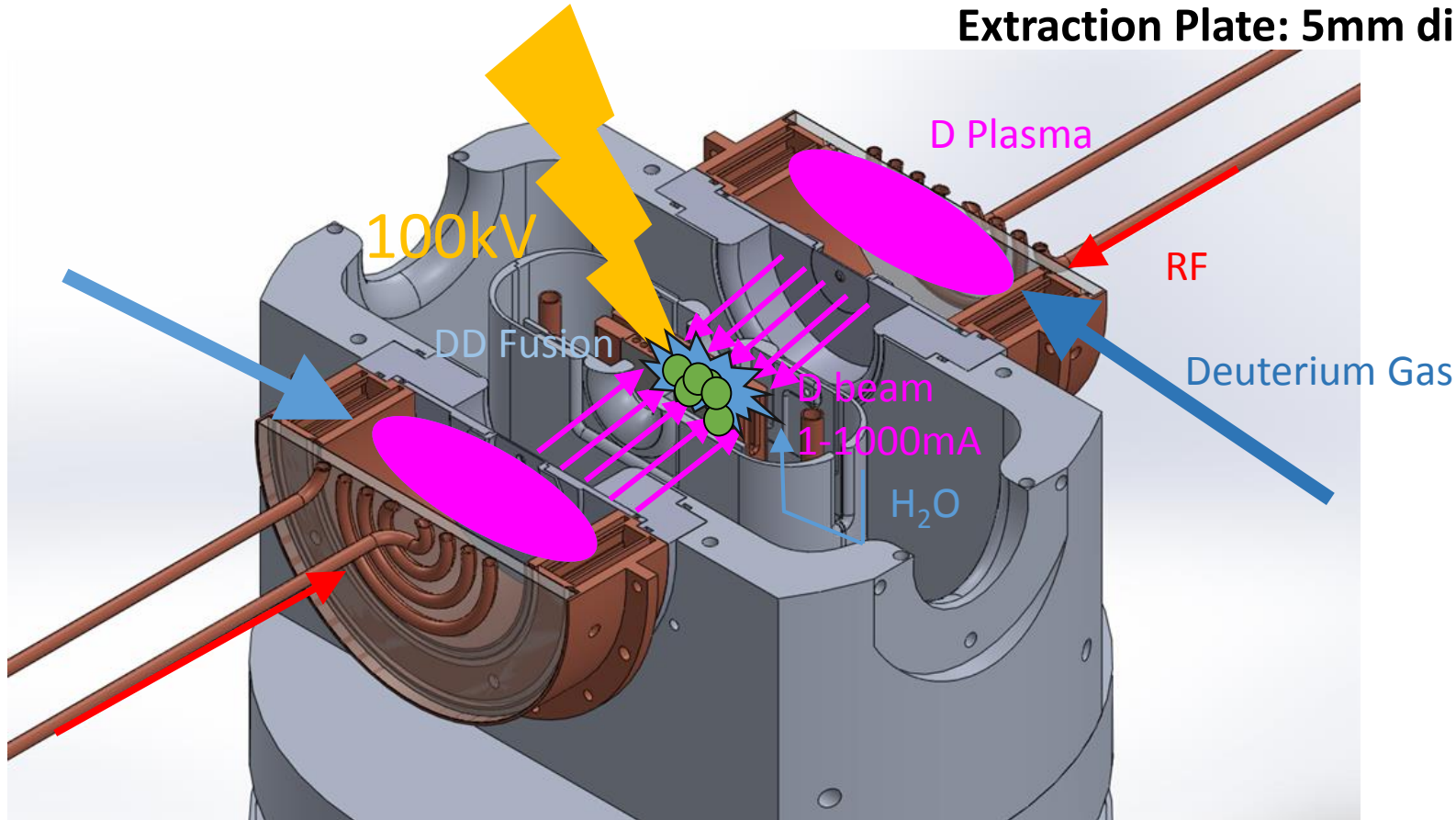
In Vivo Evaluation of Pretargeted ^{64}Cu for Tumor Imaging and Therapy

Michael R. Lewis, PhD¹; Mu Wang, MD¹; Donald B. Axworthy, BS²; Louis J. Theodore, PhD²; Robert W. Mallet, BS²; Alan R. Fritzberg, PhD²; Michael J. Welch, PhD¹; and Carolyn J. Anderson, PhD¹

¹Mallinckrodt Institute of Radiology, Washington University School of Medicine, St. Louis, Missouri;
and ²NeoRx Corporation, Seattle, Washington

The UC Berkeley High Flux Neutron Generator

**2.45 MeV neutrons, 10^7 n/s/cm²
Extraction Plate: 5mm diameter**



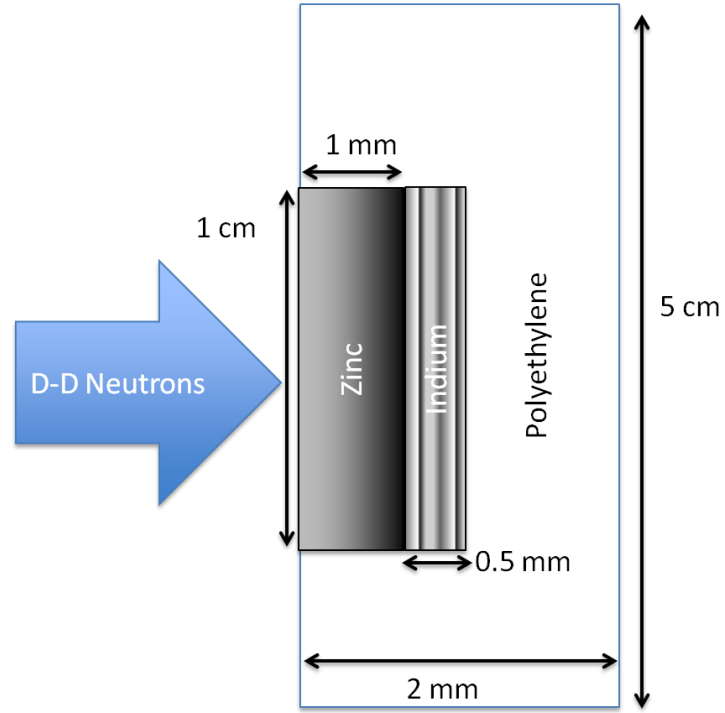
Why (n,p) via DD neutrons?

- Advantages over thermal reactors:
 - Co-production of many unwanted activities via (n, γ)
 - Far cheaper startup costs, no proliferation concerns
- Advantages over DT neutrons:
 - 14-15 MeV DT neutrons open up unwanted (n,pxn) channels, contaminating the desired product
 - No tritium handling concerns
- 2-3 MeV DD neutrons are ideal for (n,p) and (n, α) production, but often suffer from fairly low flux, and poor nuclear data

The UC Berkeley High Flux Neutron Generator

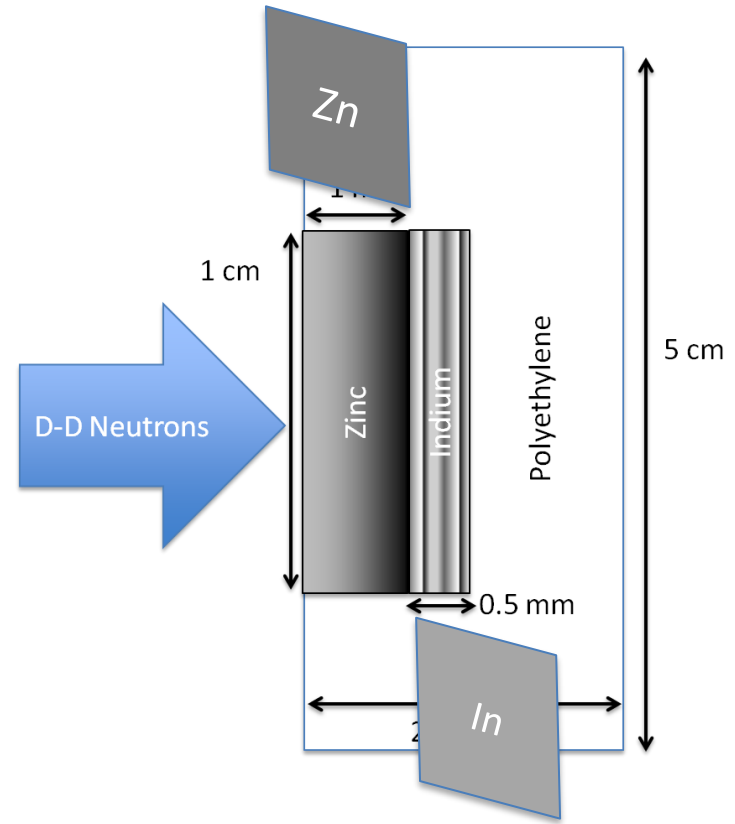
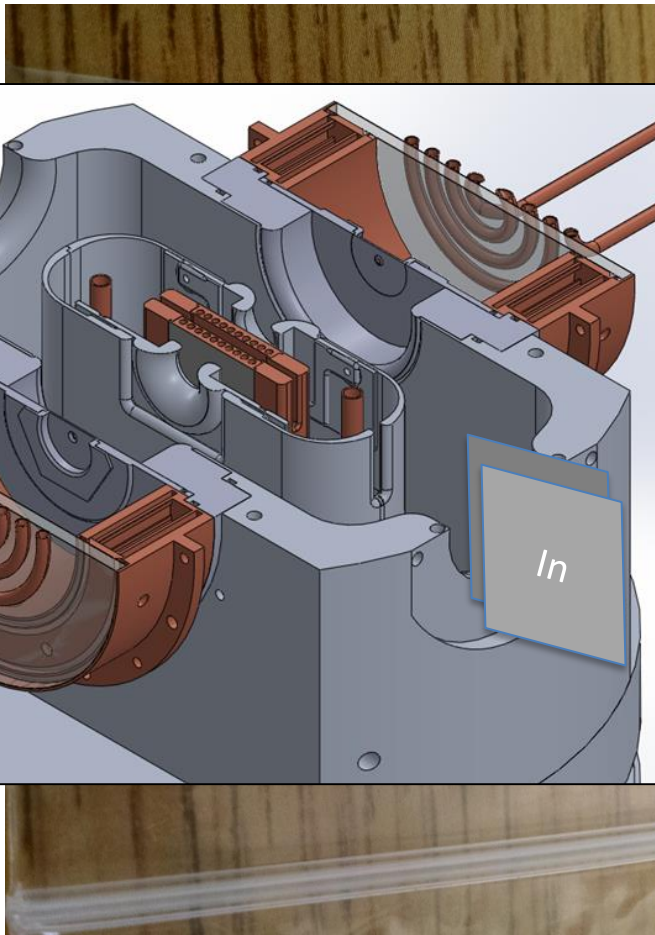


- Dosimetry: IRDFF
 $^{113}/^{115}\text{In}(n,n')$ $^{113\text{m}}/\text{m}^{115}\text{In}$ standards

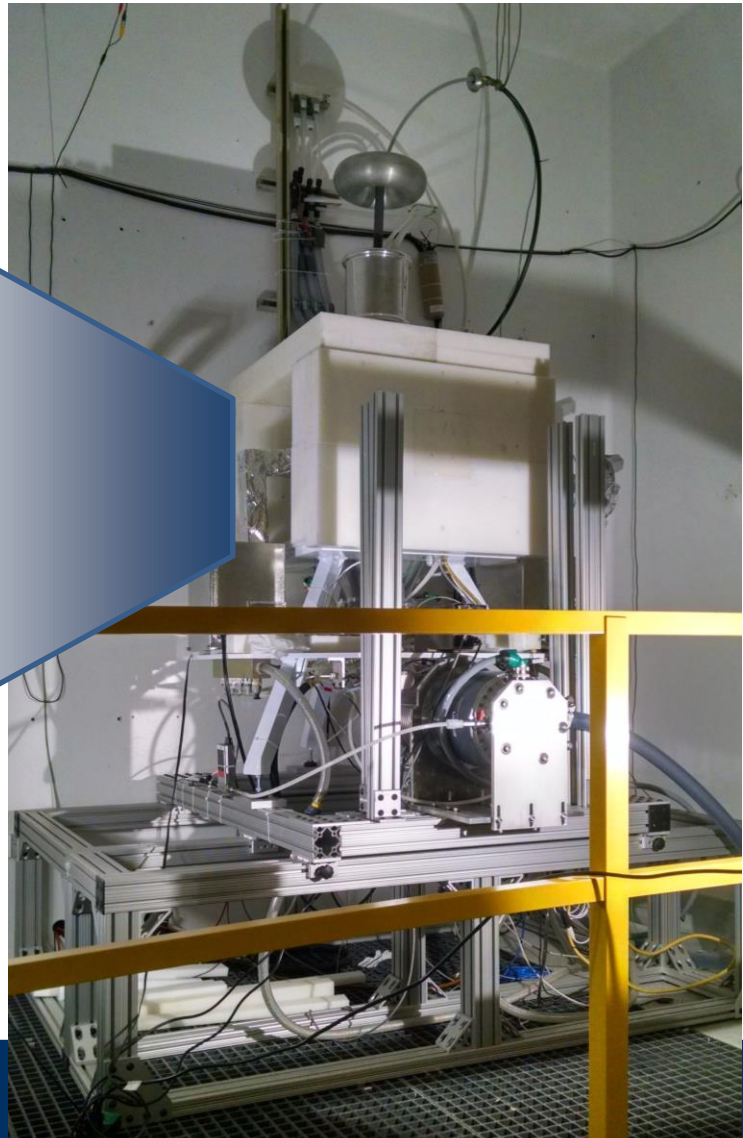
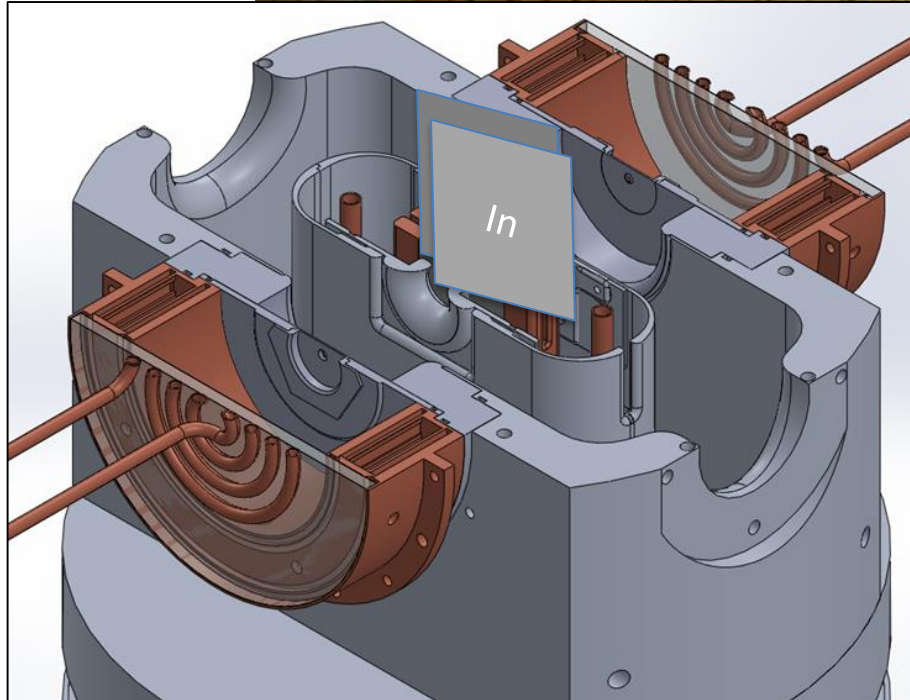


Foils Used	Metal Purity	Abundance (a/o)	Foil Density (mg/cm ²)
$^{\text{nat}}\text{In}$	> 99.999%	^{113}In (4.29%), ^{115}In (95.71%)	365.5
$^{\text{nat}}\text{Zn}$	> 99.99%	^{64}Zn (49.17%)	714.1
$^{\text{nat}}\text{Ti}$	99.999%	^{47}Ti (7.44%)	450.6

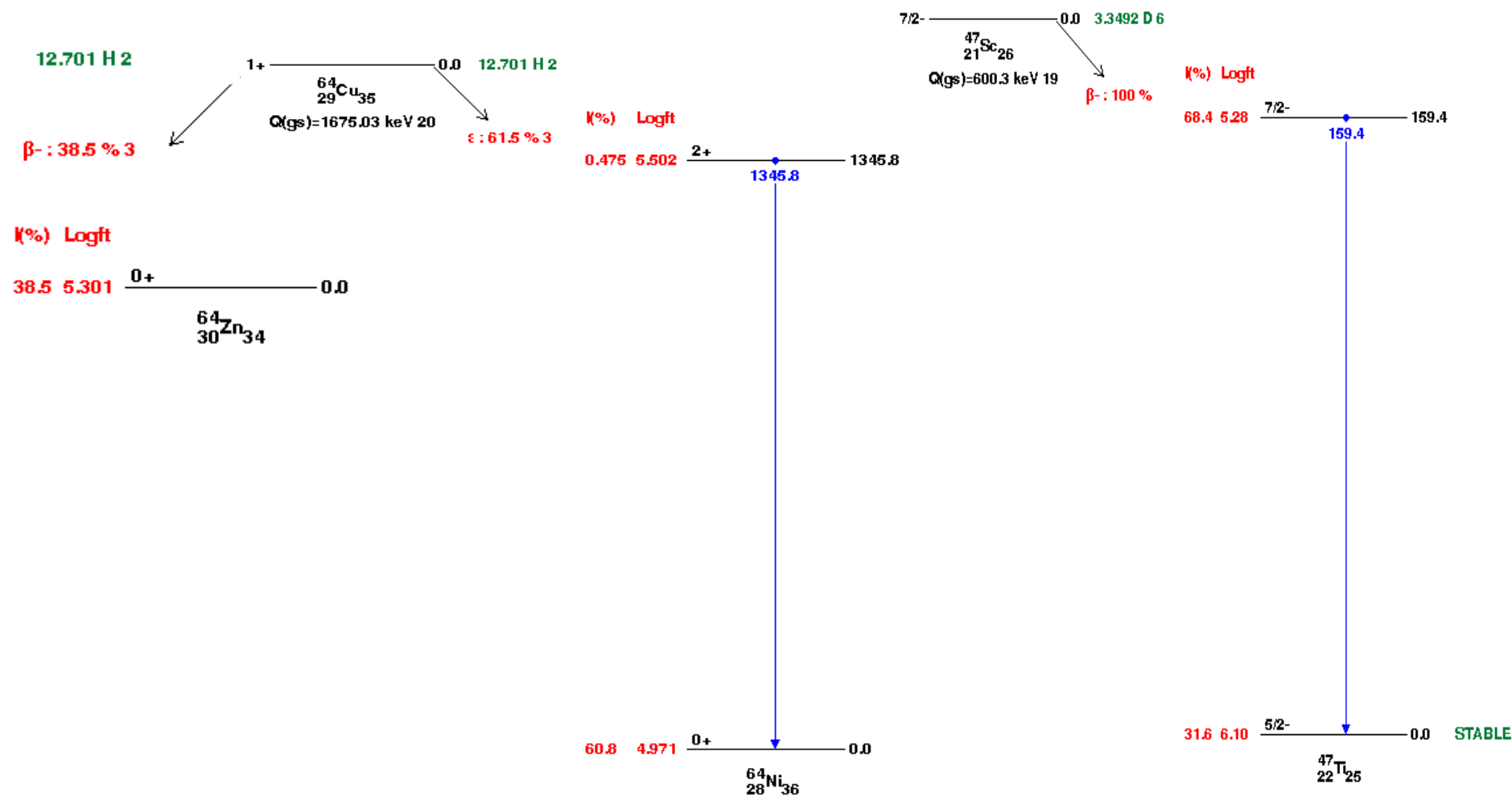
The UC Berkeley High Flux Neutron Generator



The UC Berkeley High Flux Neutron Generator



Relative Activation Measurements



Relative Activation Measurements

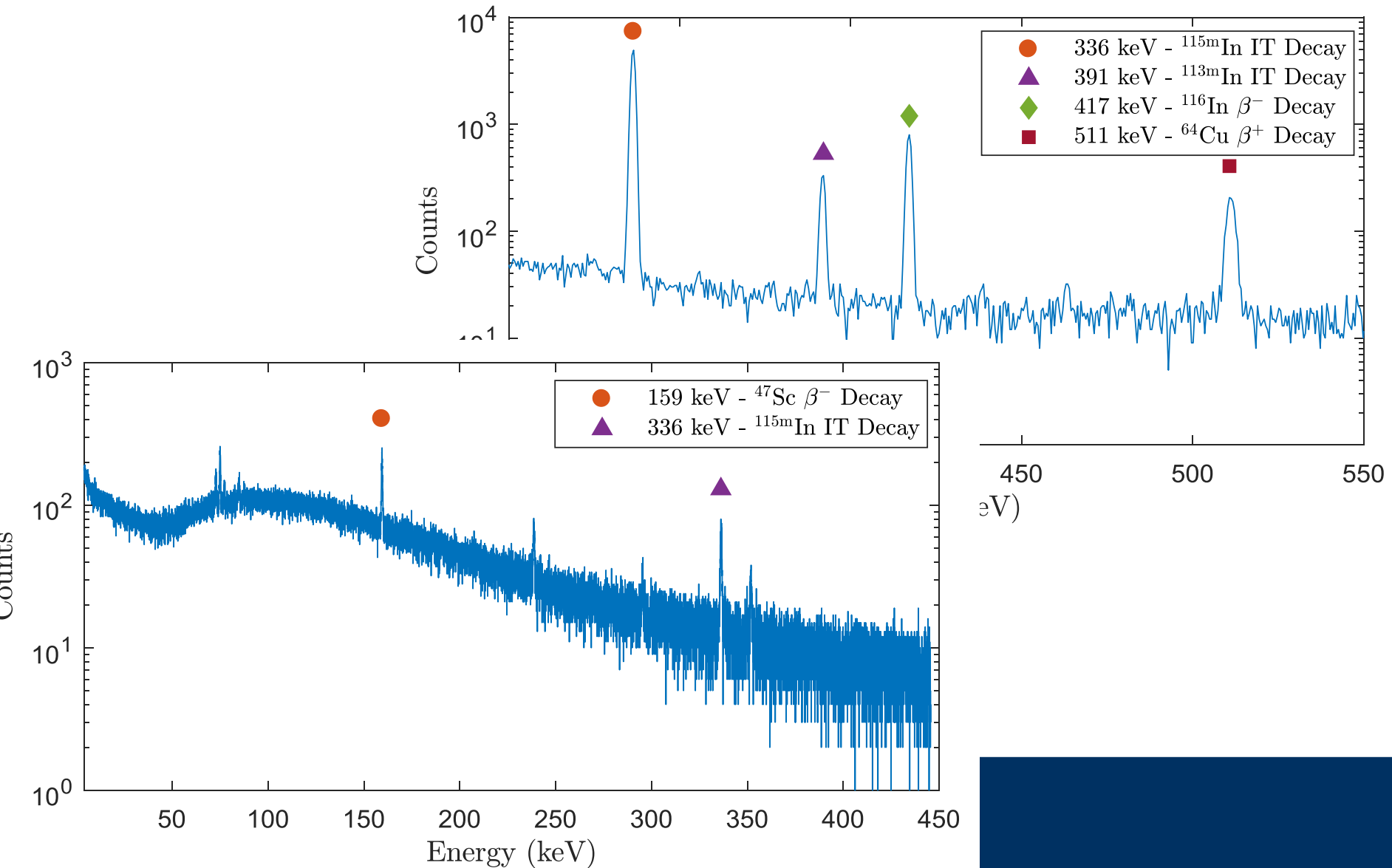


Ortec 80% HPGe detector

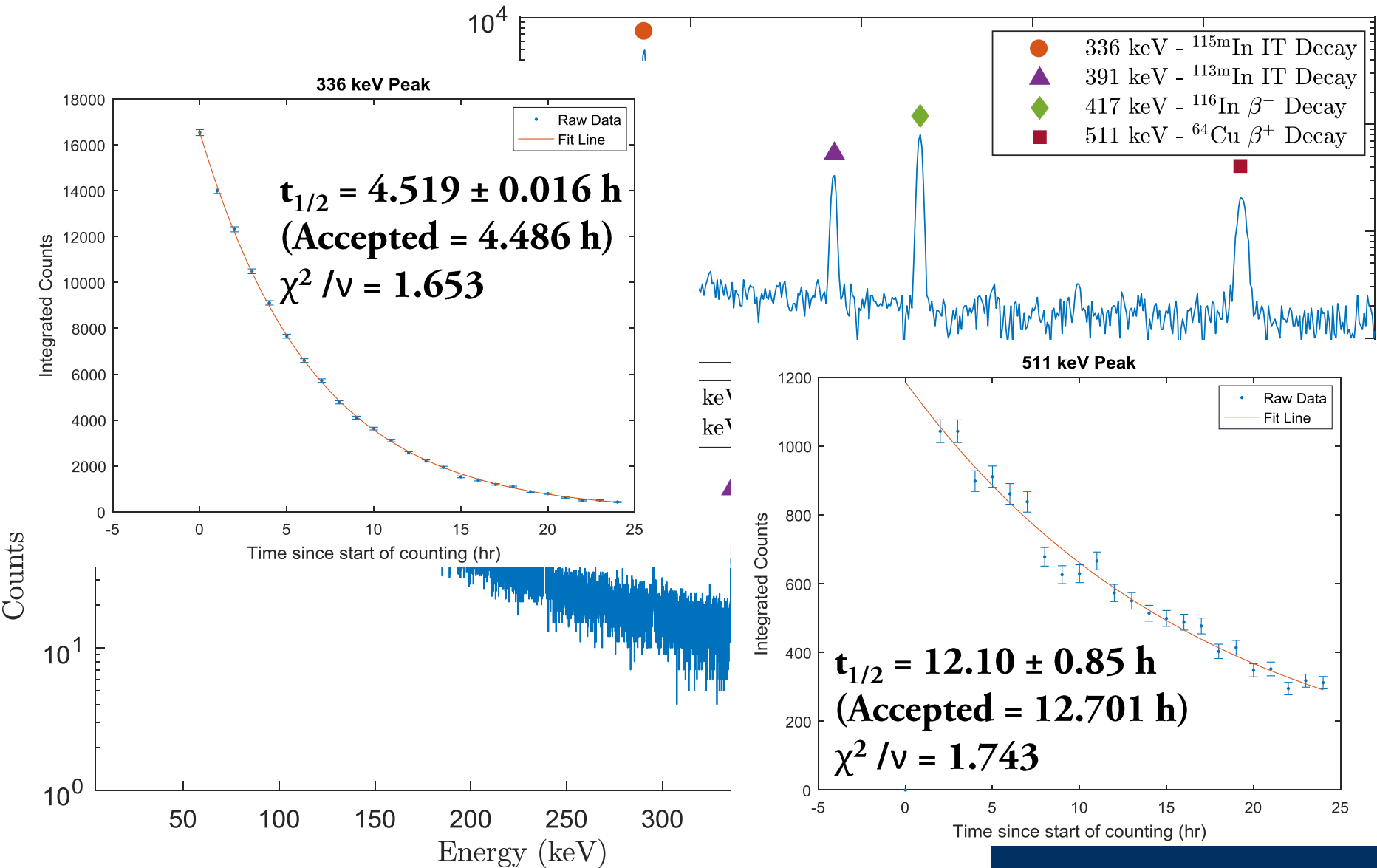


Ortec Planar LEPS detector

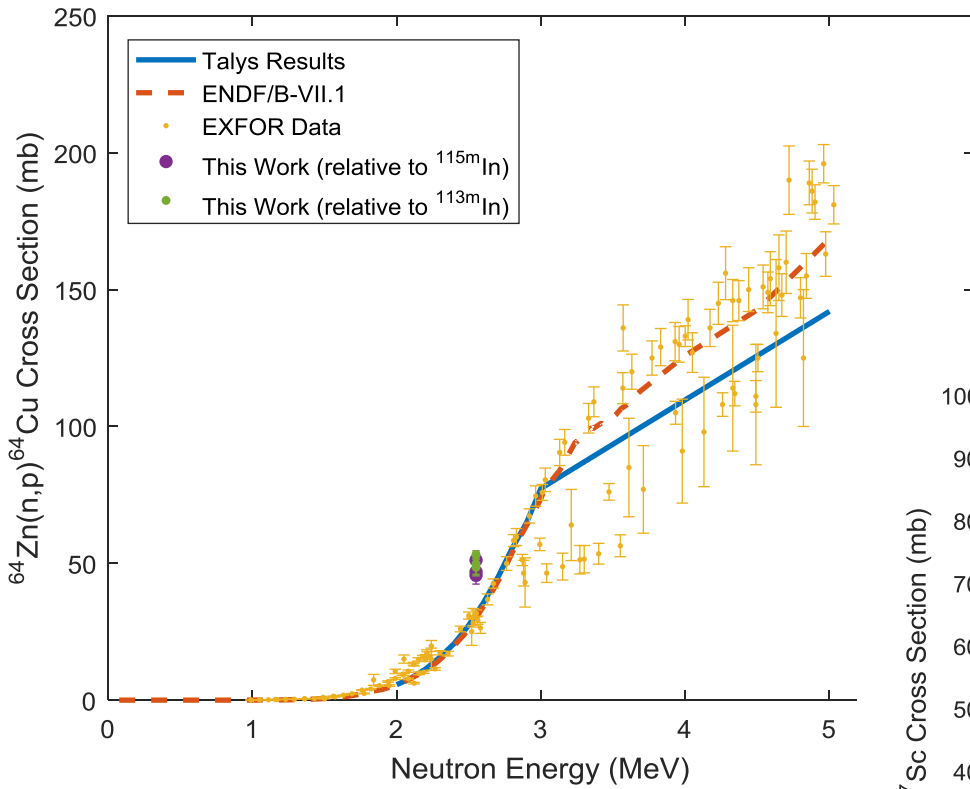
Relative Activation Measurements



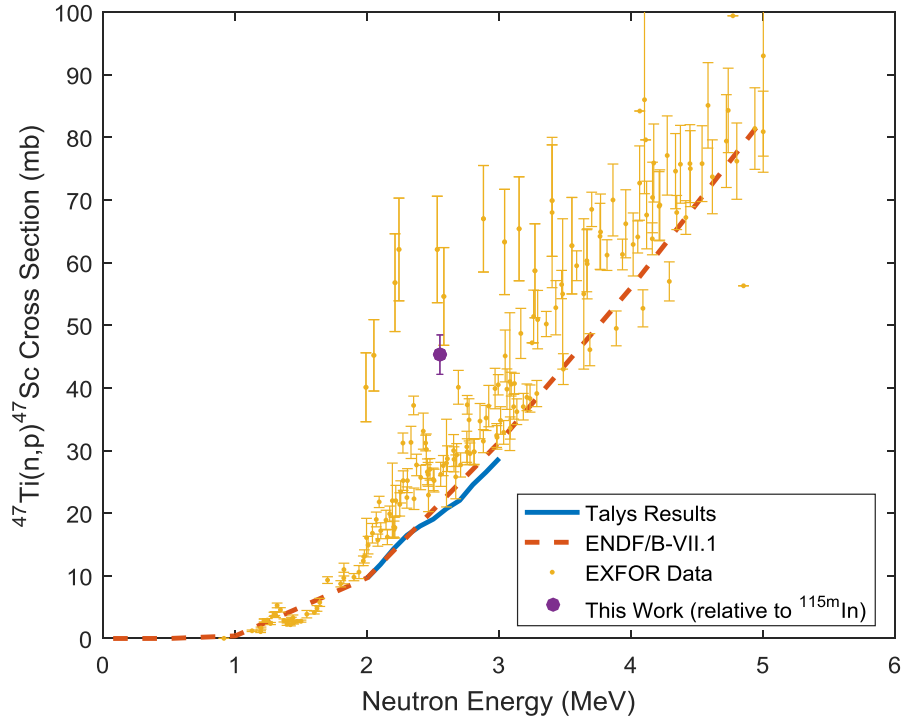
Relative Activation Measurements



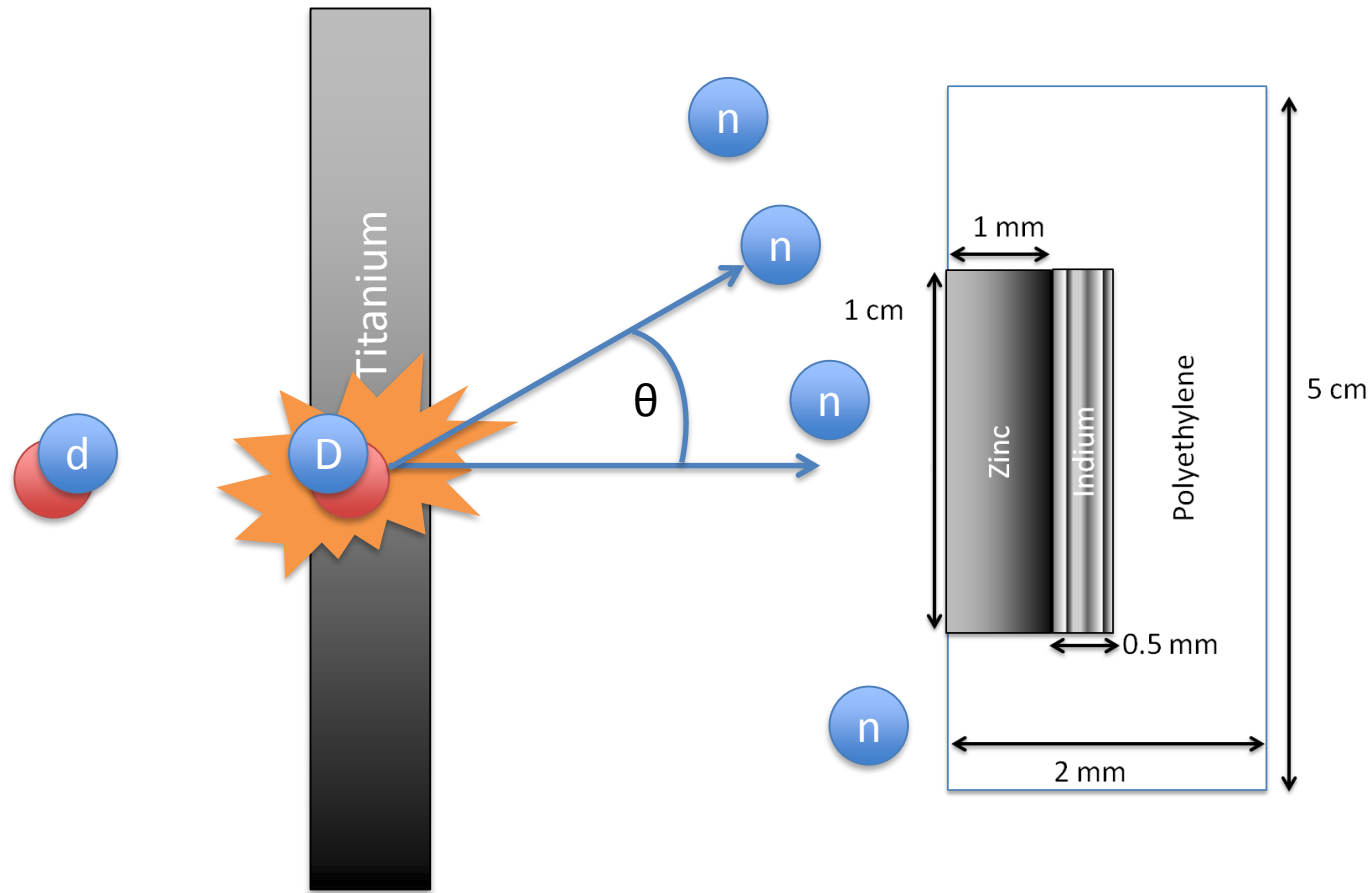
Relative Activation Measurements



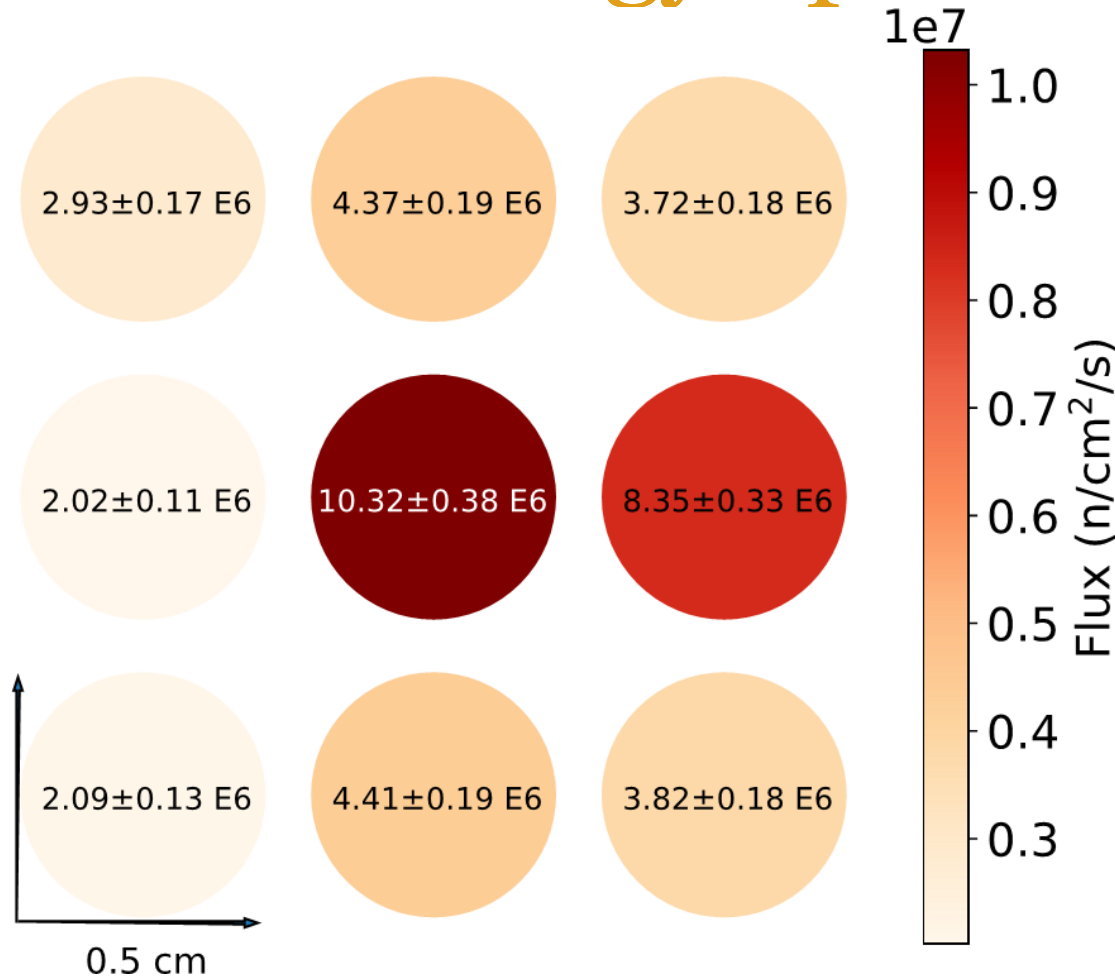
What's going on???



Neutron Energy Spread



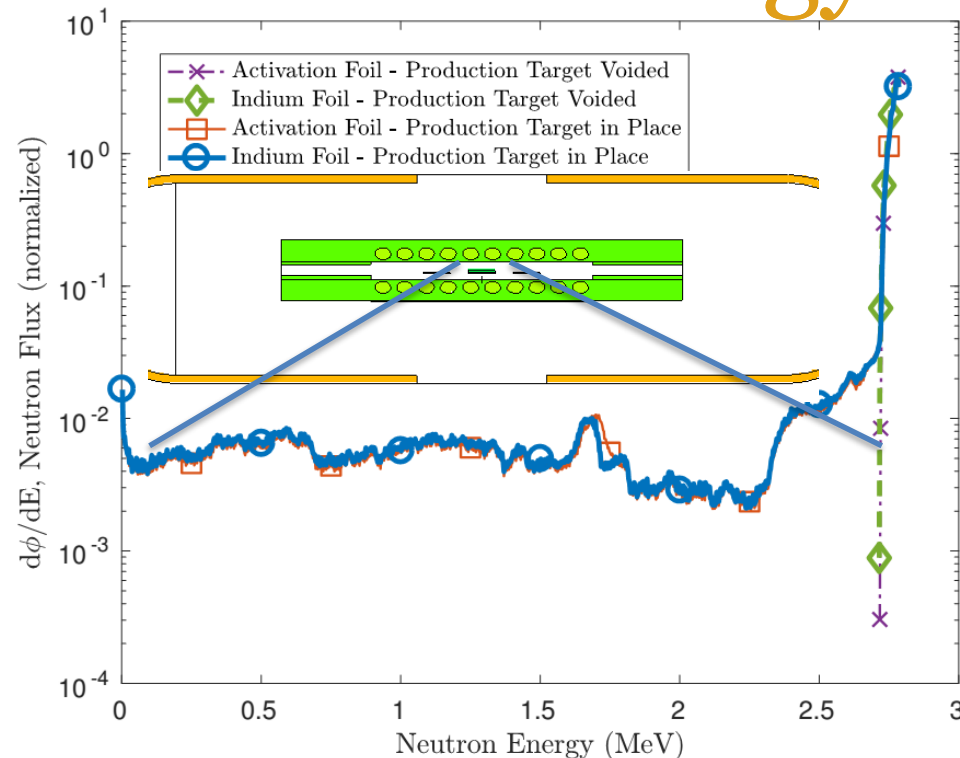
Neutron Energy Spread



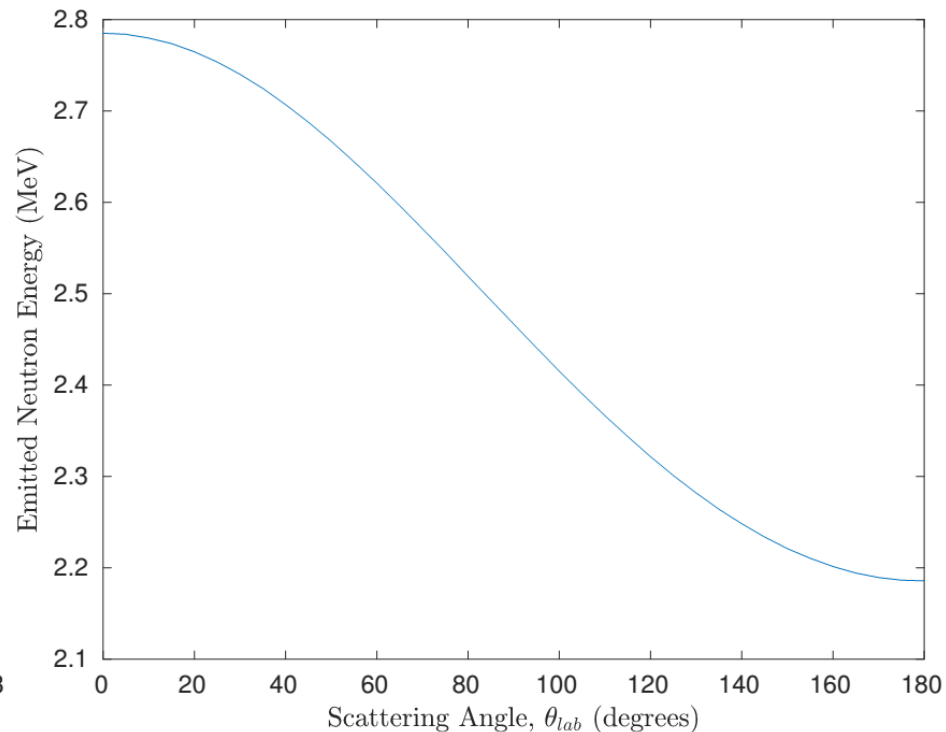
Relative fluxes as seen by a 3 x 3 array of 0.5-cm diameter indium foils. The central foil corresponds to the location in which target and monitor foils were mounted during the cross section measurements, verifying that the beam is centered on the middle of mounted foils

Neutron Energy Spread

H. Liskien *et al.*, Nucl Data Tables, vol 11, 2973

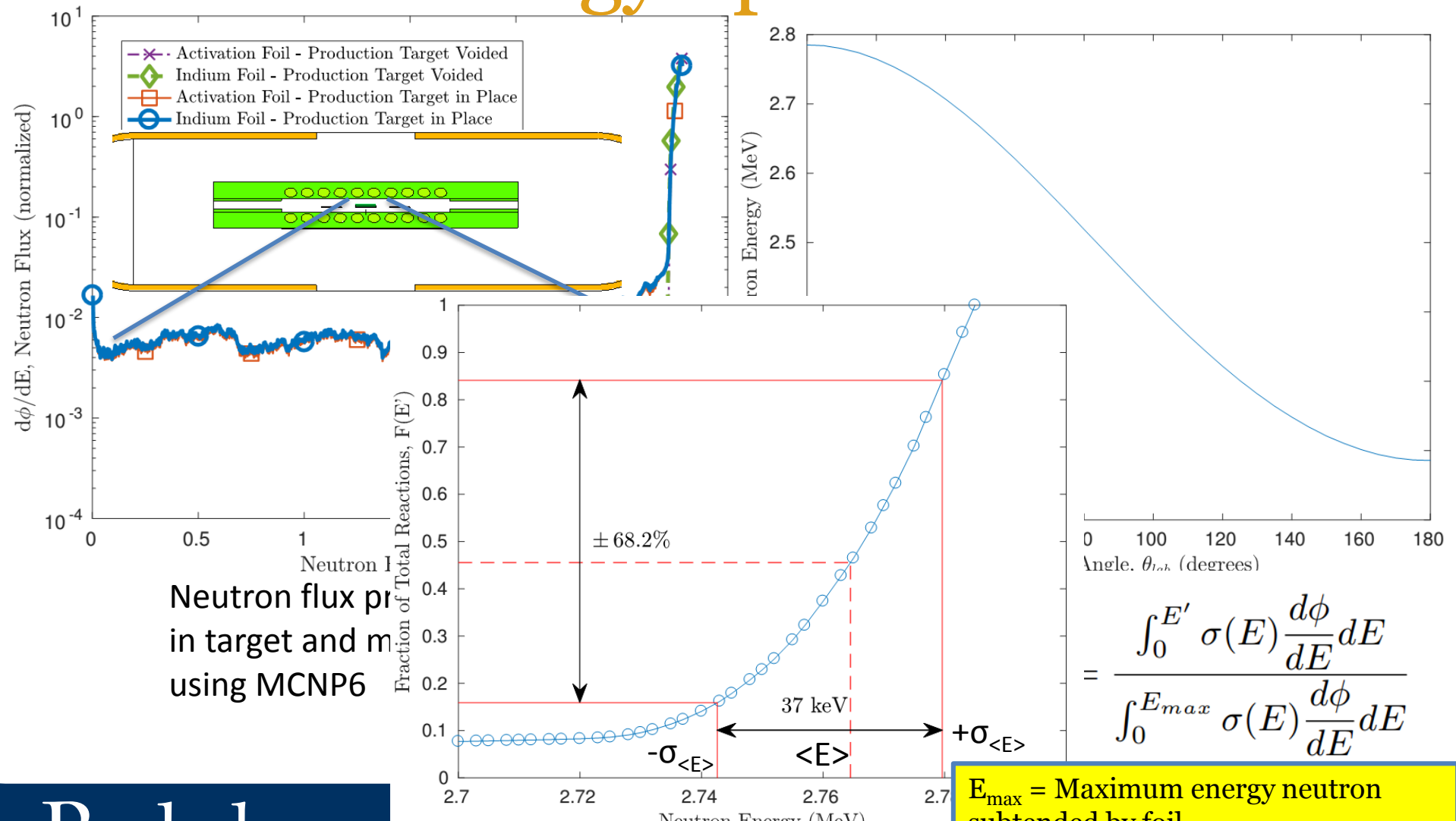


Neutron flux profile modeled
in target and monitor foil,
using MCNP6



Neutron Energy Spread

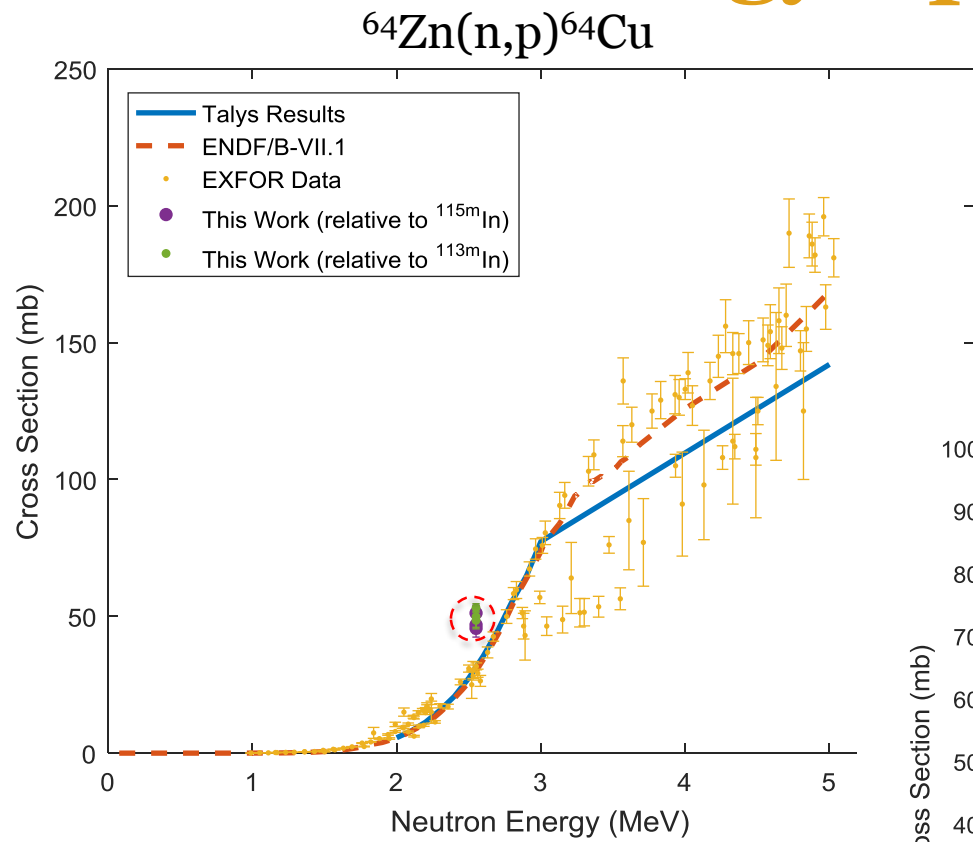
H. Liskien *et al.*, Nucl Data Tables, vol 11, 2973



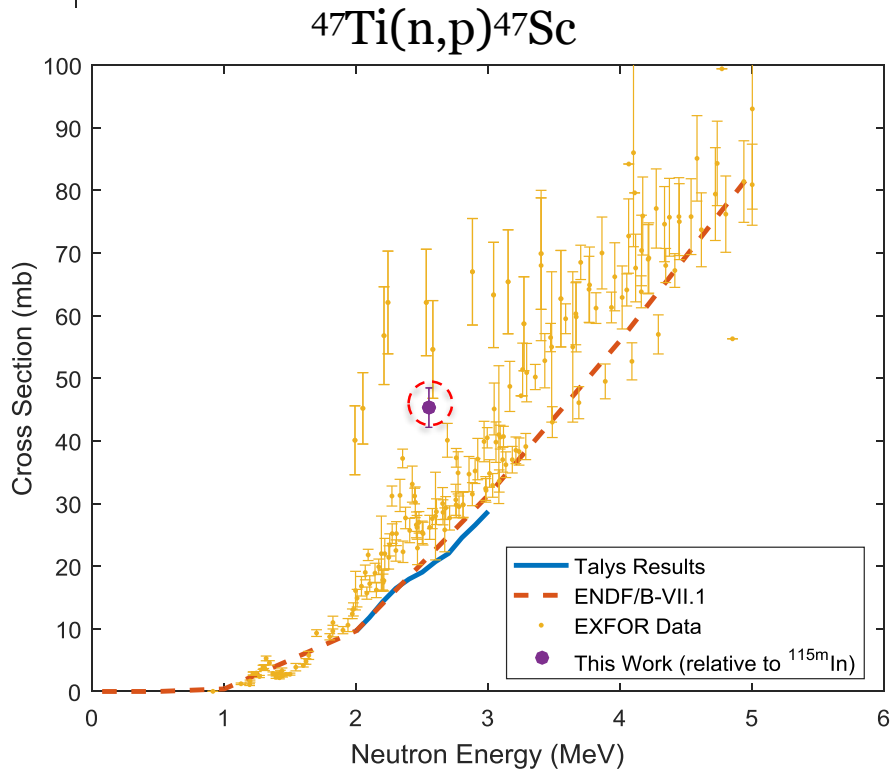
$$= \frac{\int_0^{E'} \sigma(E) \frac{d\phi}{dE} dE}{\int_0^{E_{max}} \sigma(E) \frac{d\phi}{dE} dE}$$

E_{max} = Maximum energy neutron subtended by foil
 $F(E')$ = Fraction of Total Reactions induced up to energy E'

Neutron Energy Spread



Before...



Neutron Energy Spread

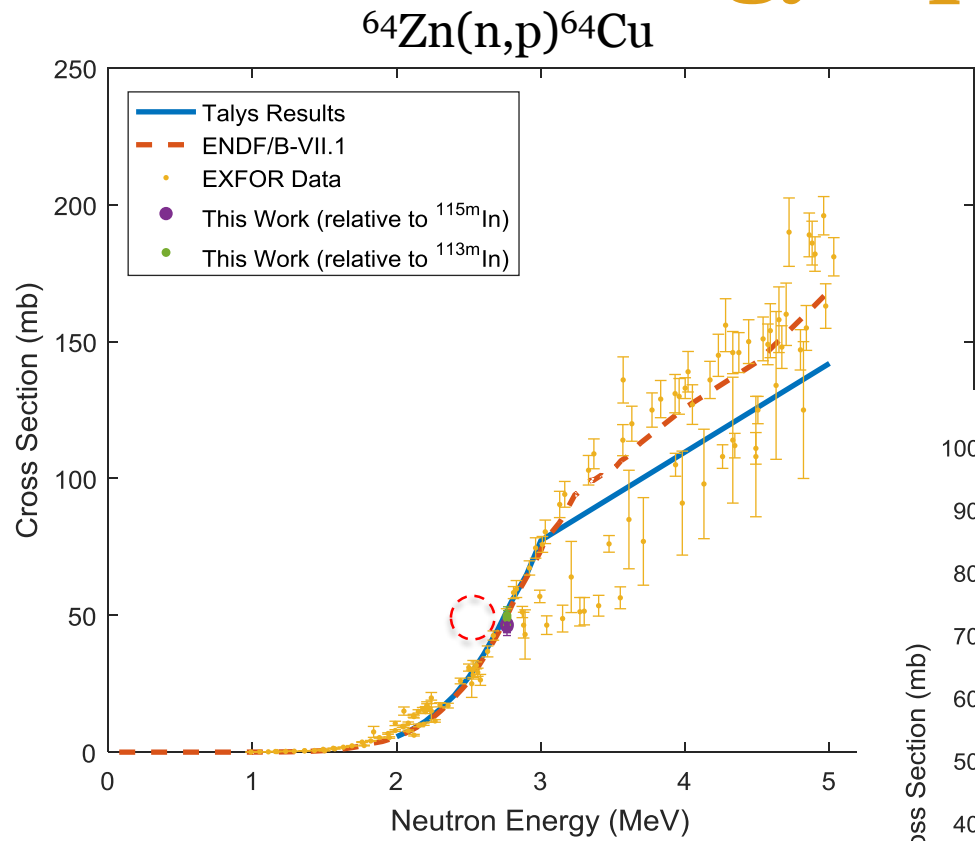
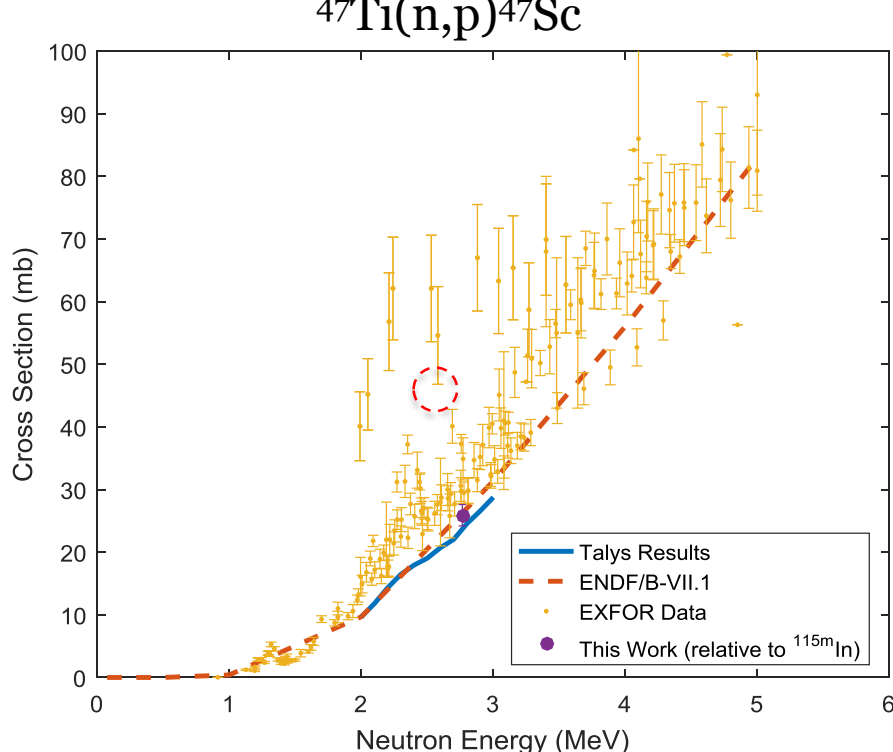


Table 3. Results of cross section measurement.

Reaction	$\sigma(E_n = 2.7645 \text{ MeV}) \text{ (mb)}$
$^{64}\text{Zn}(\text{n},\text{p})^{64}\text{Cu}$ (relative to ^{113}In)	$45.953 \pm 3.351,$ $46.493 \pm 2.805,$ 46.9 ± 3.189
$^{64}\text{Zn}(\text{n},\text{p})^{64}\text{Cu}$ (relative to ^{115}In)	$49.716 \pm 3.335,$ $49.011 \pm 2.698,$
$^{47}\text{Ti}(\text{n},\text{p})^{47}\text{Sc}$ (relative to ^{115}In)	$25.901 \pm 1.7089,$

After!



Neutron Energy Spread

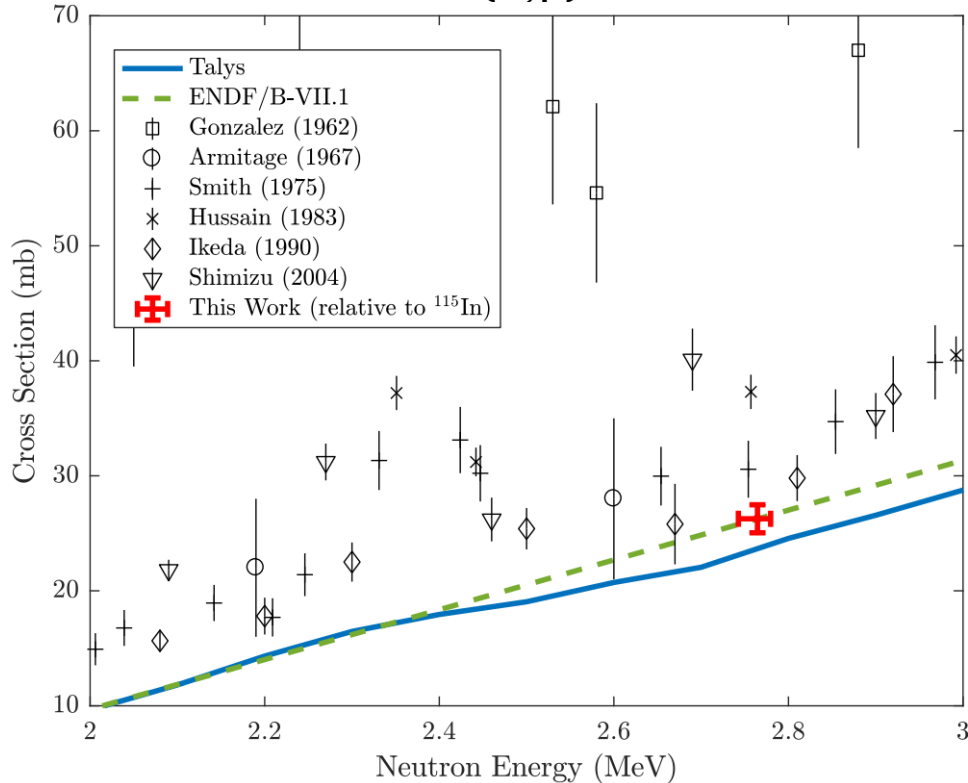
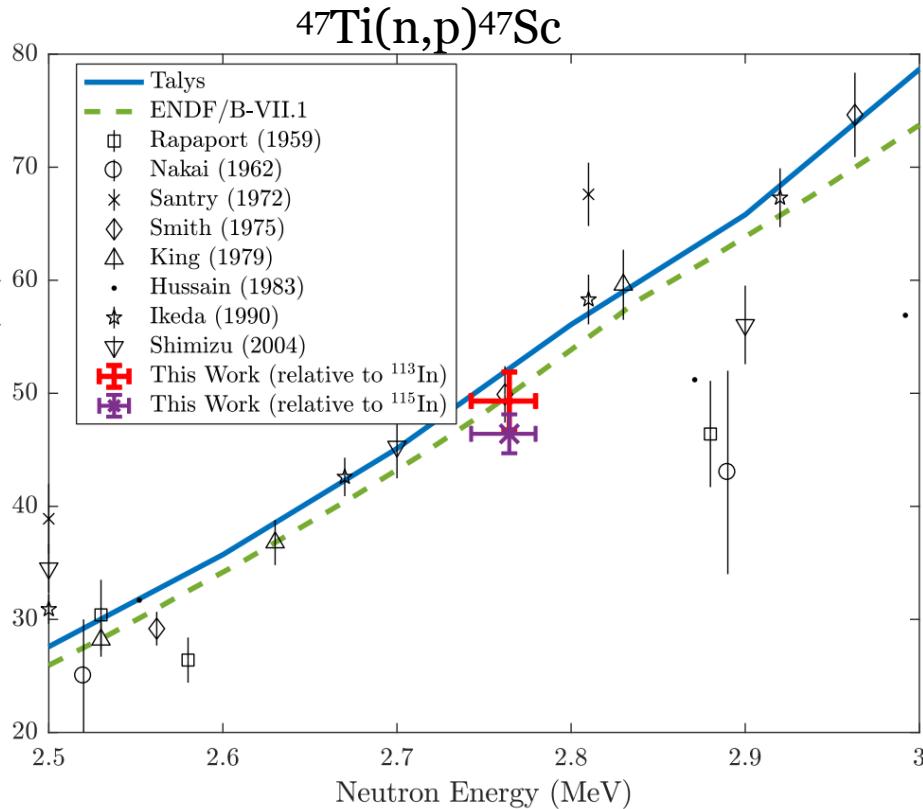


Table 3. Results of cross section measurement.

Reaction	$\sigma(E_n = 2.7645 \text{ MeV}) (\text{mb})$
$^{64}\text{Zn}(\text{n},\text{p})^{64}\text{Cu}$ (relative to ^{113}In)	$45.953 \pm 3.351,$ $46.493 \pm 2.805,$ 46.9 ± 3.189
$^{64}\text{Zn}(\text{n},\text{p})^{64}\text{Cu}$ (relative to ^{115}In)	$49.716 \pm 3.335,$ $49.011 \pm 2.698,$
$^{47}\text{Ti}(\text{n},\text{p})^{47}\text{Sc}$ (relative to ^{115}In)	$25.901 \pm 1.7089,$

After!



Neutron Energy Systematics

- Indium foils also undergo $^{115}\text{In}(\text{n}, \gamma)^{116}\text{In}$, which emits a 417 keV γ following β^- decay
 - Capture is strongly subject to thermal neutron contamination, as the (n, γ) cross section at 25 meV is ~ 2000 x that at 2.7 MeV
 - MCNP neutron energy spectrum estimates thermal & epithermal neutrons comprise 0.0771% of all neutrons
 - Confirmed experimentally - production of ^{116}In was consistent with an effective neutron energy of 2.45 MeV
 - Activation consistent with predominantly fast neutron capture confirms paucity of "room return" thermal neutrons
 - Highlights the possibility of using HFNG-like designs for (n, p) isotope production free from (n, γ) contamination products!

Neutron Energy Systematics

- Use of Indium activation to assign the effective energy window for activation foils introduces a small systematic uncertainty, as the two have differing reaction threshold energies
 - Convolution of IRDFF In(n,n') cross sections with our MCNP neutron flux profile predicts that the total activity in the In produced by the low energy neutrons (below the "knee" near 2.25 MeV is 2.17%).
 - If we trust the (n,p) excitation functions for Zn and Ti from TALYS, the corresponding values from TALYS for the Cu and Sc activity are 0.24% and 0.85%, respectively.
 - If we assume an uncertainty of $\pm 50\%$ in the TALYS calculations in this energy region, this would lead to a shift in (n,p) cross sections for the Cu and Sc activities of 0.12% and 0.42%, respectively.

Neutron Utilization

$$R_{production} = R_{decay} = \lambda N_{product} \quad A_{saturation} = \eta R_n$$

$$\eta = \frac{1}{R_n} \int_{\text{production target}} \phi(\mathbf{r}) \bar{\sigma} \rho_{target}(\mathbf{r}) d\mathbf{V},$$

$$d\mathbf{V} = \mathbf{r}^2 dr \sin \theta d\theta d\varphi$$

$$A(t_i) = \eta R_n (1 - e^{-\lambda t_i})$$

Neutron Utilization

$$A(t_i) = \eta R_n (1 - e^{-\lambda t_i})$$

- Theoretical saturation activities are currently estimated at 1.5 kBq of ^{64}Cu , 0.11 kBq of ^{47}Sc
 - Measured production rates were 453.8 Bq of ^{64}Cu , 31.6 Bq of ^{47}Sc
 - **Implies $\eta \approx 3 \times 10^{-5}$ (^{64}Cu), $\eta \approx 1 \times 10^{-5}$ (^{47}Sc)**

Stacked-target Charged Particle Excitation Functions

Low Energy – LBNL

Why charged particle production?

- Cyclotron
 - Many hospitals have small K~15 medical cyclotrons for PET tracer production
 - Leverage existing infrastructure
 - Explore higher energies for regional research cyclotrons, basic science
- Linac
 - Commonly used for high-energy production (LANL – IPF)
 - Useful for anchoring to complementary low-energy measurements

$^{51,52}\text{Mn}$ - Motivation

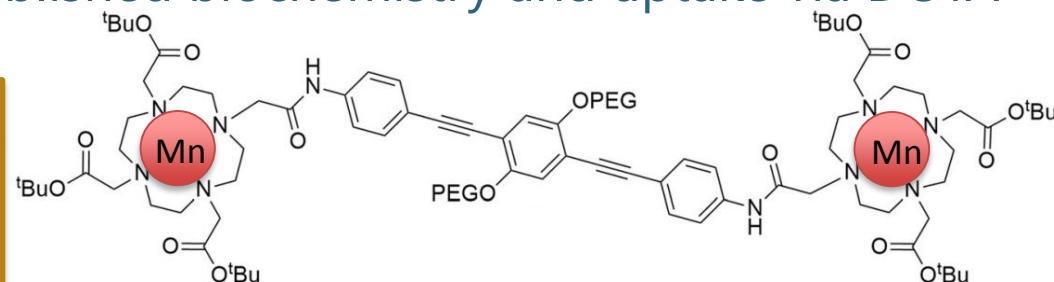
- Emerging medical radionuclides
 - ^{51}Mn ($t_{1/2} = 46$ min, 97% β^+) – short-lived PET tracer for metabolic studies
 - ^{52}Mn ($t_{1/2} = 5.6$ d, 29% β^+) – long-lived PET tracer for neuron tracking, immune studies

Preparation and *in vivo* characterization of $^{51}\text{MnCl}_2$ as PET tracer of Ca^{2+} channel-mediated transport

Stephen A. Graves¹, Reinier Hernandez¹, Hector F. Valdovinos¹, Paul A. Ellison¹, Jonathan W. Engle^{1*}
Todd E. Barnhart¹, Weibo Cai^{1,2,3}, Robert J. Nickles^{1*}

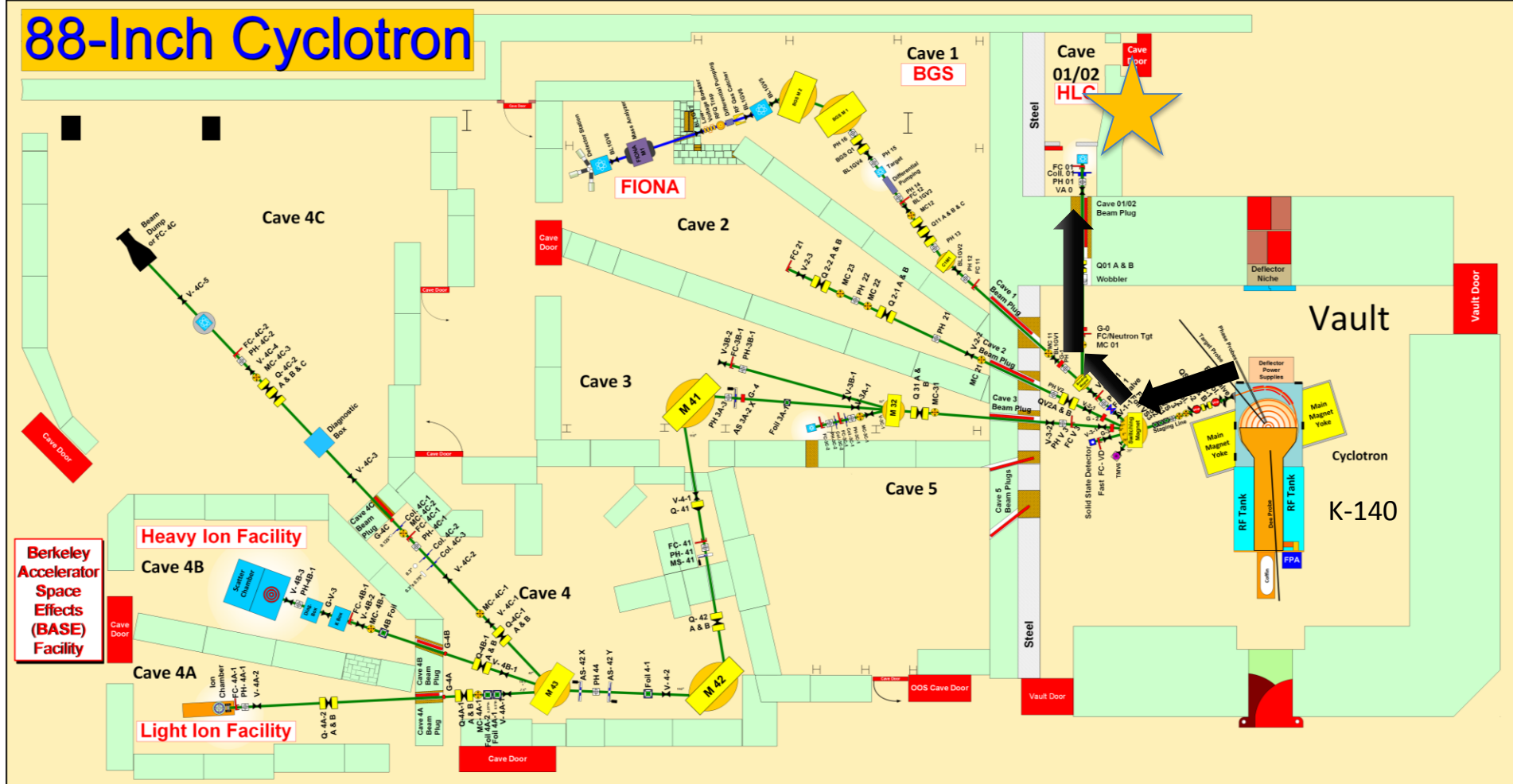
- Manganese has well-established biochemistry and uptake via DOTA-based chelation

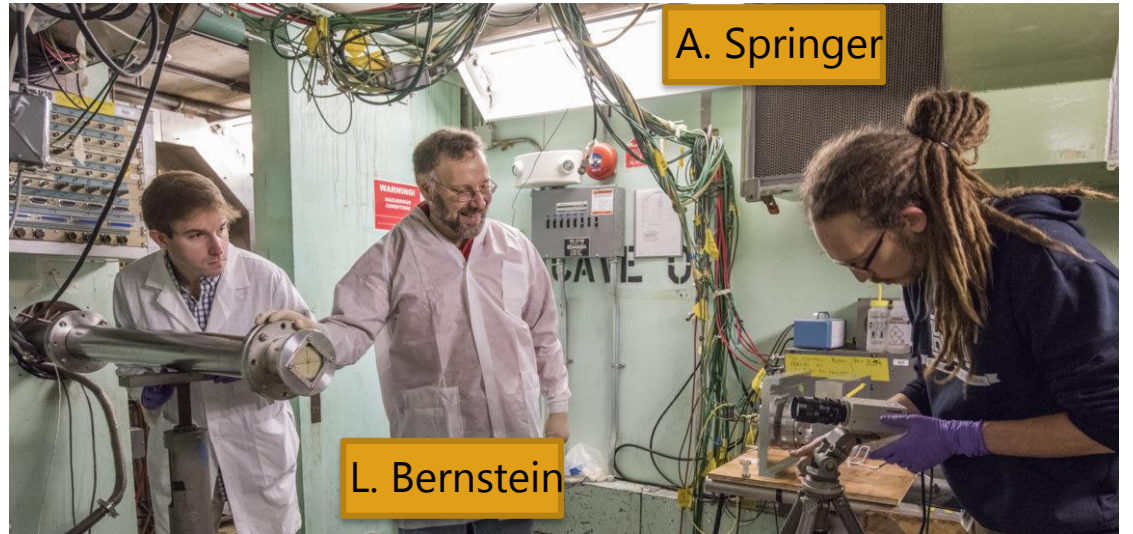
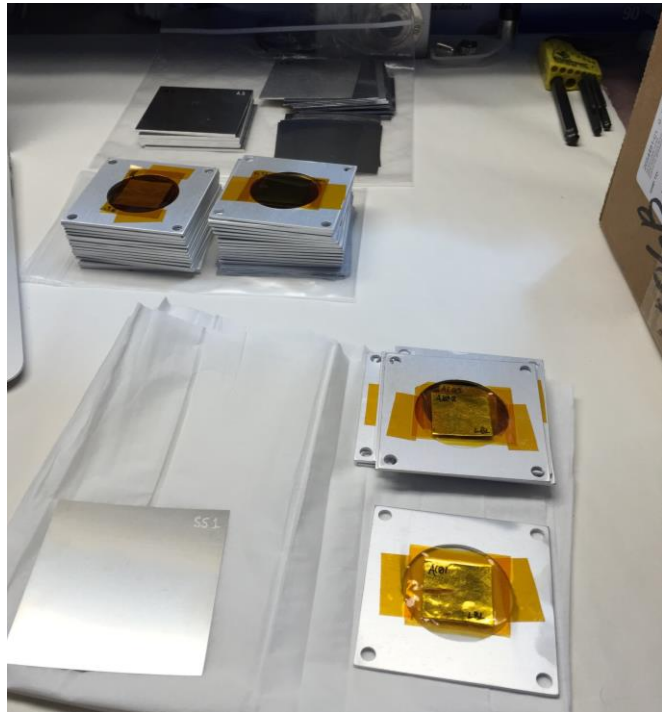
Almost no Fe(p,x) XS measurements exist – can use these to probe spin physics in the $A \approx 50$ region



Methology

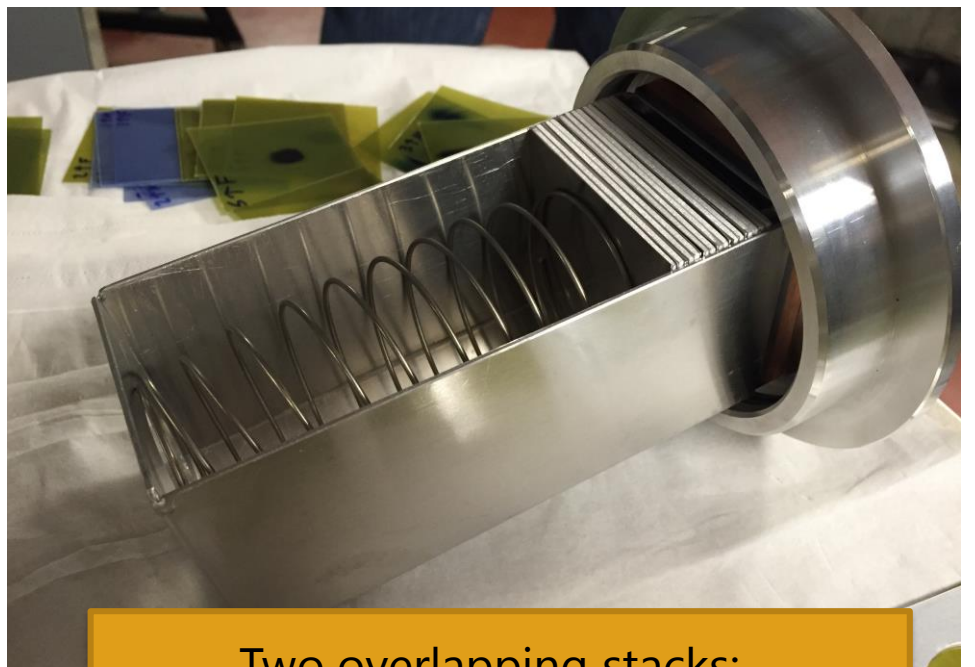
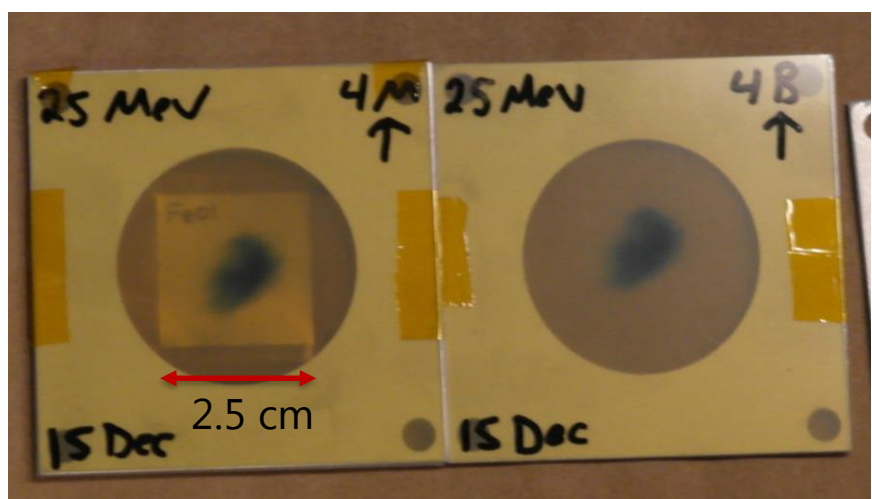
88-Inch Cyclotron





A. Springer

L. Bernstein



Two overlapping stacks:
 $E_p = 55 \rightarrow 21 \text{ MeV}, 25 \rightarrow 11 \text{ MeV}$
(120 nA@10 min, 100 nA@20 min)

Methodology

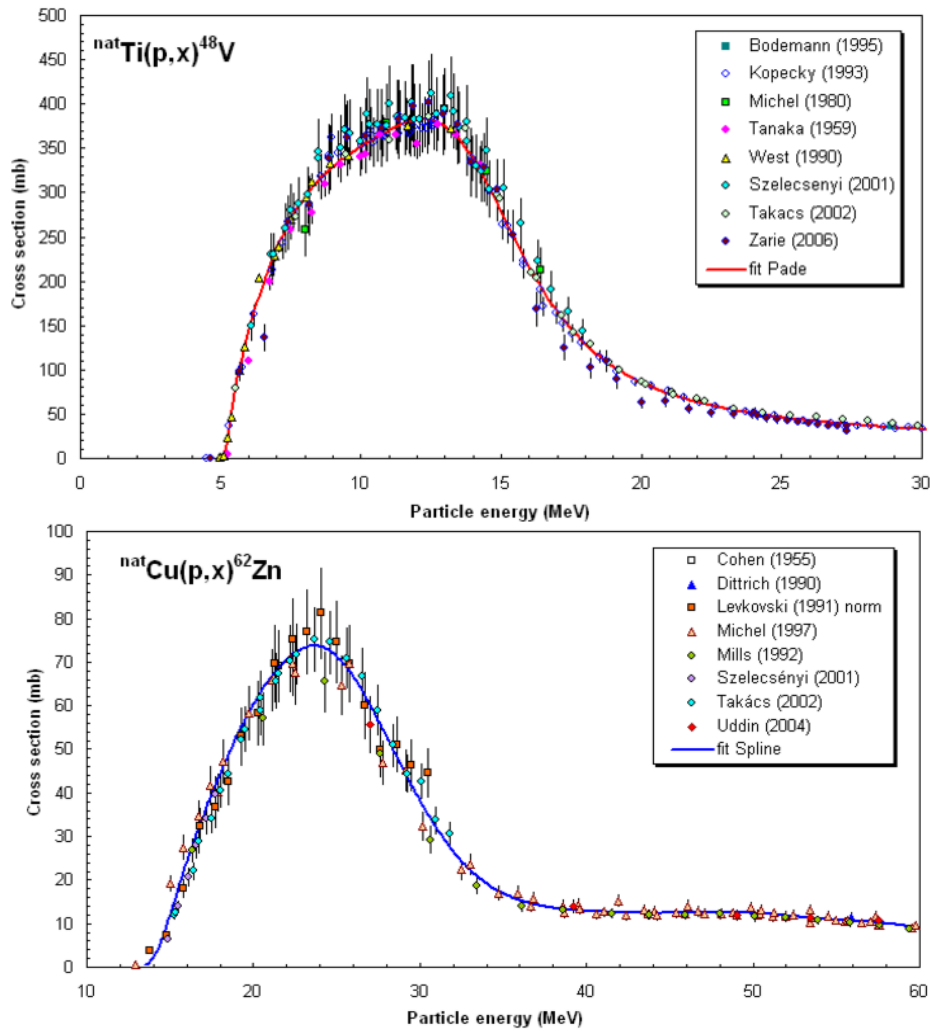
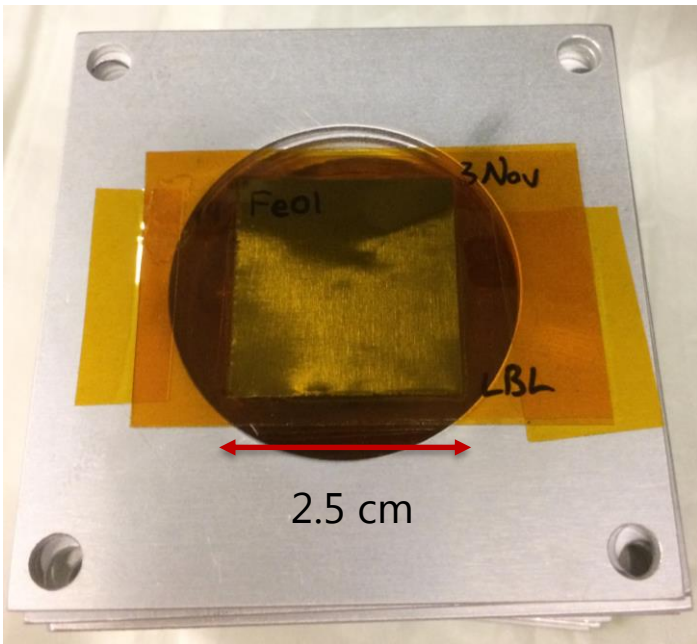
- Initial stack design planned using analytic Anderson & Ziegler stopping power formalism (SRIM)¹
 - Contains empirical corrections to Bethe-Bloch for nuclear stopping, low-energy stopping power

Stack 25MeV p on natFe

Projectile Data			Beam Energy		Precision		Target Stack Data				Name	
Name	Z-number	Mass					Incident Energy	Exit Energy	Energy Loss	Stopping Power		
H	1	1.008	25	100			[MeV]	[MeV]	[MeV]	MeV/(g/cm ²)		
1	316 SS	103	0.125	100.573			7.930	100.6	25.000	23.514	1.486	14.78 SS 5
2	Kapton	105	0.025				1.420	3.6	23.514	23.439	0.075	21.10
3	Fe	26	0.025	19.800			7.866	19.8	23.439	23.138	0.301	15.21 Fe01
4	Kapton	105	0.025				1.420	3.6	23.138	23.062	0.076	21.38
5	Kapton	105	0.025				1.420	3.6	23.062	22.986	0.076	21.43
6	Ti	22	0.025	10.900			4.519	10.9	22.986	22.813	0.173	15.85 Ti14
7	Kapton	105	0.025				1.420	3.6	22.813	22.736	0.077	21.62
8	Kapton	105	0.025				1.420	3.6	22.736	22.659	0.077	21.68
9	Cu	29	0.025	17.500			8.949	17.5	22.659	22.400	0.259	14.80 Cu14
10	Kapton	105	0.025				1.420	3.6	22.400	22.322	0.078	21.95
11	Al	13	0.254				2.698	68.5	22.322	21.052	1.271	18.54 E9
12	Kapton	105	0.025				1.420	3.6	21.052	20.970	0.082	23.08
13	Fe	26	0.025	19.800			7.866	19.8	20.970	20.641	0.328	16.58 Fe02
14	Kapton	105	0.025				1.420	3.6	20.641	20.558	0.083	23.45
15	Kapton	105	0.025				1.420	3.6	20.558	20.475	0.084	23.53
16	Ti	22	0.025	10.900			4.519	10.9	20.475	20.286	0.189	17.34 Ti15
17	Kapton	105	0.025				1.420	3.6	20.286	20.201	0.084	23.79
18	Kapton	105	0.025				1.420	3.6	20.201	20.116	0.085	23.87
19	Cu	29	0.025	17.500			8.949	17.5	20.116	19.833	0.284	16.20 Cu15
20	Kapton	105	0.025				1.420	3.6	19.833	19.747	0.086	24.23
21	Al	13	0.127				2.698	34.3	19.747	19.053	0.694	20.24 H01
22	Kapton	105	0.025				1.420	3.6	19.053	18.964	0.089	25.03
23	Fe	26	0.025	19.800			7.866	19.8	18.964	18.610	0.355	17.92 Fe03
24	Kapton	105	0.025				1.420	3.6	18.610	18.519	0.091	25.52
25	Kapton	105	0.025				1.420	3.6	18.519	18.428	0.091	25.62
26	Ti	22	0.025	10.900			4.519	10.9	18.428	18.223	0.205	18.82 Ti16

$$-\left\langle \frac{dE}{dx} \right\rangle = \frac{4\pi}{m_e c^2} \cdot \frac{n z^2}{\beta^2} \cdot \left(\frac{e^2}{4\pi\epsilon_0} \right)^2 \cdot \left[\ln\left(\frac{2m_e c^2 \beta^2}{I \cdot (1 - \beta^2)} \right) - \beta^2 \right]$$

- 25 μm -thin ${}^{\text{nat}}\text{Fe}$, ${}^{\text{nat}}\text{Cu}$, ${}^{\text{nat}}\text{Ti}$ foils in 0.1" Al frames



- Dosimetry: IAEA charged particle beam monitor reactions:
 - ${}^{\text{nat}}\text{Ti}(\text{p},\text{x}){}^{48}\text{V}$
 - ${}^{\text{nat}}\text{Cu}(\text{p},\text{x}){}^{62,63,65}\text{Zn}$

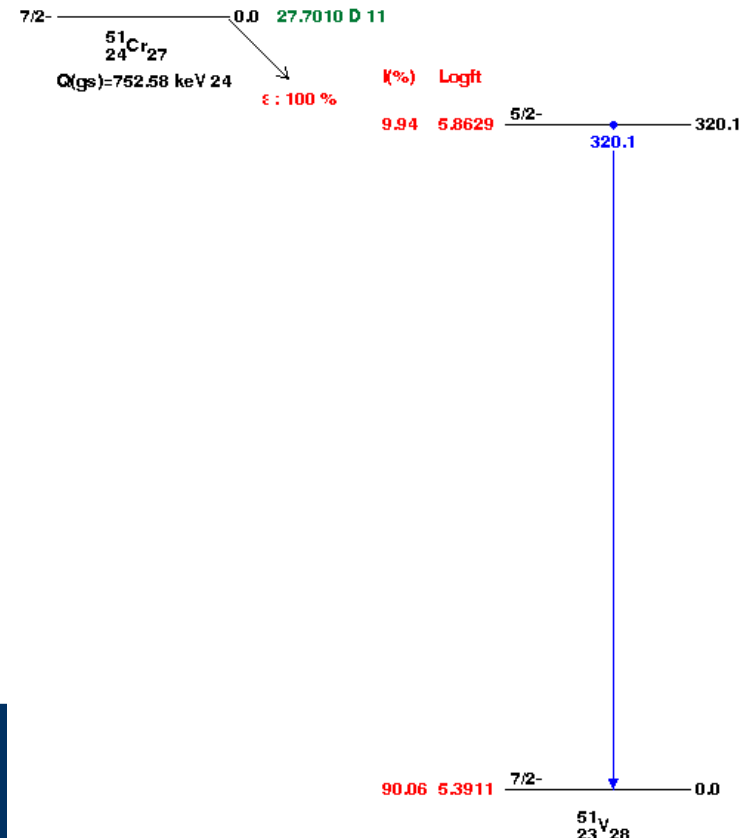
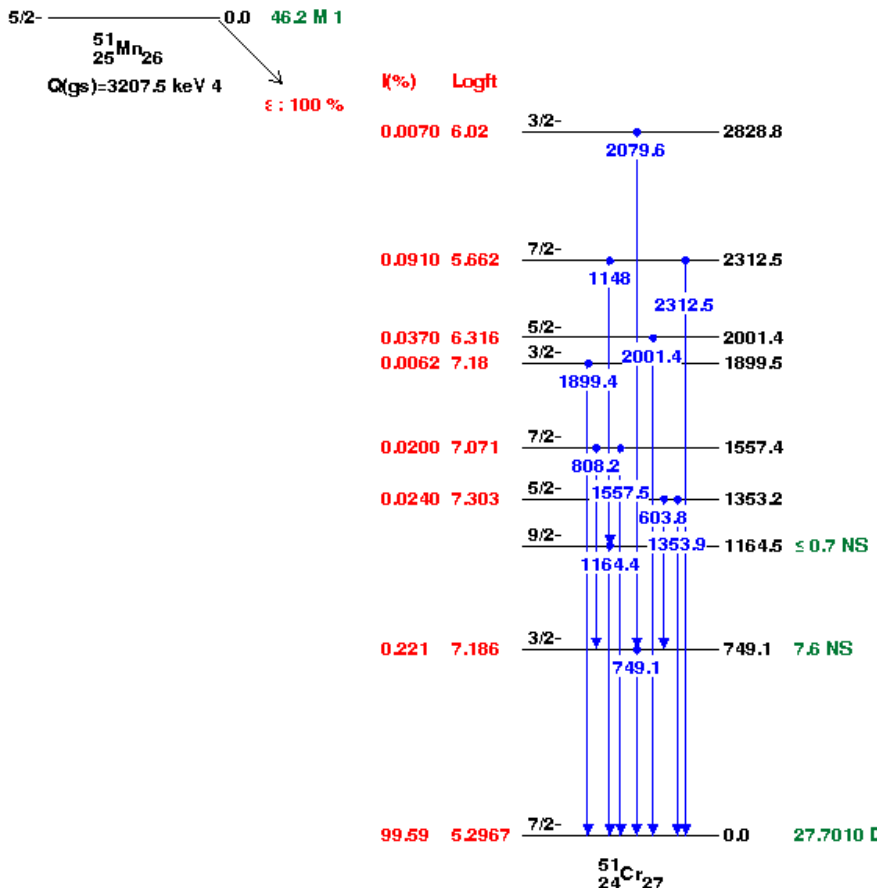
nds.iaea.org/medical/monitor_reactions.html

Spectroscopy

$\epsilon, t_{1/2} = 27.7 \text{ d}$



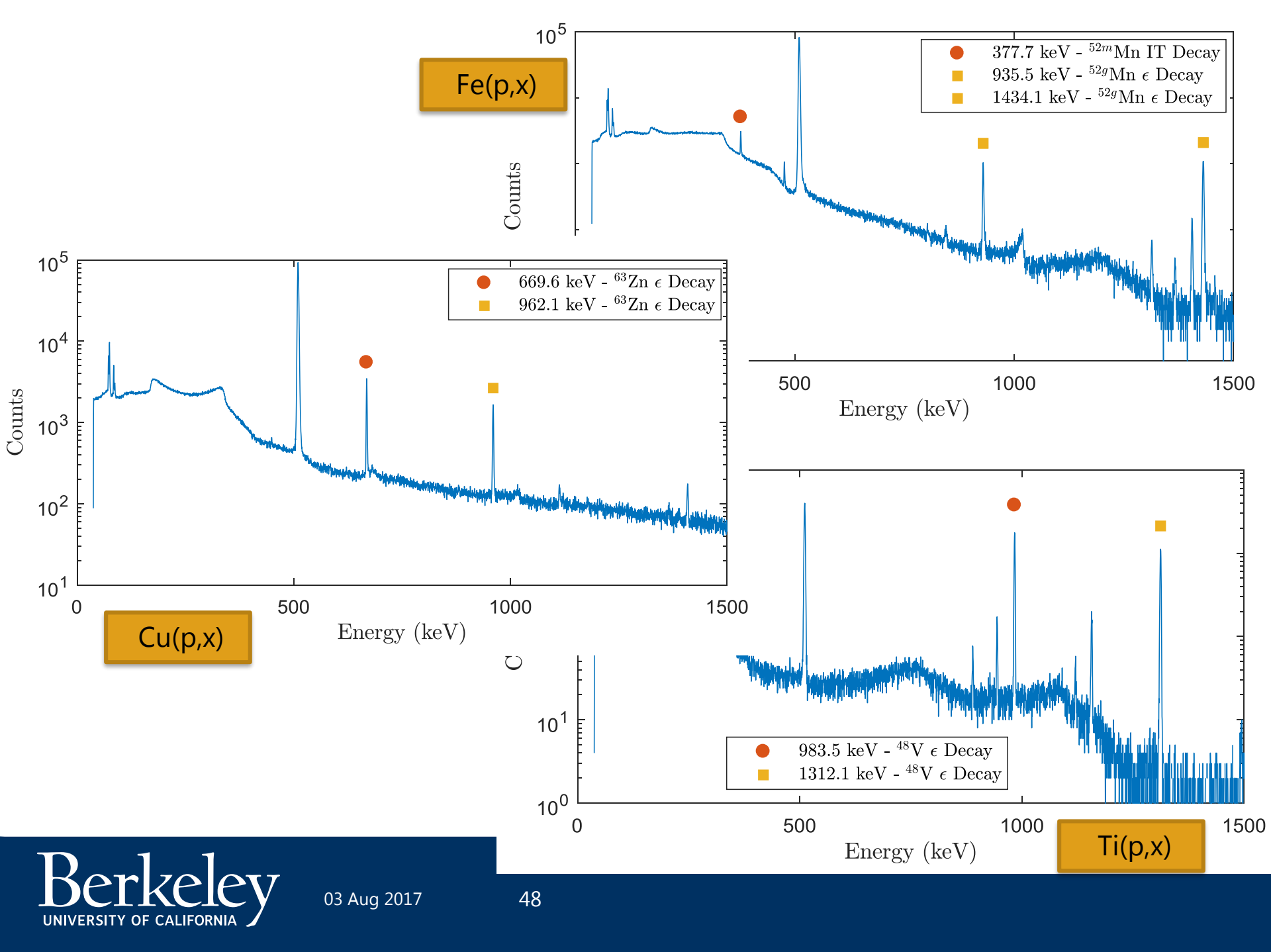
- ${}^{51}\text{Mn}$ decay has no strong gammas, just annihilation 511's
- Production is quantified using the ${}^{51}\text{Cr}$ decay 320.1 keV line



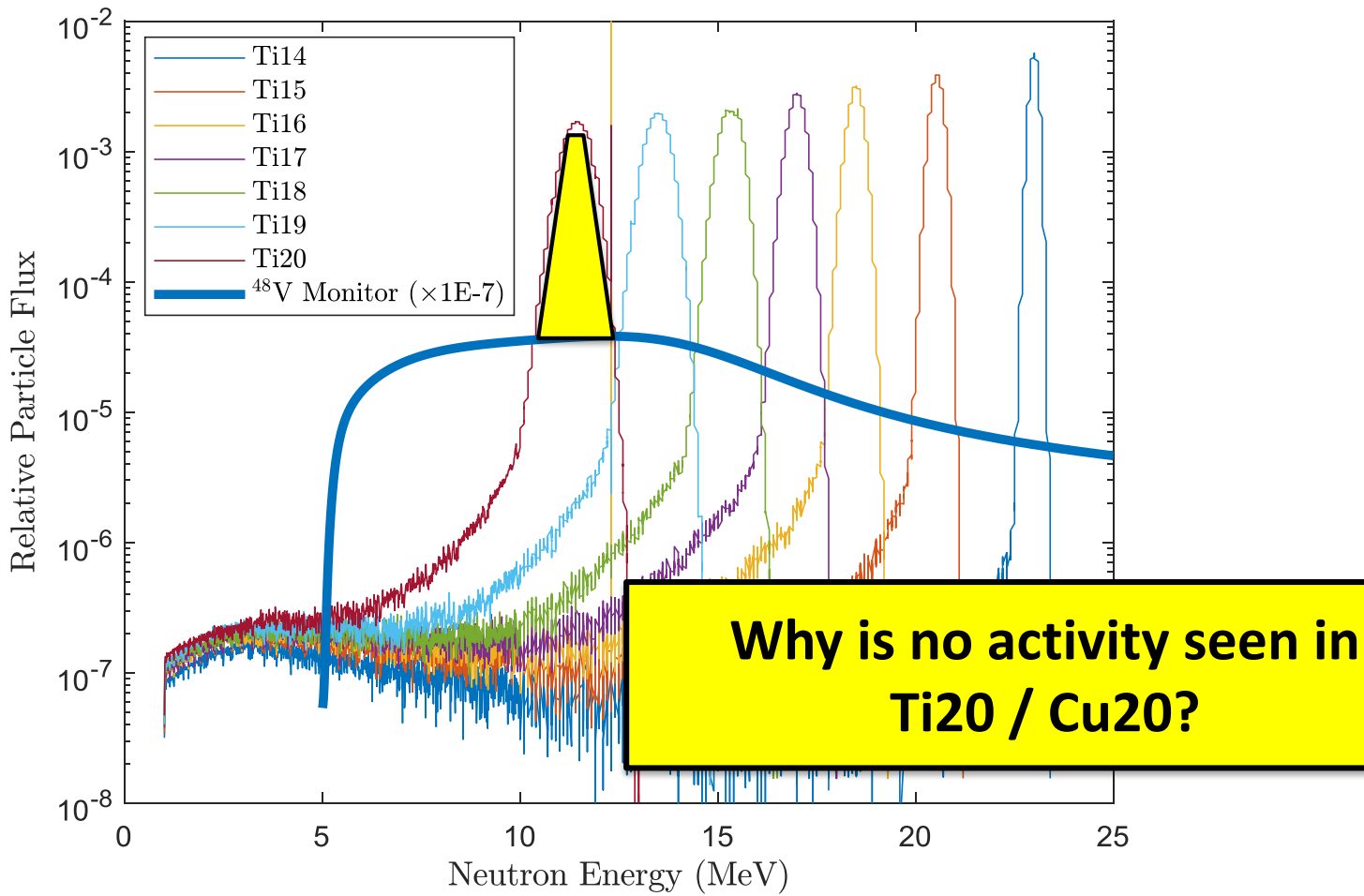
Spectroscopy



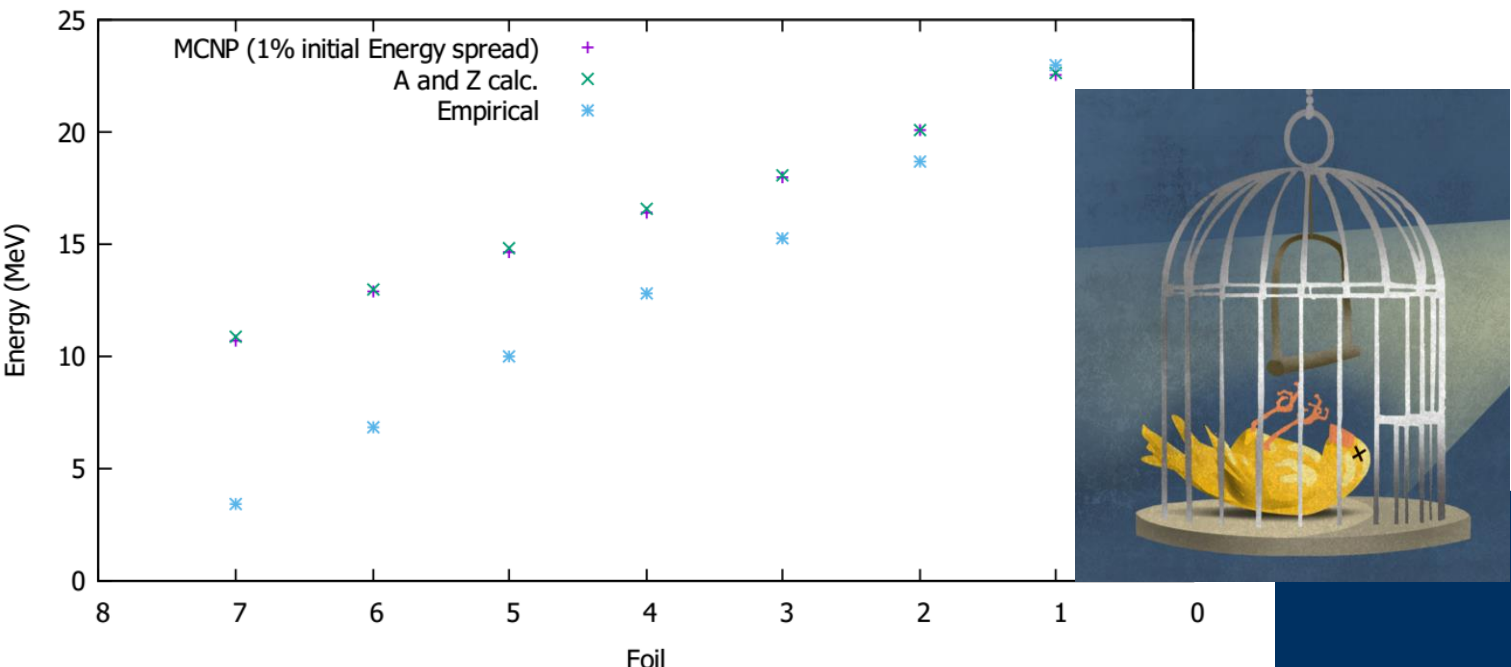
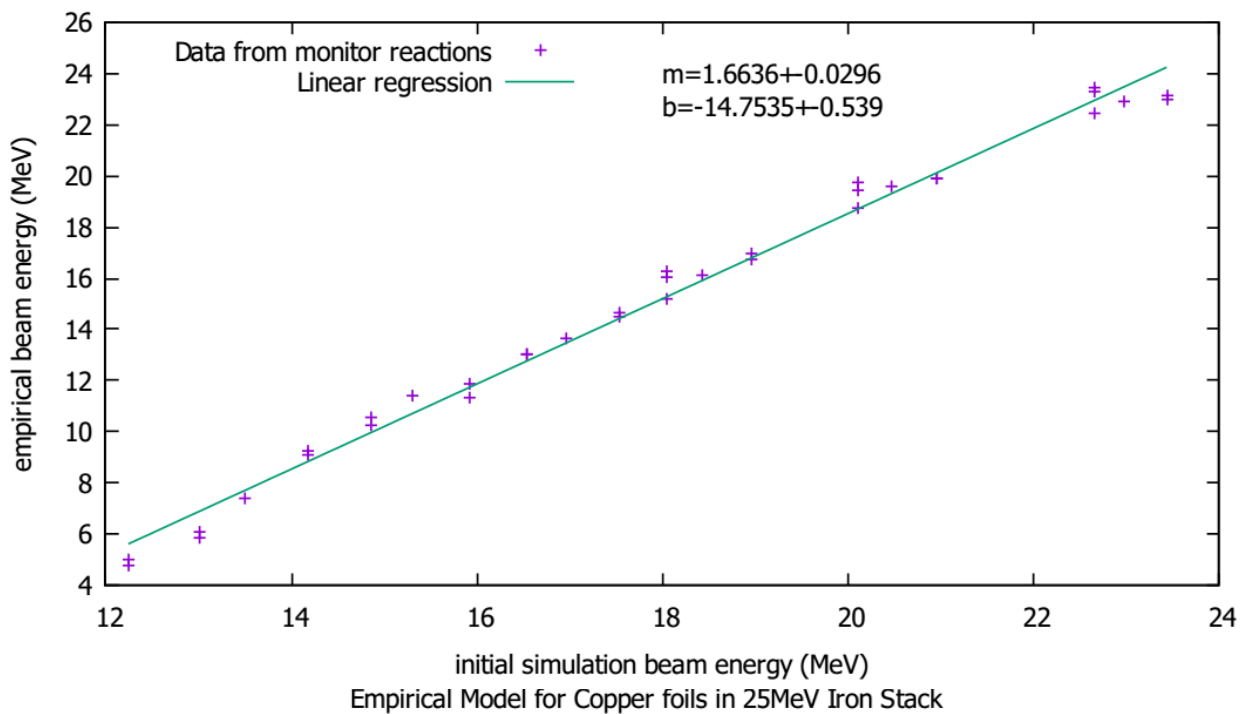
- ^{51}Mn β 's have max energy of 963.67 keV
- NIST ESTAR tables list aluminum CSDA range of 0.4873 g/cm² = 0.18 cm



Data Analysis Issues



Empirical beam energy model



Corrected Energy Assignments

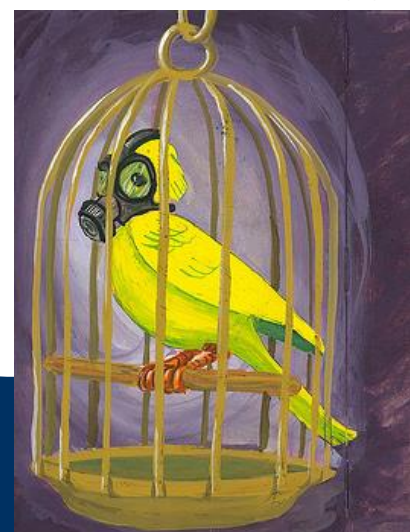
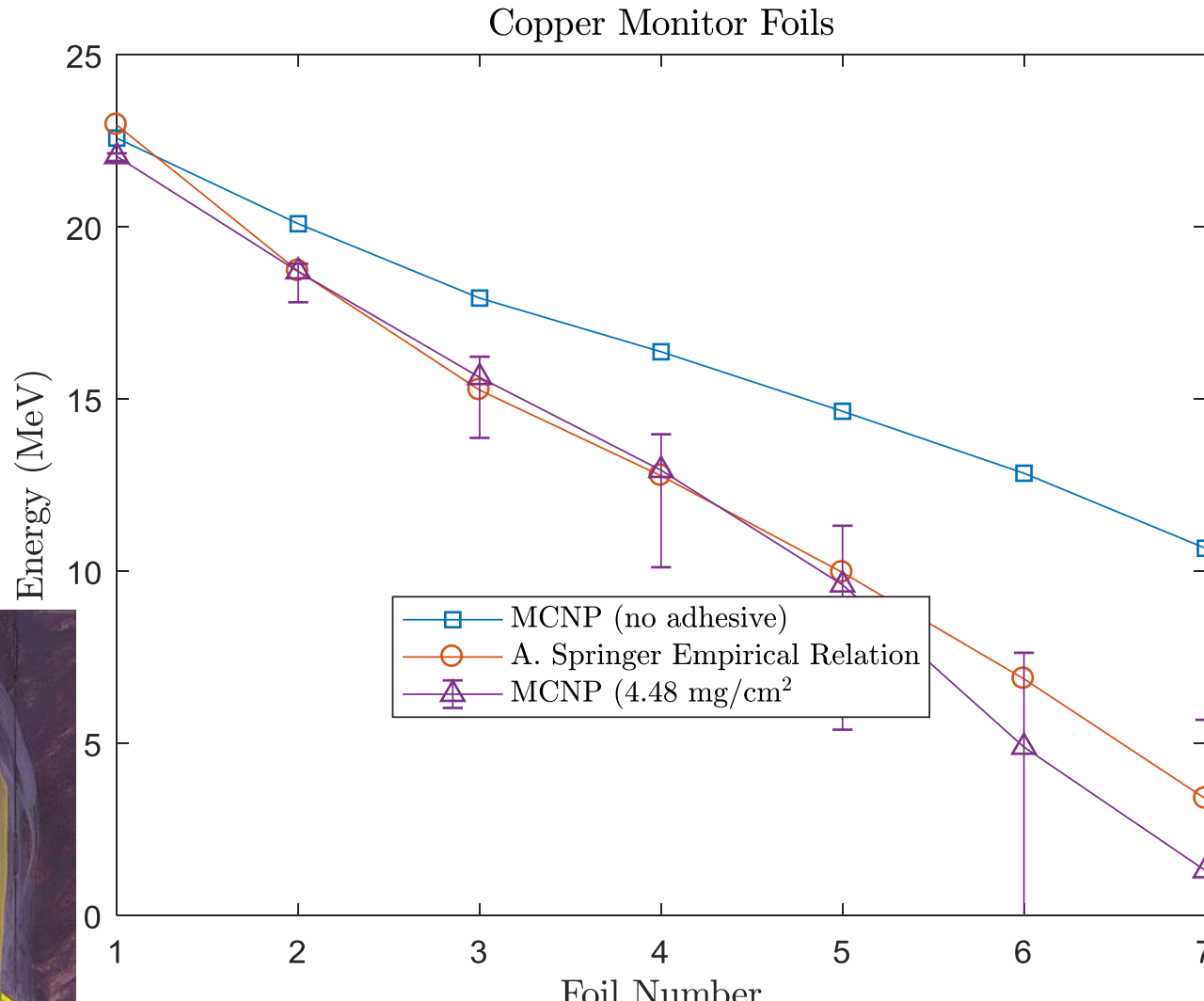


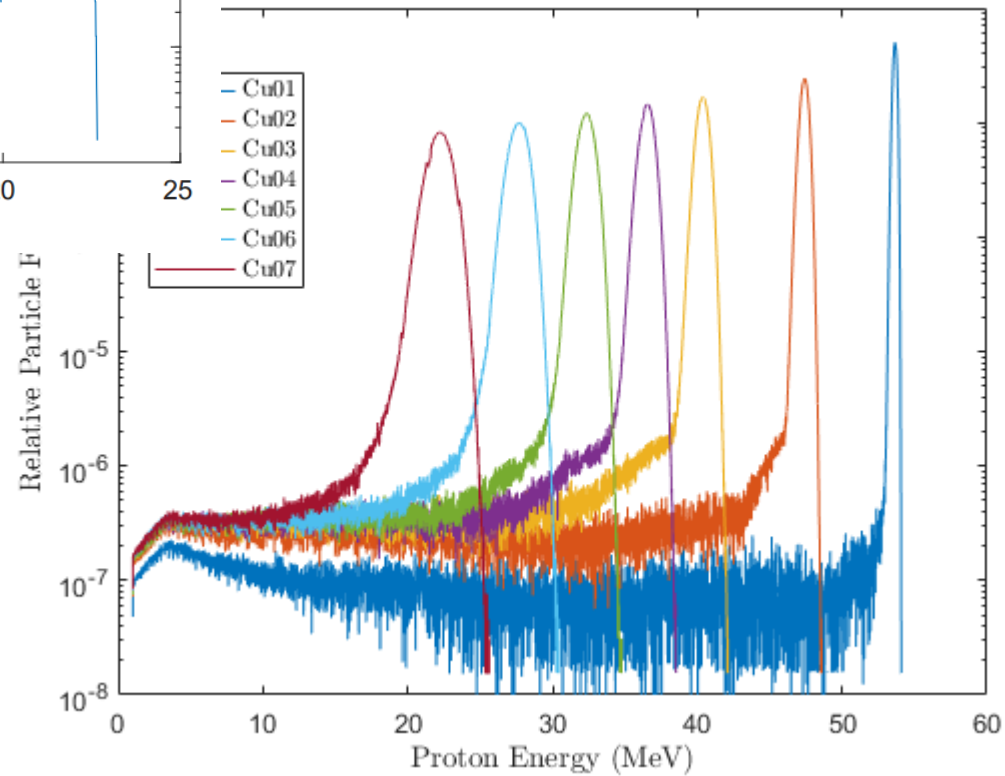
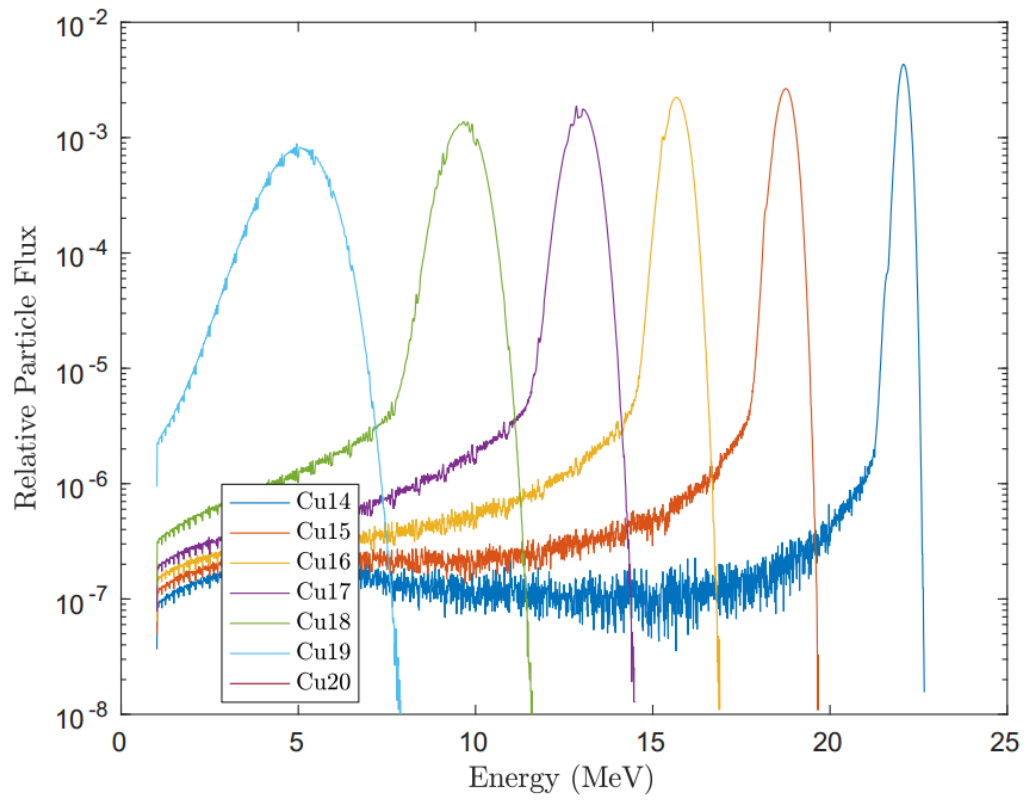
25 μm = 11 - 23 mg/cm 2

38 μm @ 1.18 g/cm 3 = 4.48 mg/cm 2

38 μm @ 1.42 g/cm 3 = 3.55 mg/cm 2

Corrected Energy Assignments





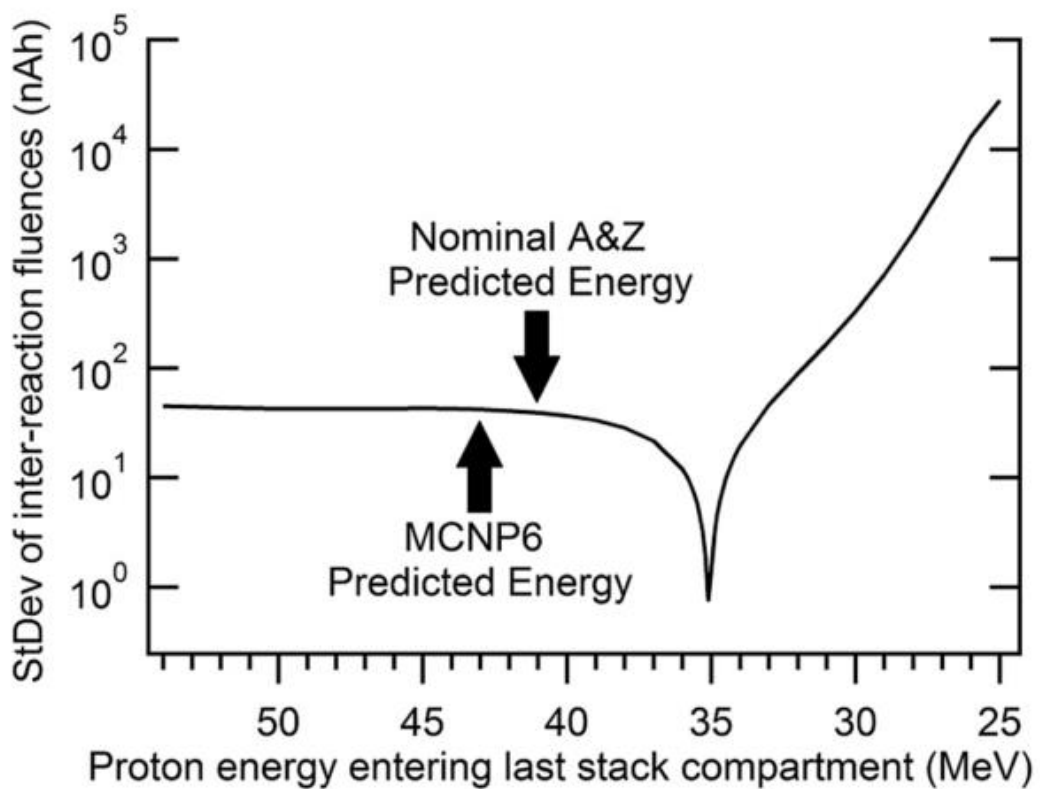


Fig. 3. Results of varying degrader density in analytic A&Z calculations on inter-monitor reaction fluence standard deviation. Varying degrader density has the effect of non-linearly varying the average beam energy in each compartment. This non-linear dependence on density has nearly the same functional impact as variations in the incident beam energy. Arrows indicate the predicted average beam energy in the last stack compartment by MCNP6 simulation and nominal A&Z calculations. A clear minimum from this approach is seen at 35.1 MeV, suggesting the initial beam energy estimations by nominal A&Z calculations and by MCNP6 simulation are significantly higher than what was experimentally observed.

LANL sees the
same issue...

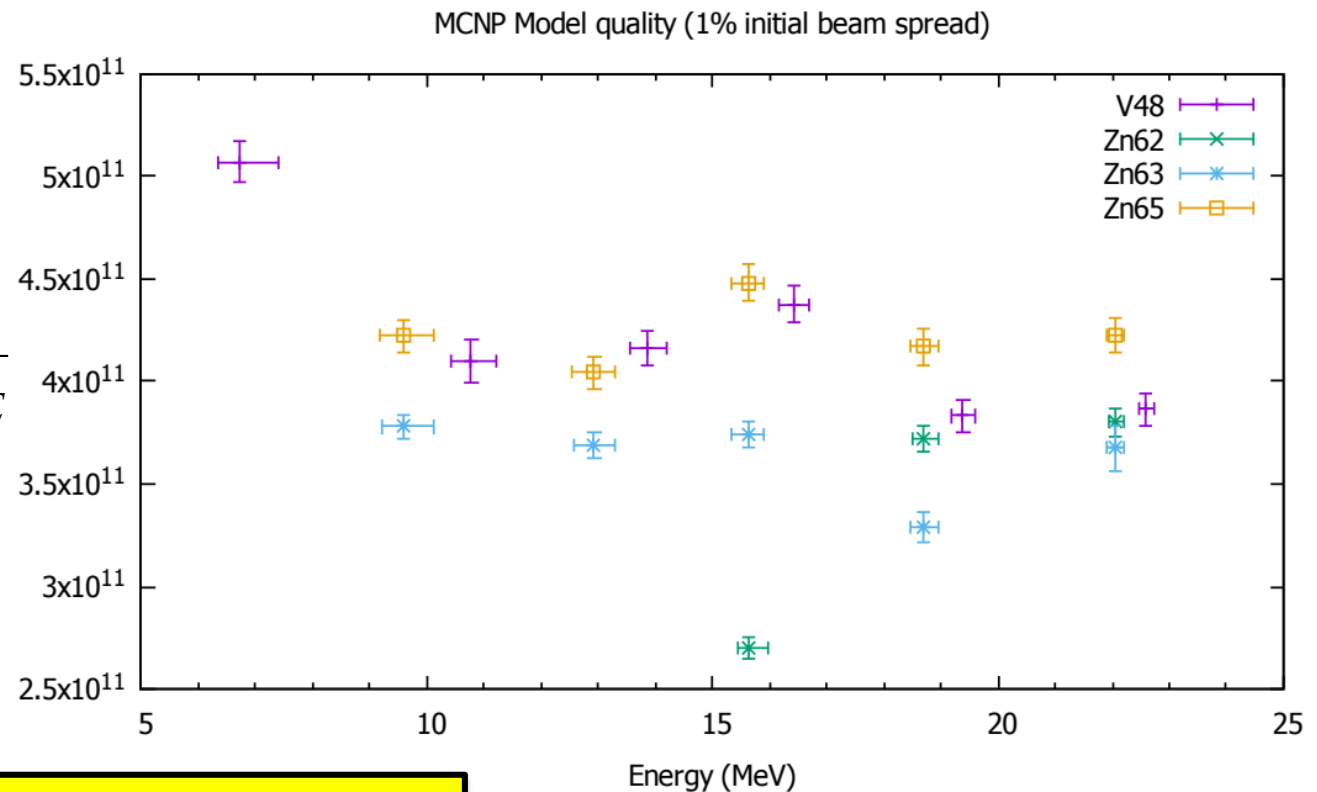
Corrected Energy Assignments

- Minimize in 2D:
 - Effective adhesive areal density ($\pm 20\%$, in 1% steps = 41 trials)
 - Initial beam energy dispersion (0.5%, 1%, 1.5%, 2% = 4 trials)
 - 164 simulations → Running on UCB Savio HPC
 - Adhesive should have a much stronger impact than beam dispersion

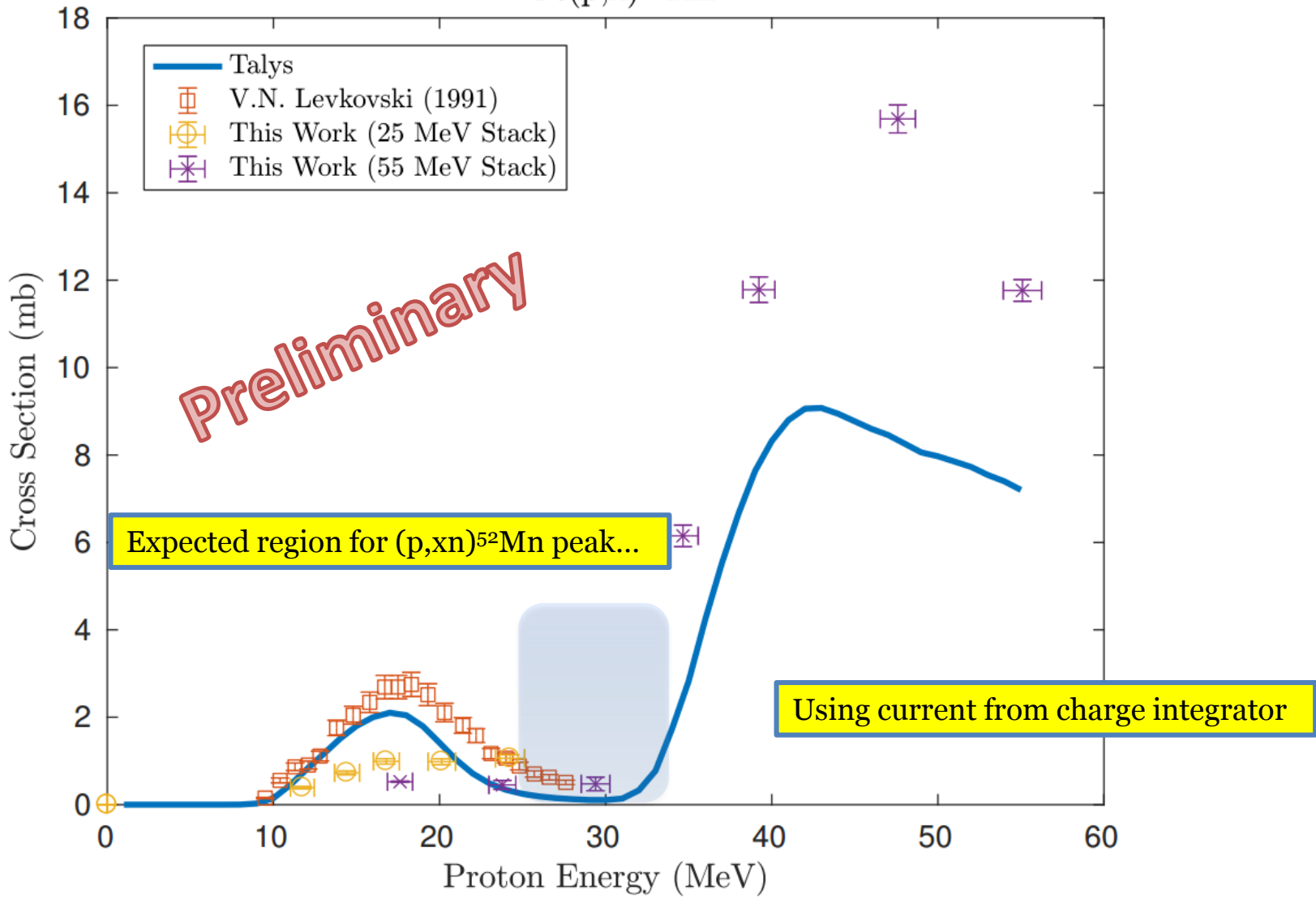
$$\chi = \frac{R_{prod}}{\int \sigma_{IAEA}(E) \frac{d\phi_{MCNP}}{dE} \rho \Delta r dE}$$

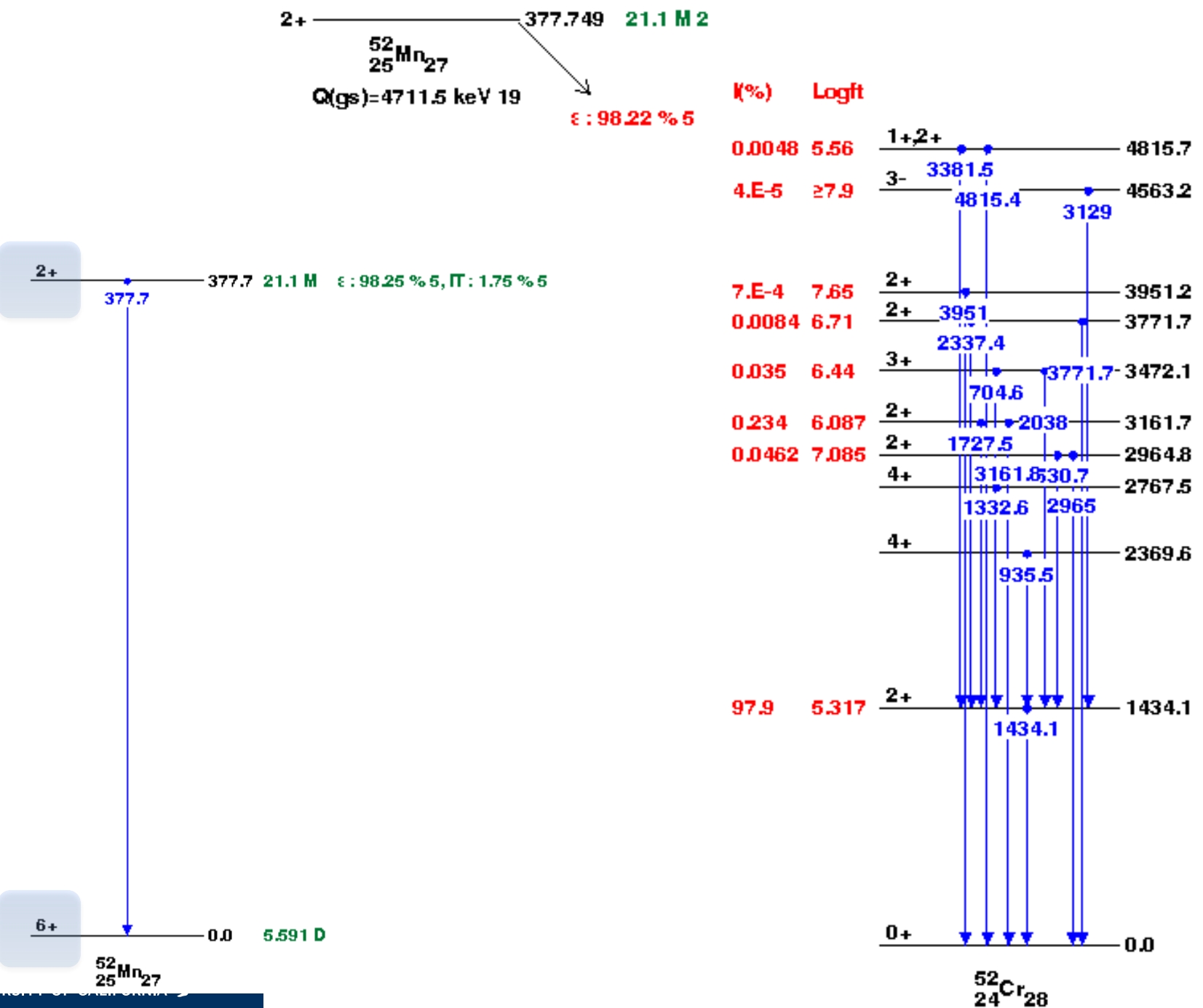
Corrected Energy Assignments

$$\chi = \frac{R_{prod}}{\int \sigma_{IAEA}(E) \frac{d\phi_{MCNP}}{dE} \rho \Delta r dE}$$

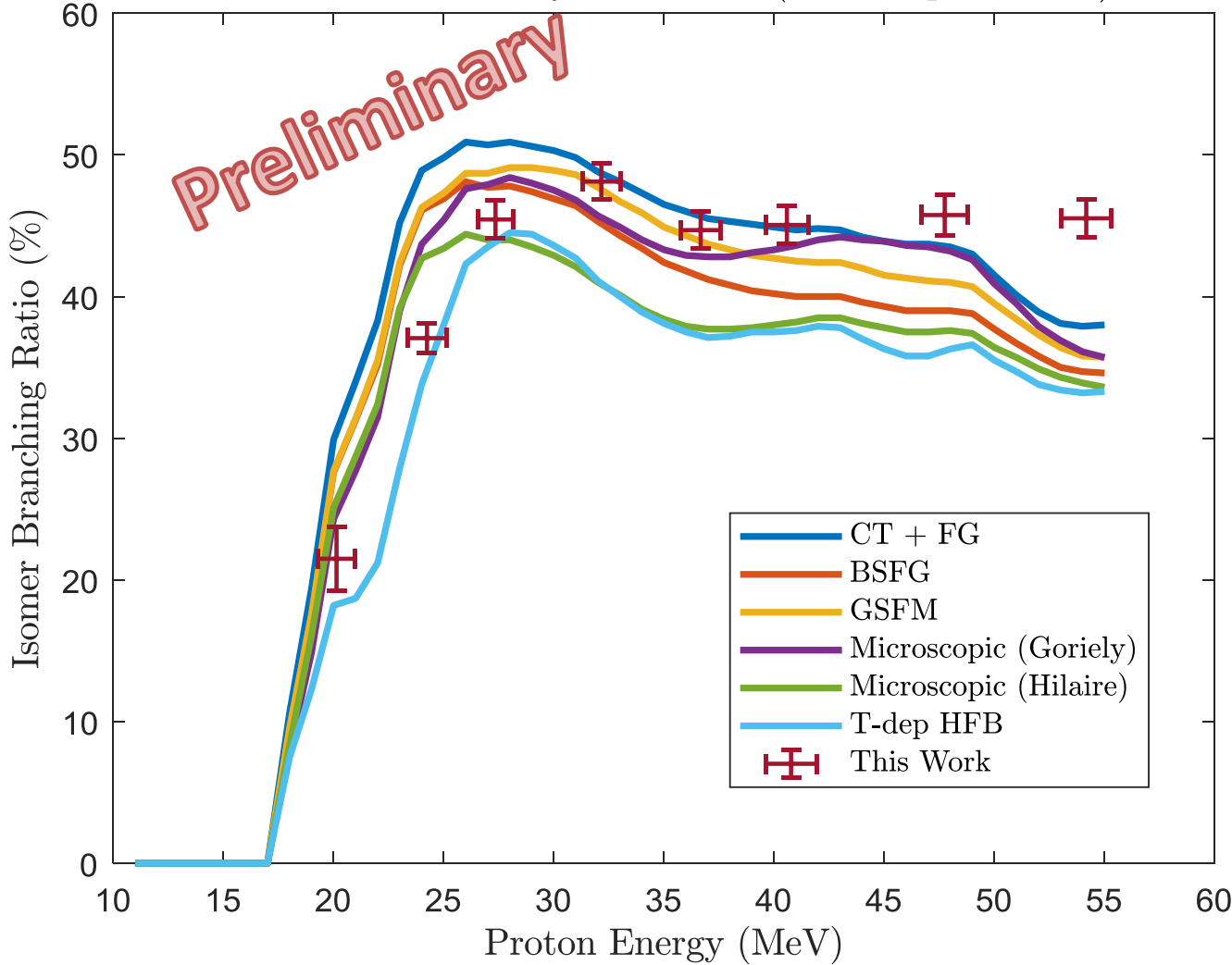


Goal: Minimize standard deviation of χ





^{52m}Mn (2+)/ ^{52g}Mn (6+) vs. Energy for $^{56}\text{Fe}(\text{p},\alpha\text{n})$
TALYS Level Density Models 1-6 (default spin cut-off)



Spin Distribution

- Constant Temperature + Fermi Gas:

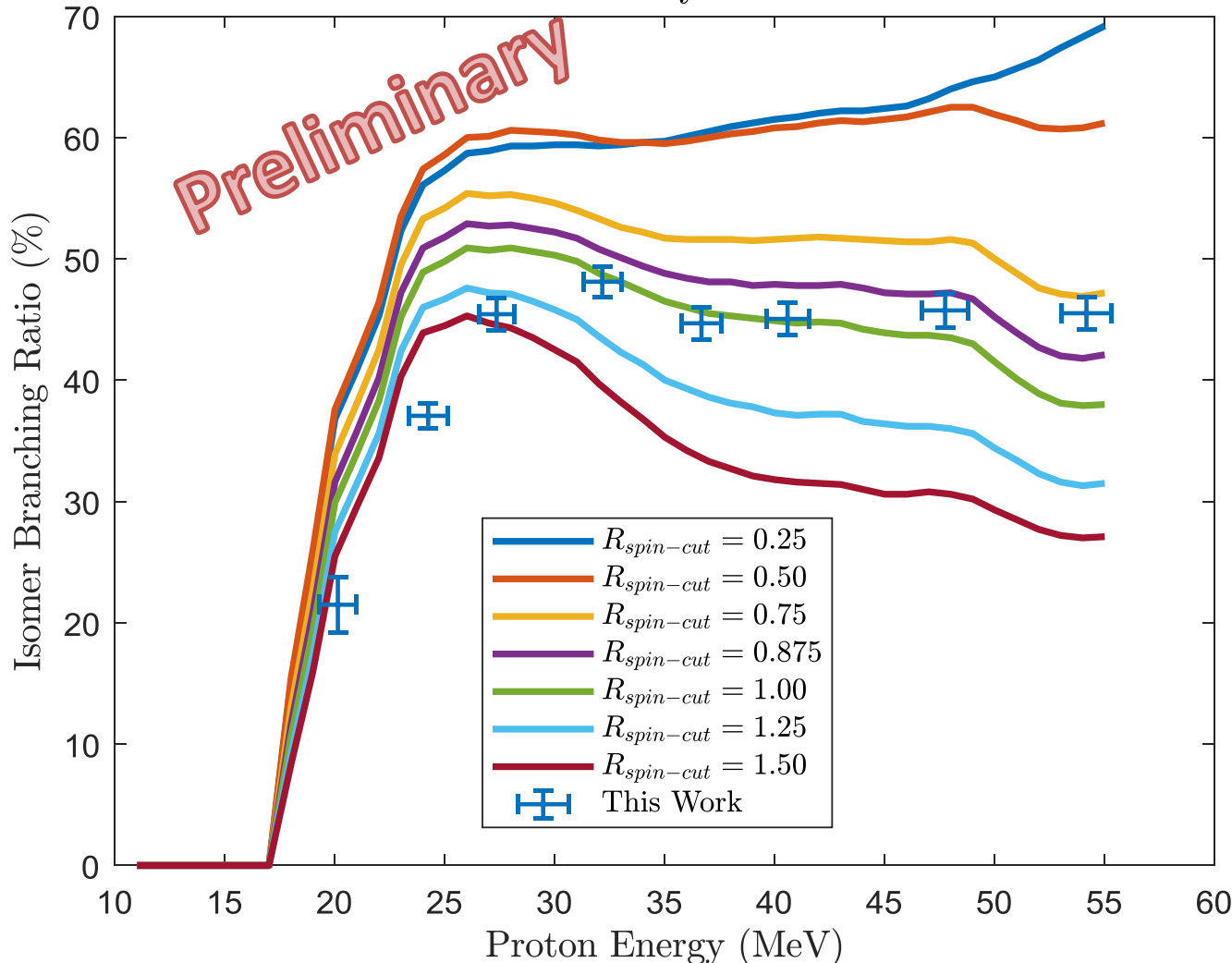
$$\rho(E, J) = f(J)\rho(E)$$

$$f(J, \sigma) = e^{-J^2/2\sigma^2} - e^{-(J+1)^2/2\sigma^2} \approx \frac{2J+1}{2\sigma^2} e^{-J(J+1/2)/2\sigma^2}$$

- In TALYS, $R_{spin-cut}$ is used as a tunable scaling parameter for σ^2

$$\sigma^2 = \eta \frac{\Theta_{\text{rig}} T}{\hbar^2}$$

^{52m}Mn (2+)/ ^{52g}Mn (6+) vs. Energy for $^{56}\text{Fe}(\text{p},\alpha\text{n})$
TALYS Level Density Model CT + FG



Results consistent with $R \approx 1$ at high energy.
At low energy, results are ambiguous due to energy straggling.

Spin Distribution Application

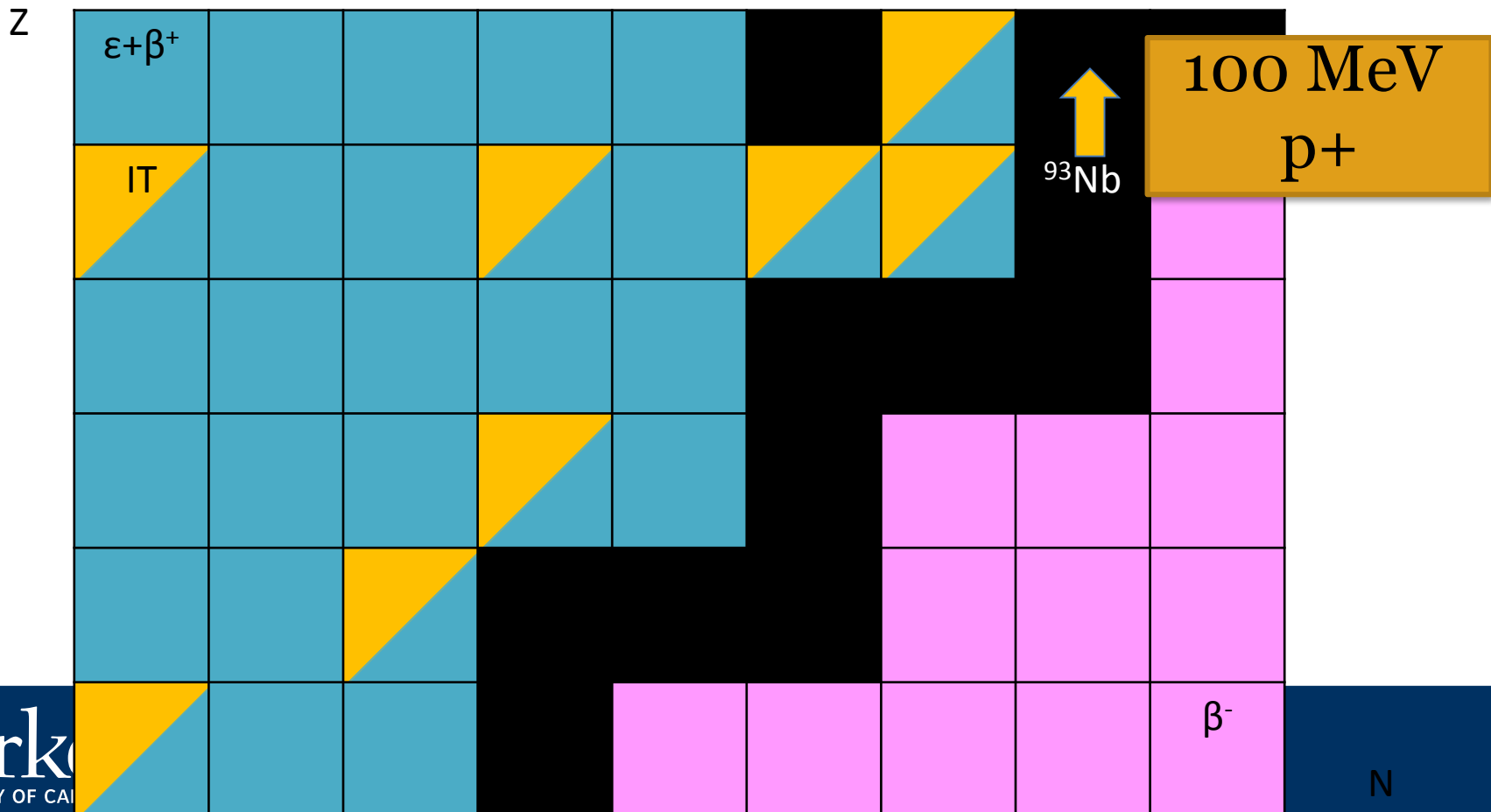
- Through its impact on nuclear level densities, the spin cut-off parameter has a strong impact on the favoring of higher-spin isomers in charged particle-induced reactions – a “tuning parameter” for isomer-to-ground state branching ratio
 - Reaction physics codes can be used to model (σ_m/σ_g) when experimental data is unavailable
 - Case study: ^{177}Lu
 - ^{177g}Lu ($t_{1/2} = 6.7$ d) – emerging β^- therapy agent
 - ^{177m}Lu ($t_{1/2} = 160$ d) – contributes extra dose to patient, without therapeutic or diagnostic benefit
 - Improved spin distribution measurements can improve modeling to guide production studies

Stacked-target Charged Particle Excitation Functions

Moderate Energy – LANL

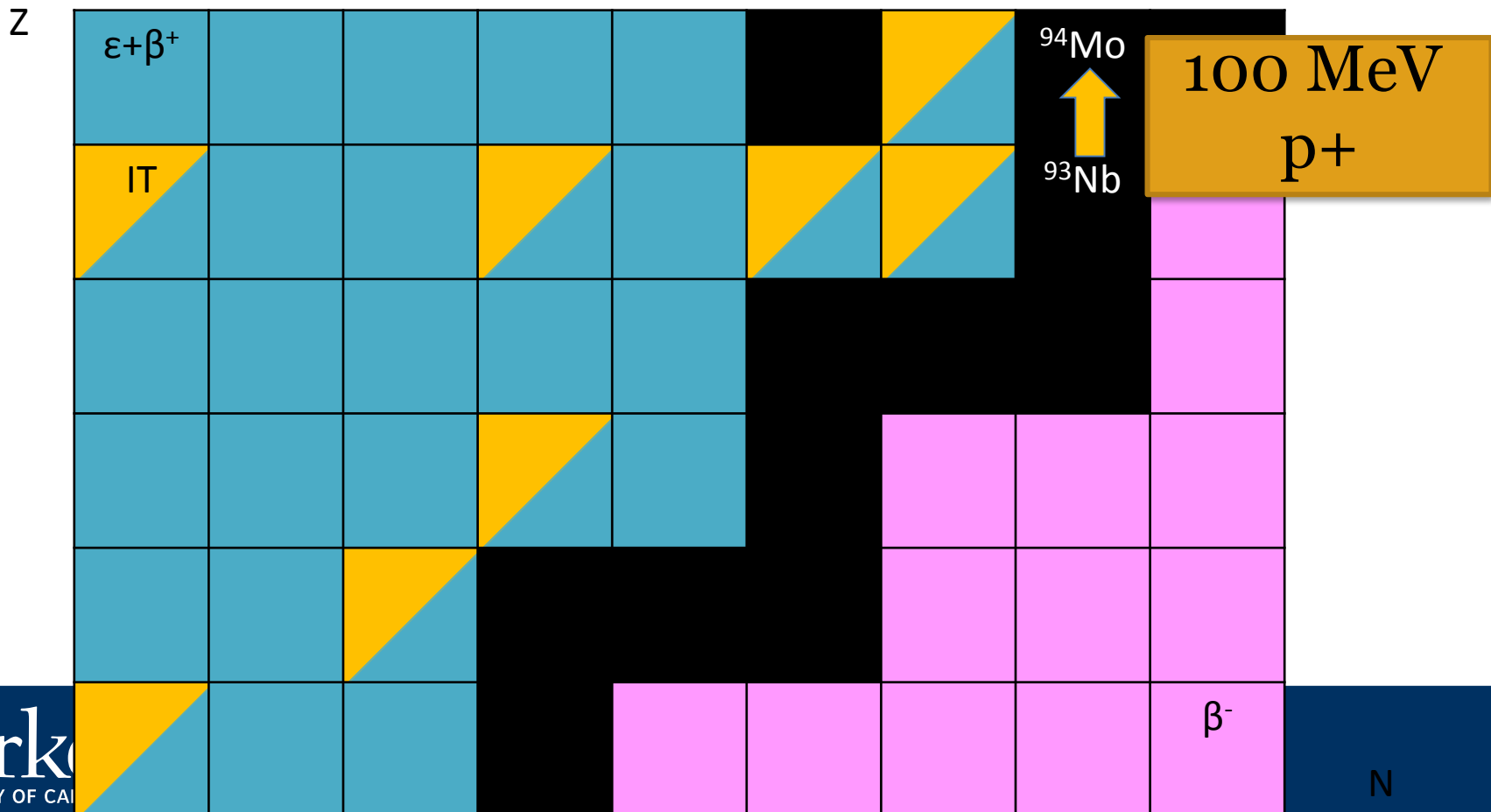
Measurements @ LANL – Nb(p,x)

- $^{nat}\text{Nb}(p,4n)^{90}\text{Mo}$ is a high-priority objective as a new proton beam dosimetry standard for $E_p \approx 50 - 100$ MeV
 - Other emerging radionuclides: ^{82m}Rb , ^{86}Y , ^{89}Zr , ^{90}Nb



Measurements @ LANL – Nb(p,x)

- $^{nat}\text{Nb}(p,4n)^{90}\text{Mo}$ is a high-priority objective as a new proton beam dosimetry standard for $E_p \approx 50 - 100$ MeV
 - Other emerging radionuclides: ^{82m}Rb , ^{86}Y , ^{89}Zr , ^{90}Nb

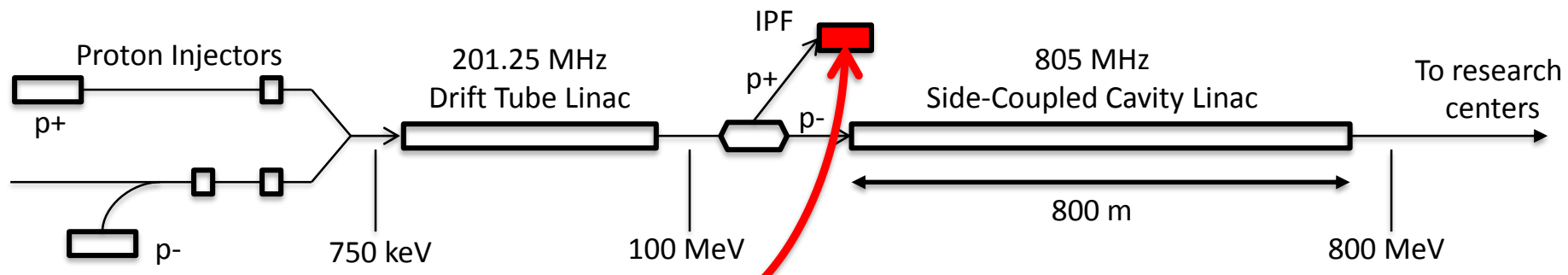


Measurements @ LANL – Nb(p,x)

- $^{nat}\text{Nb}(p,4n)^{90}\text{Mo}$ is a high-priority objective as a new proton beam dosimetry standard for $E_p \approx 50 - 100$ MeV
 - Other emerging radionuclides: ^{82m}Rb , ^{86}Y , ^{89}Zr , ^{90}Nb

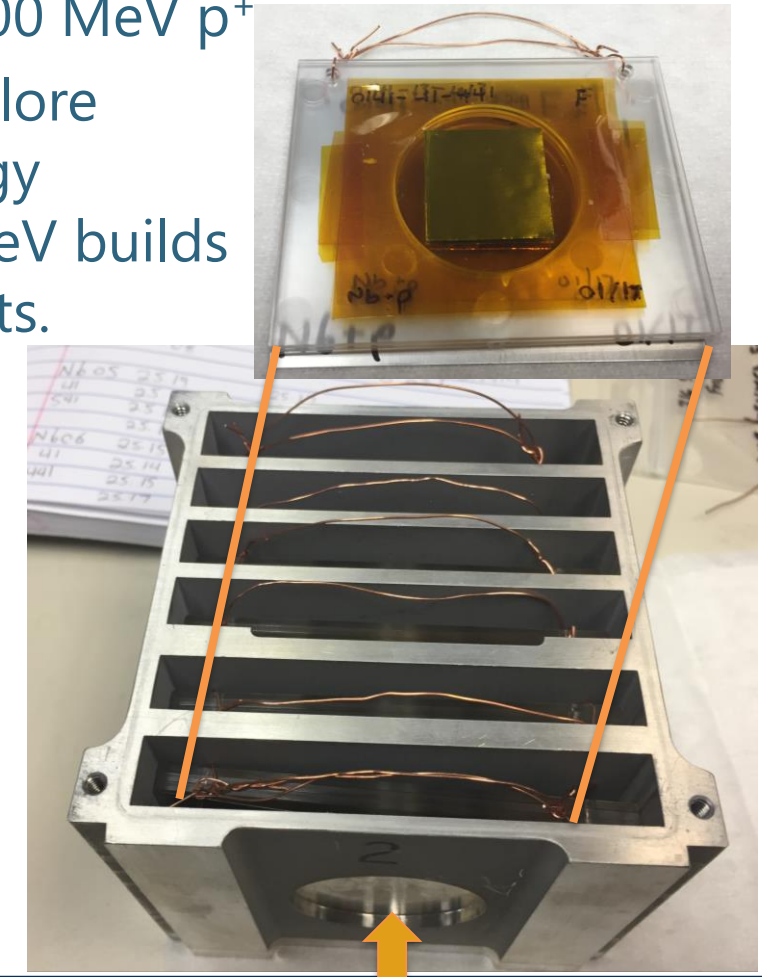


Measurements @ LANL – Nb(p,x)

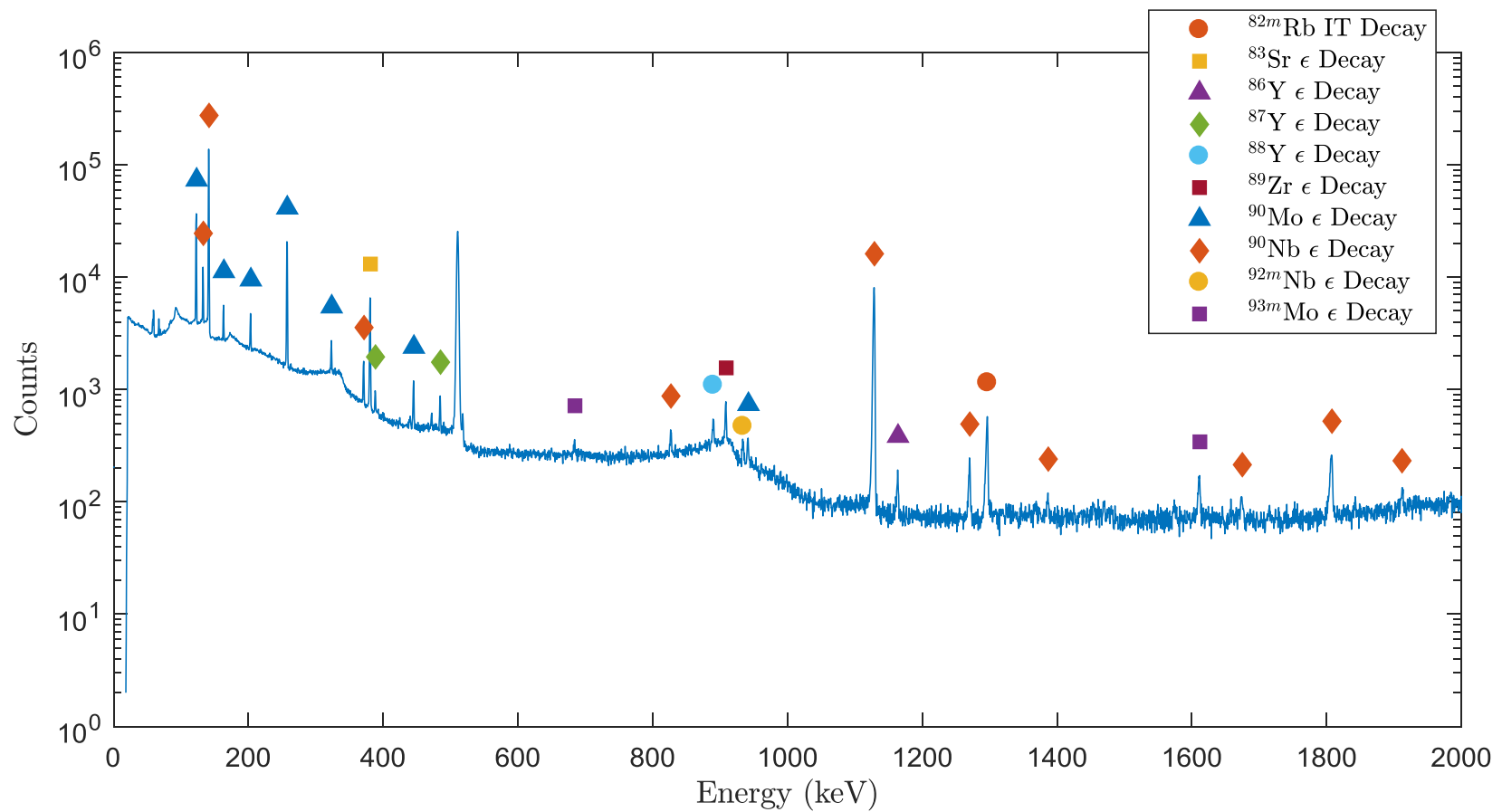


Measurements @ LANL – Nb(p,x)

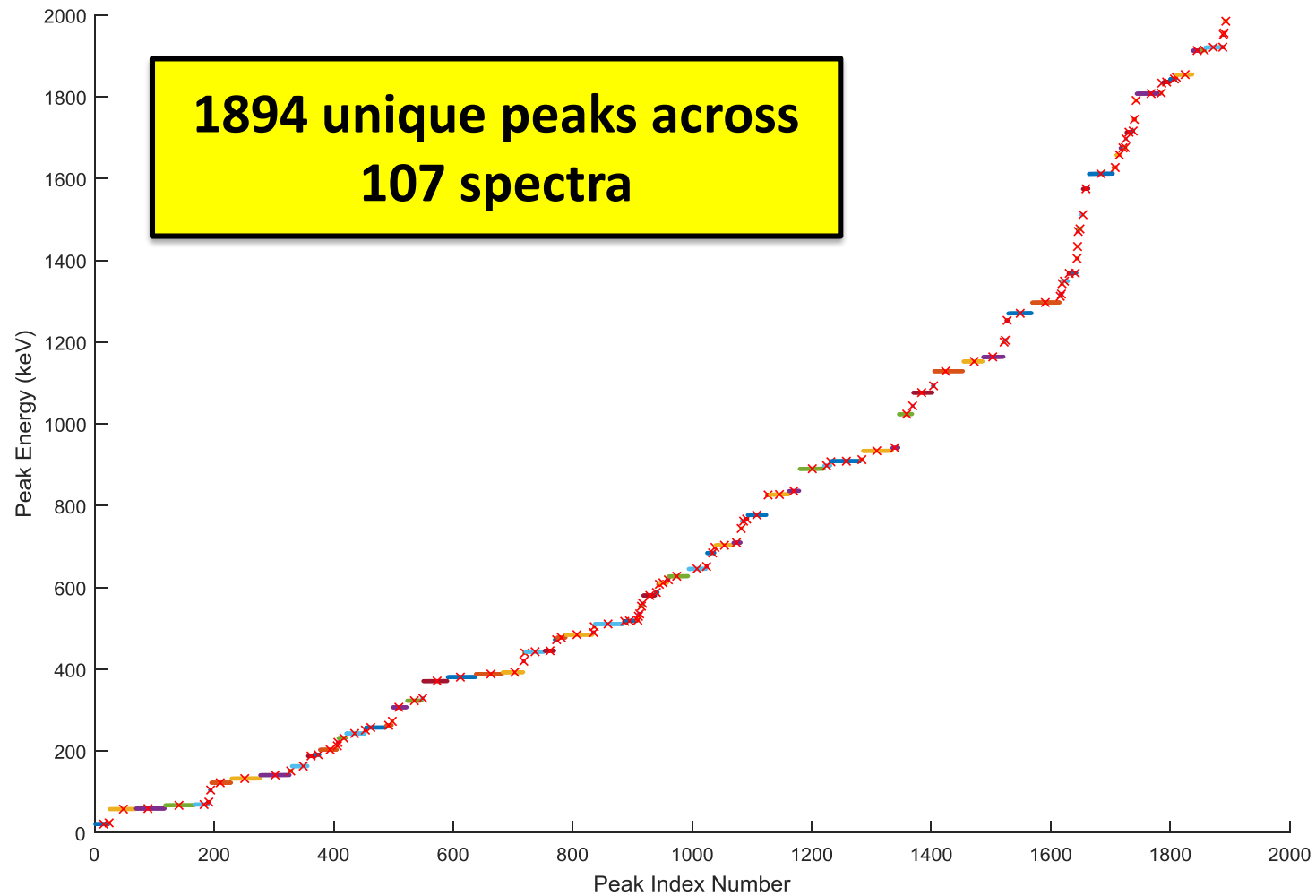
- LBNL: 5 – 55 MeV / A, LANL: 45 – 100 MeV p⁺
- Complementary measurements explore reaction dynamics in different energy regimes, overlap region of 45-55 MeV builds confidence and consistency in results.



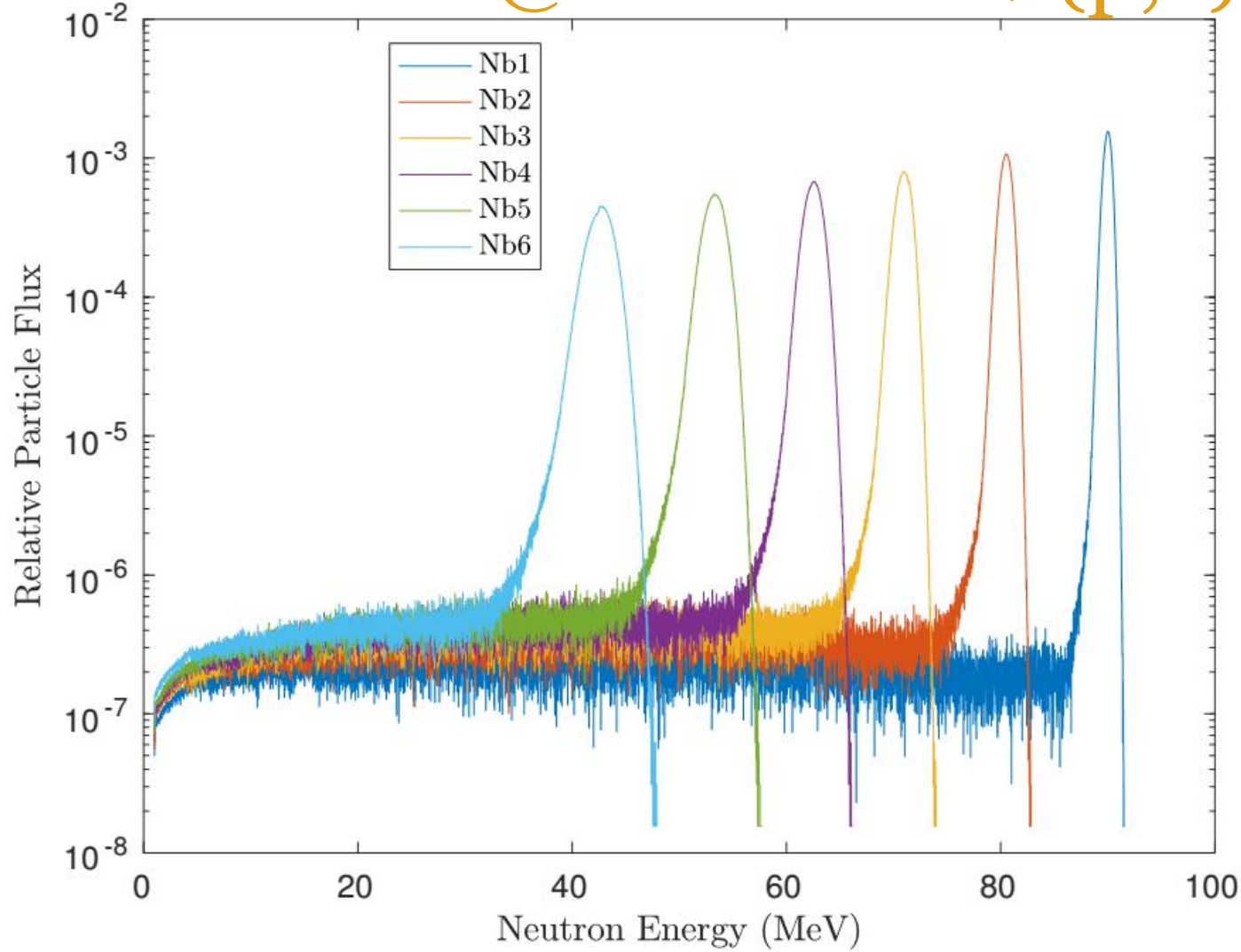
Measurements @ LANL – Nb(p,x)



Measurements @ LANL – Nb(p,x)



Measurements @ LANL – Nb(p,x)



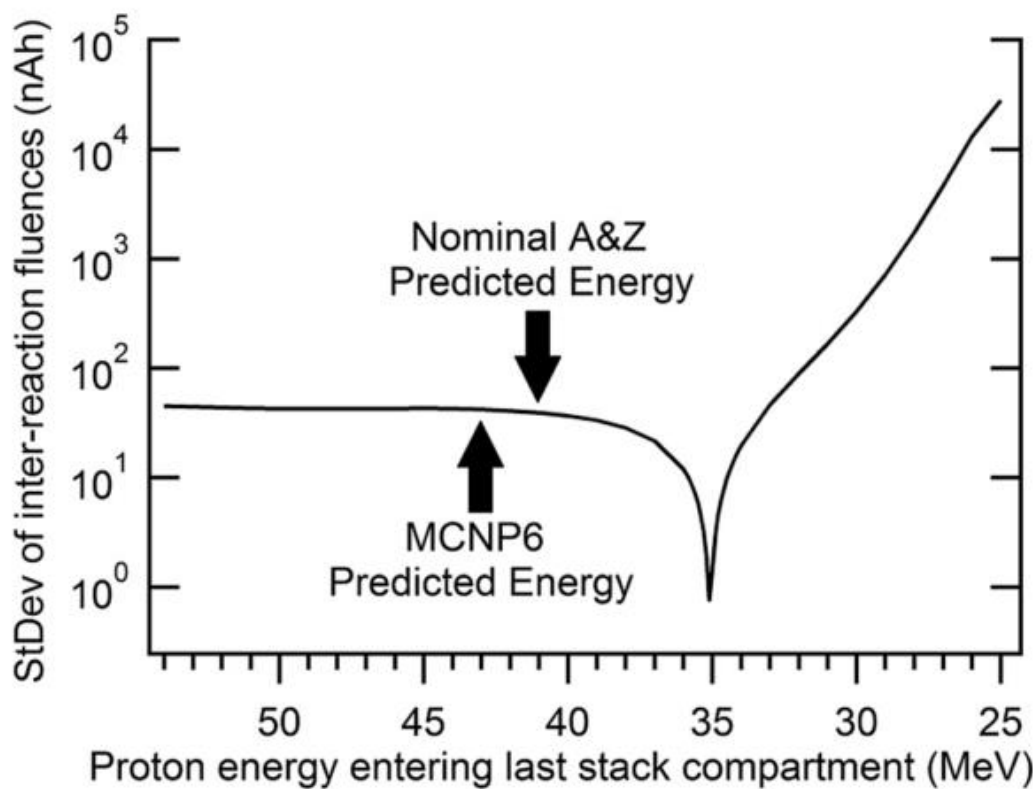
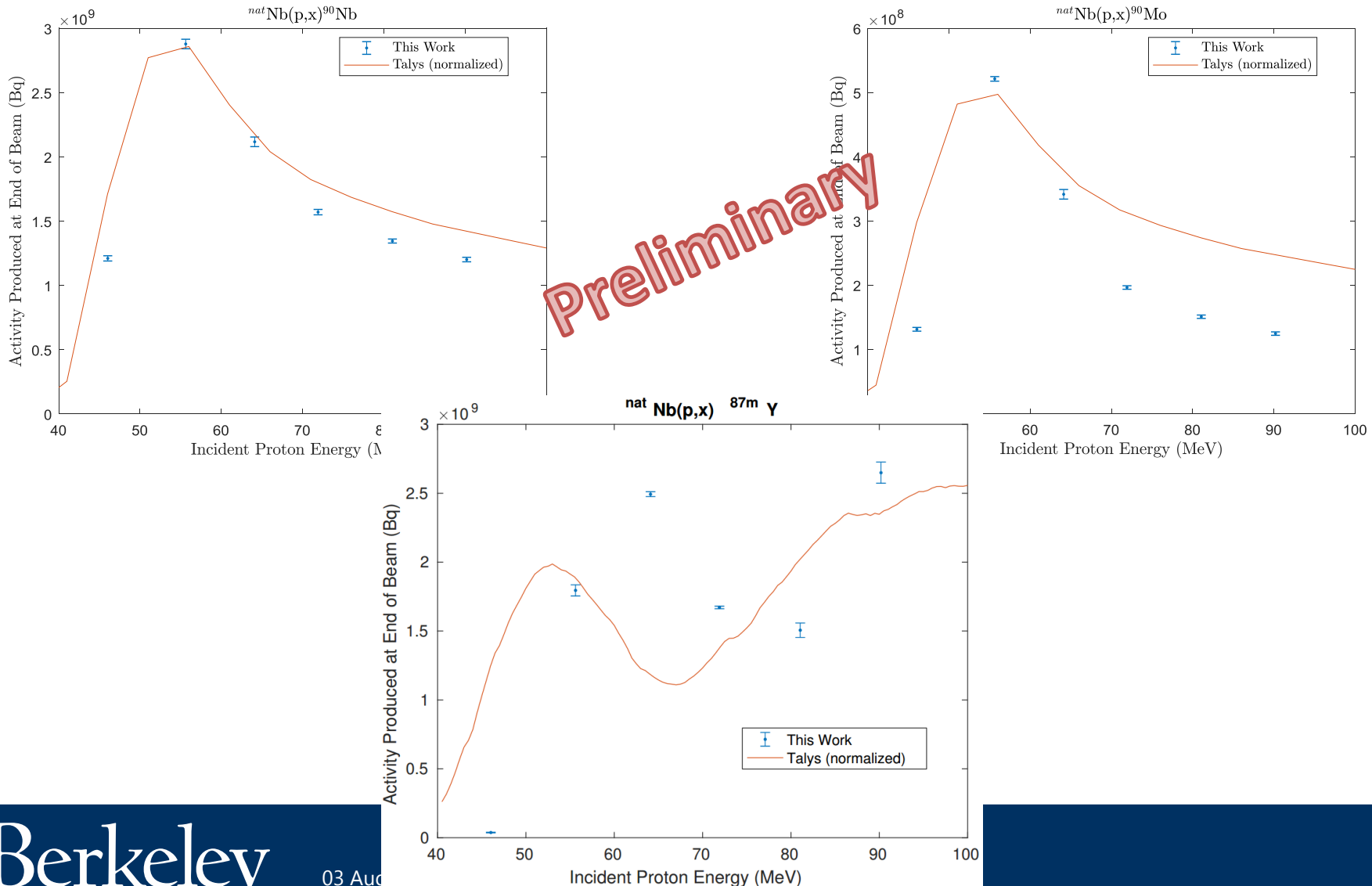
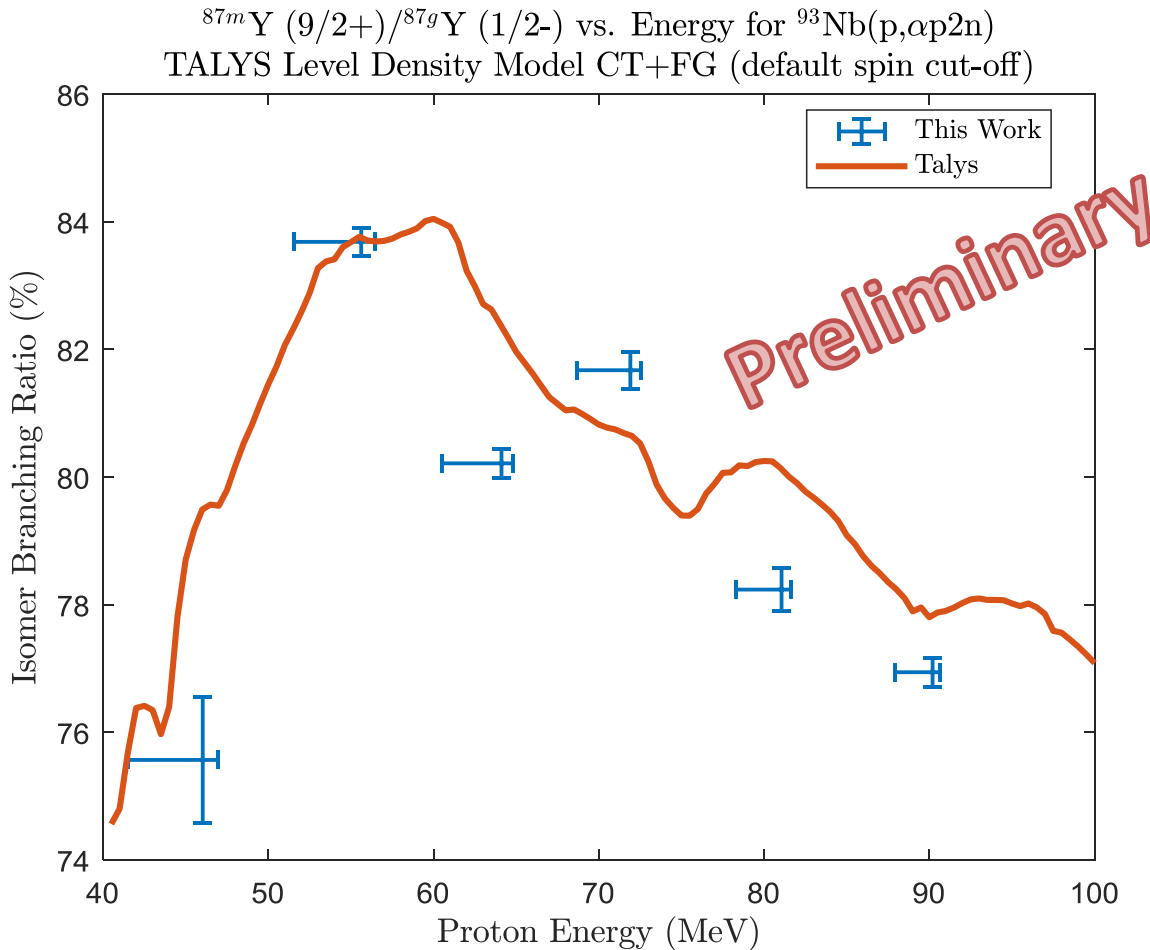


Fig. 3. Results of varying degrader density in analytic A&Z calculations on inter-monitor reaction fluence standard deviation. Varying degrader density has the effect of non-linearly varying the average beam energy in each compartment. This non-linear dependence on density has nearly the same functional impact as variations in the incident beam energy. Arrows indicate the predicted average beam energy in the last stack compartment by MCNP6 simulation and nominal A&Z calculations. A clear minimum from this approach is seen at 35.1 MeV, suggesting the initial beam energy estimations by nominal A&Z calculations and by MCNP6 simulation are significantly higher than what was experimentally observed.

Measurements @ LANL – Nb(p,x)



Measurements @ LANL – Nb(p,x)



Summary

Demonstrated ability to measure excitation functions for emerging medical radionuclides through 3 different production paradigms

- Provides first / vastly improved production measurements for each of the isotopes listed here
- Thin-target measurements in this work provide an ideal jumping-off point to begin thick-target yields for commercial application, as well as radiochemical workup

Path Forward

- ${}^{\text{nat}}\text{Fe}(\text{p},\text{x})$
 - Complete minimization of inter-reaction fluences for final energy assignment and stack fluence
 - Identify and quantify additional activities produced
- $\text{Nb}(\text{p},\text{x})$
 - Complete minimization of inter-reaction fluences for final energy assignment and stack fluence
 - All activities are quantified – energy assignments are all that remain to normalize into absolute cross sections
 - Finish spin distribution analysis for isomers produced
- 08 September - ${}^{\text{nat}}\text{La}(\text{p},6\text{n}){}^{134}\text{Ce}$ @ 88
 - Positron analogue for ${}^{225}\text{Ac}$ development



Thank you!

Extra Slides

Cross-Section Systematics

$$R = N_T \int_0^{E_{max}} \sigma(E) \frac{d\phi}{dE} dE = N_T \sigma(\bar{E}) \phi(\bar{E})$$

$$N_\gamma = N_D \epsilon_\gamma I_\gamma$$

$$= \epsilon_\gamma I_\gamma \frac{N_T \sigma(\bar{E}) \phi(\bar{E})}{\lambda} (1 - e^{-\lambda t_i}) e^{-\lambda t_d} (1 - e^{-\lambda t_c})$$

$$\sigma(\bar{E}) = \frac{N_\gamma \lambda}{N_T \epsilon_\gamma I_\gamma \phi(\bar{E}) (1 - e^{-\lambda t_i}) e^{-\lambda t_d} (1 - e^{-\lambda t_c})}$$

$$\begin{aligned} \frac{\sigma_P}{\sigma_{In}} &= \frac{N_{\gamma,P}}{N_{\gamma,In}} \frac{N_{T,In}}{N_{T,P}} \frac{\lambda_P}{\lambda_{In}} \left(\frac{1 - e^{-\lambda_{In} t_i}}{1 - e^{-\lambda_P t_i}} \right) \frac{e^{-\lambda_{In} t_d}}{e^{-\lambda_P t_d}} \times \\ &\quad \times \left(\frac{1 - e^{-\lambda_{In} t_c}}{1 - e^{-\lambda_P t_c}} \right) \frac{\epsilon_{In}}{\epsilon_P} \frac{I_{\gamma,In}}{I_{\gamma,P}} \frac{e^{-\mu_{In} x_{In}/2} \times e^{-\mu_{In} x_P}}{e^{-\mu_P x_P/2}} \end{aligned}$$

Neutron Utilization

$$A(t_i) = \eta \Phi_n (1 - e^{-\lambda t_i})$$

- Theoretical saturation activities are currently estimated at 1.5 kBq of ^{64}Cu , 0.11 kBq of ^{47}Sc
 - Measured production rates were 453.8 Bq of ^{64}Cu , 31.6 Bq of ^{47}Sc
 - **Implies $\eta \approx 29.9\%$**
- Path to upgrades:
 - Thicker activation target (1 cm) → factor 10
 - Increased current, run second ion source → factor 60
 - Switch to DT operation → factor 80
 - Higher (n,p) cross section at DT energies → factor 3
 - **Estimated saturation activities of 6 mCi ^{64}Cu , 0.5 mCi ^{47}Sc**

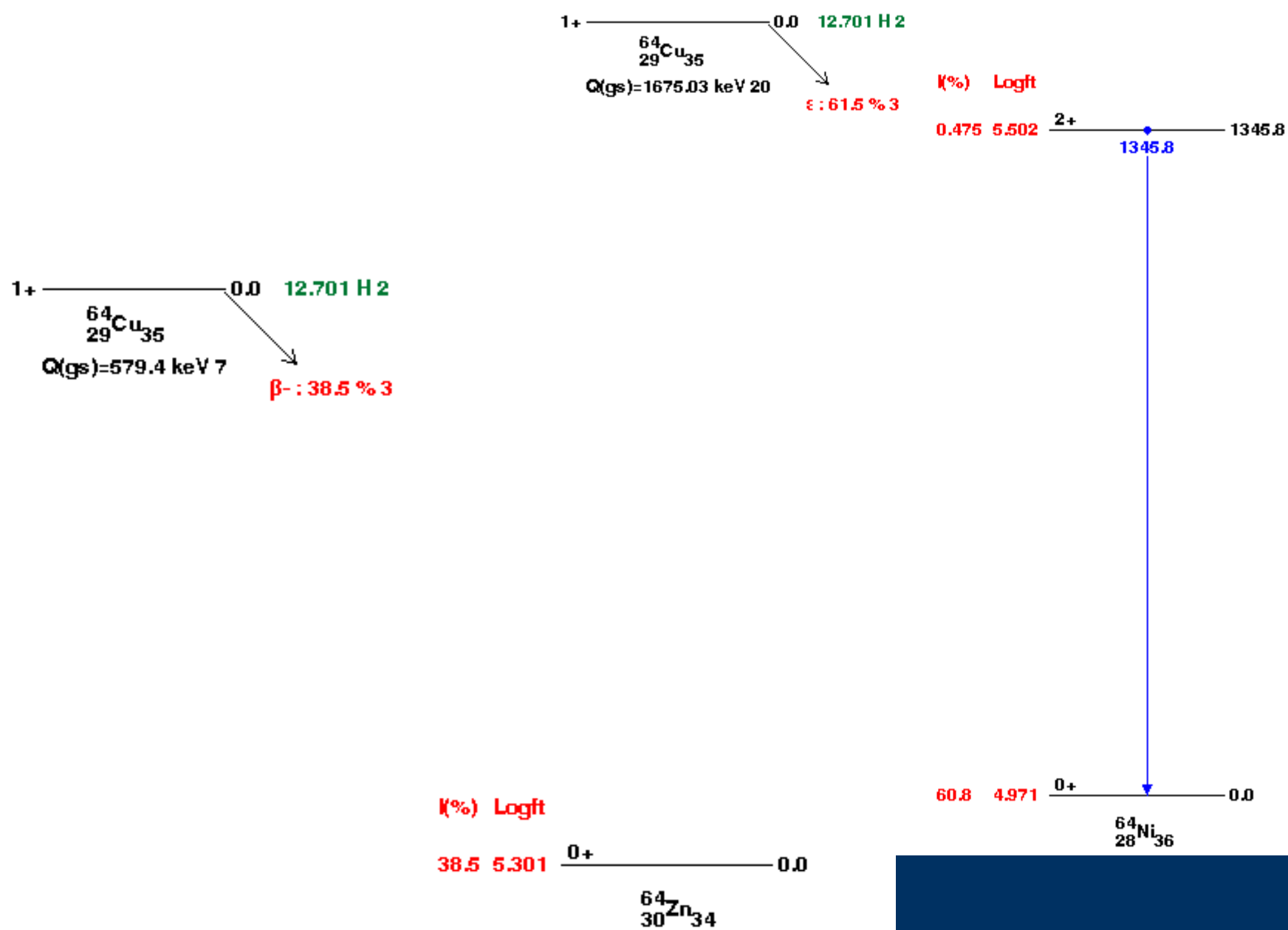
Decay Schemes

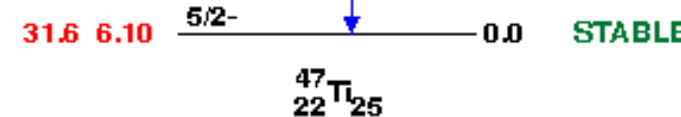
$\frac{1}{2}^-$ 391.7 1.6579 H $\pi: 100\%$

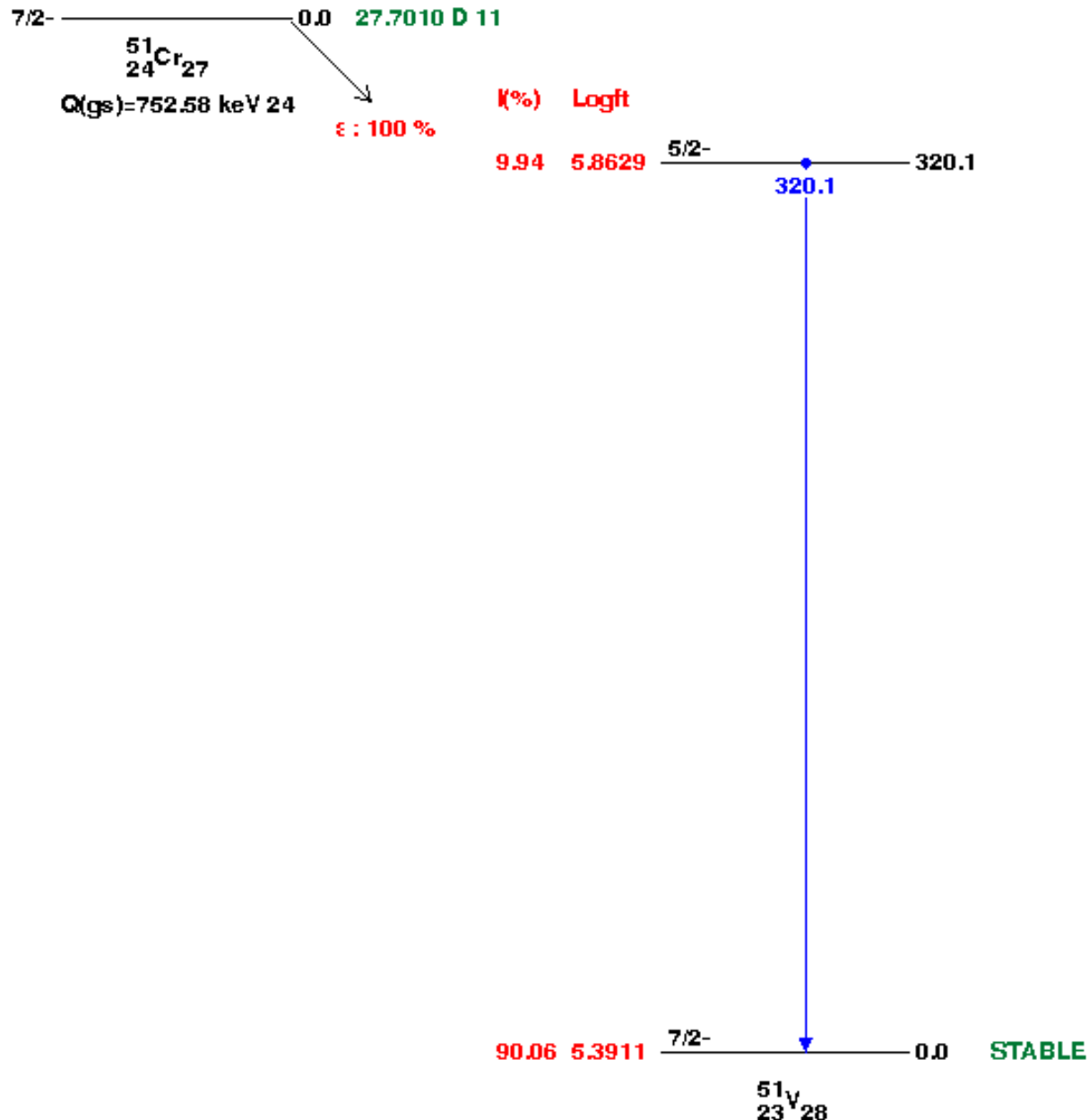
$\frac{9}{2}^+$ 0.0 STABLE
 $^{113}_{49}\text{In}_{64}$

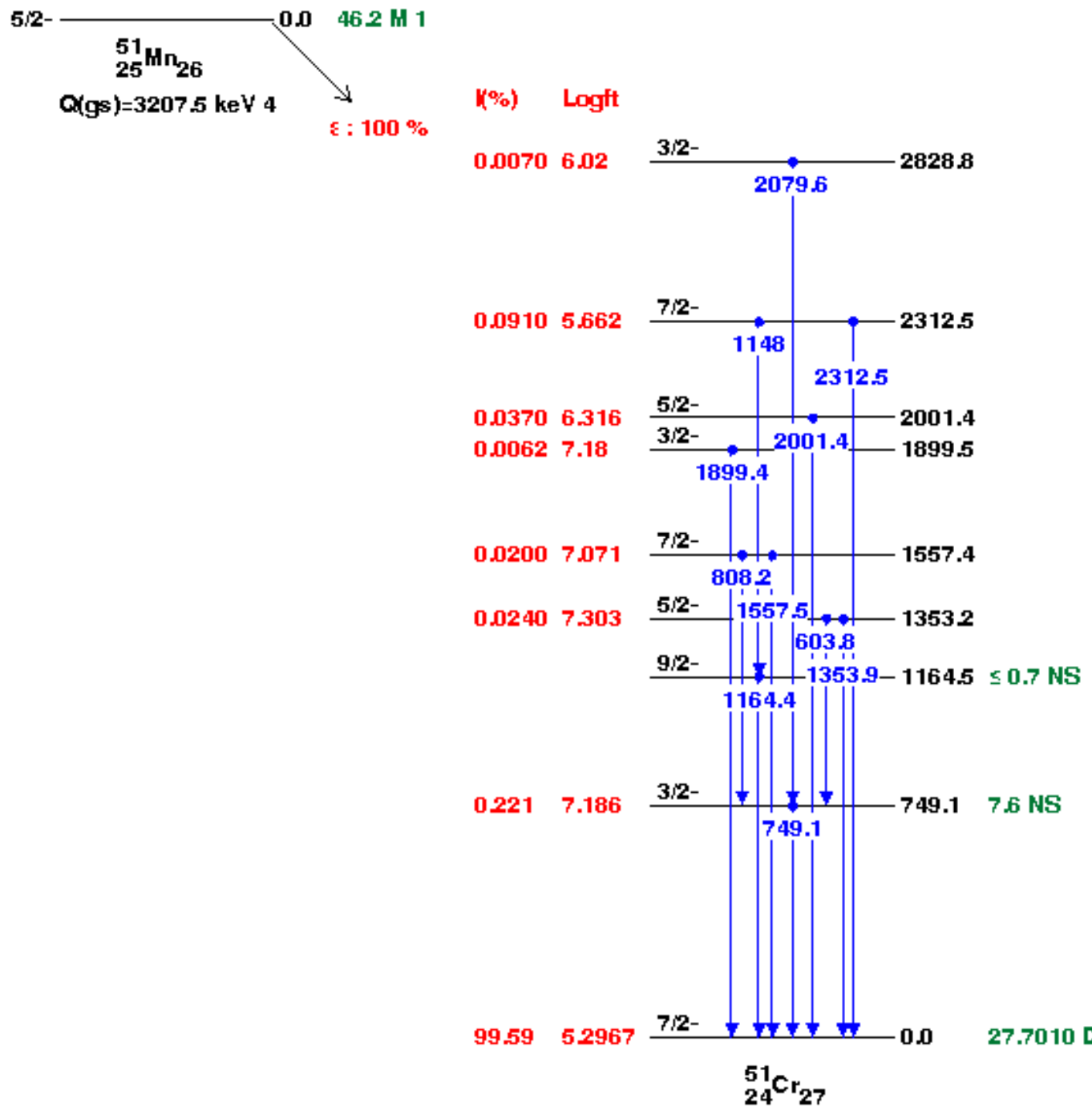
$\frac{1}{2}^-$ 336.2 4.486 H $\pi: 95.0\% \gamma$

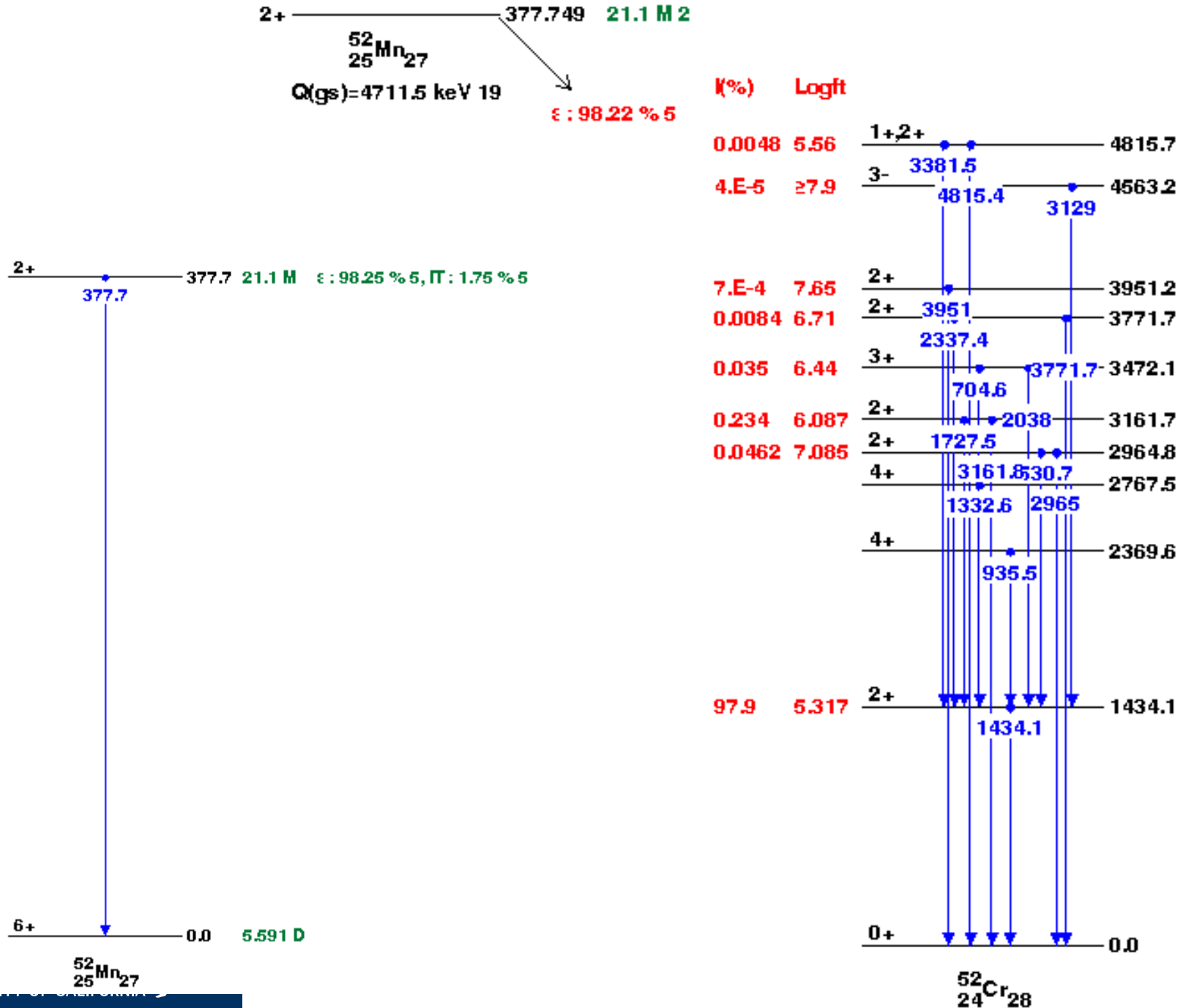
$\frac{9}{2}^+$ 0.0 $4.41\text{E}+14$ Y
 $^{115}_{49}\text{In}_{66}$

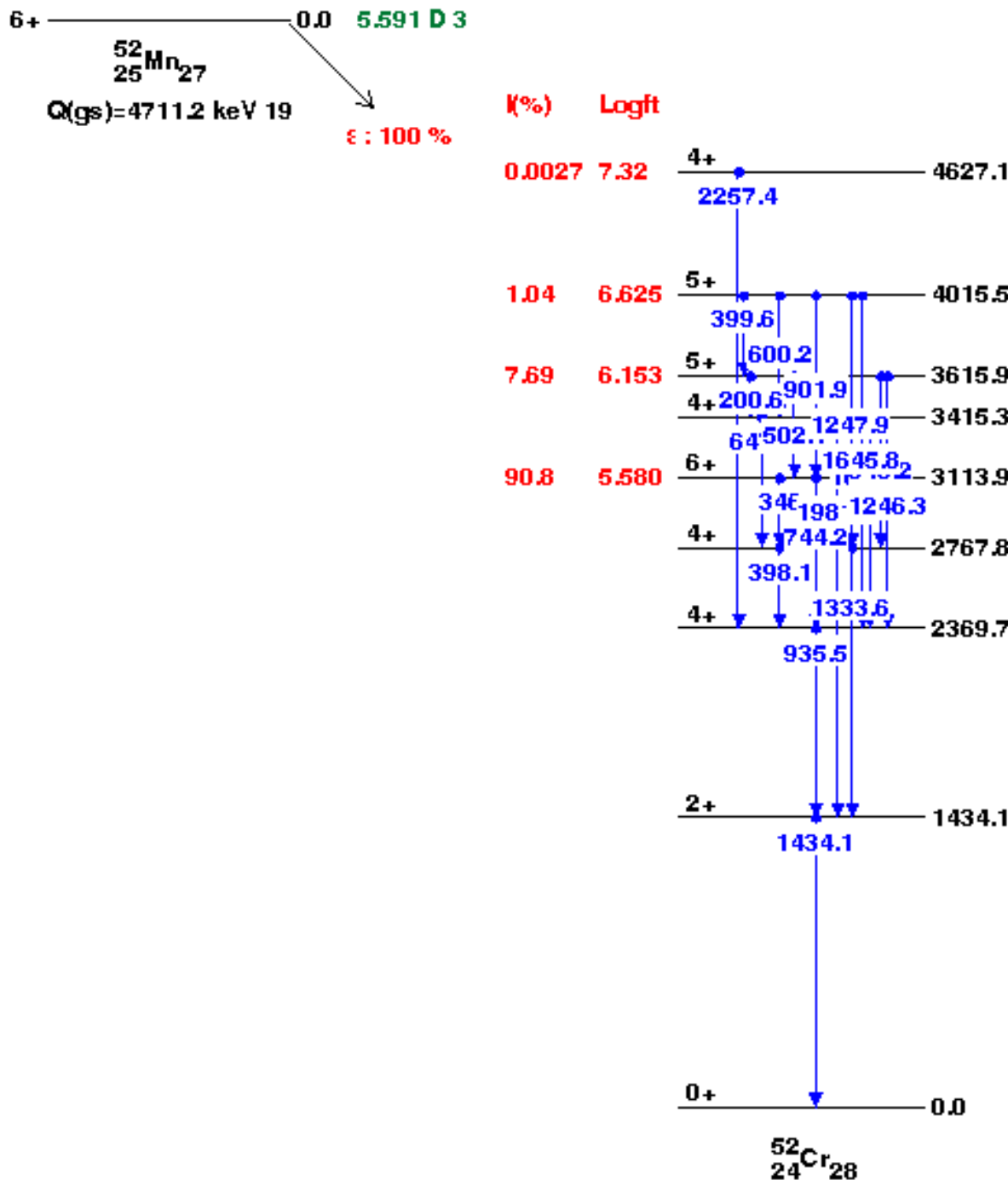




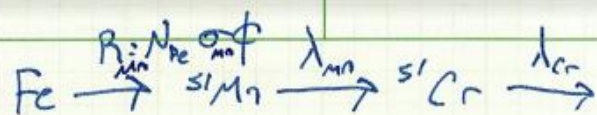








Granddaughter Decay Spectroscopy



During irradiation :

$$\frac{dN_m}{dt} = R_m - \lambda_m N_m \Rightarrow N_m(t) = \frac{R_m}{\lambda_m} (1 - e^{-\lambda_m t})$$

$$\begin{aligned} \frac{dN_c}{dt} &= R_c + \lambda_m N_m - \lambda_c N_c \\ \Rightarrow N_c(t) &= \frac{R_c + R_m}{\lambda_c} + \frac{R_m}{\lambda_m - \lambda_c} e^{-\lambda_m t} - \frac{R_c(\lambda_m - \lambda_c) + \lambda_m R_m}{\lambda_c(\lambda_c - \lambda_m)} e^{-\lambda_c t} \end{aligned}$$

i) $EoB:$ $N_m(t=t_1) = N_m^\circ$
 $t=0 \rightarrow t_1$ $N_c(t=t_1) = N_c^\circ$

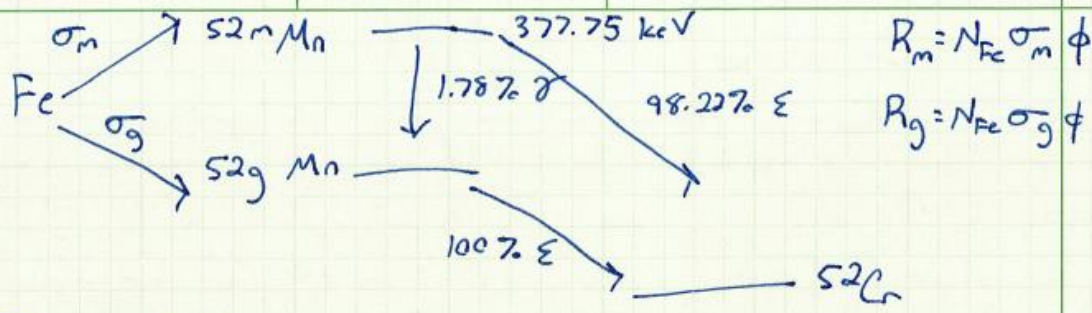
Delay: $t=t_1 \rightarrow t_2$

$$\frac{dN_m}{dt} = -\lambda_m N_m \Rightarrow N_m(t) = N_m^\circ e^{-\lambda_m t}$$

$$\frac{dN_c}{dt} = -\lambda_c N_c + \lambda_m N_m \Rightarrow N_c(t) = N_c^\circ e^{-\lambda_c t} + \frac{N_m^\circ \lambda_m}{\lambda_c - \lambda_m} (e^{-\lambda_m t} - e^{-\lambda_c t})$$

Decay during counts: $t=t_2 \rightarrow t_3$

$$\left. \begin{aligned} \Delta N_m &= N_m(t_2) - N_m(t_3) \\ \Delta N_c &= N_c(t_2) - N_c(t_3) \end{aligned} \right\}$$



During irradiation:

$$\frac{dN_m}{dt} = R_m - \lambda_m N_m \Rightarrow N_m(t) = \frac{R_m}{\lambda_m} (1 - e^{-\lambda_m t})$$

$$\begin{aligned} \frac{dN_g}{dt} &= R_g + 0.0178 \lambda_m N_m - \lambda_g N_g \\ \Rightarrow N_g(t) &= \frac{R_g + 0.0178 R_m}{\lambda_g} + \frac{0.0178 R_m}{\lambda_m - \lambda_g} e^{-\lambda_m t} + \frac{[R_g(\lambda_m - \lambda_g) + 0.0178 R_m]}{\lambda_g(\lambda_g - \lambda_m)} e^{-\lambda_g t} \end{aligned}$$

E_cB: $t = 0 \rightarrow t_1$, $N_m(t = t_1) = N_m^\circ$
 $N_g(t = t_1) = N_g^\circ$

Delay: $t = t_1 \rightarrow t_2$

$$\frac{dN_m}{dt} = -\lambda_m N_m \Rightarrow N_m^\circ e^{-\lambda_m t}$$

$$\frac{dN_g}{dt} = -\lambda_g N_g + 0.0178 \lambda_m N_m^\circ \Rightarrow N_g(t) = \frac{0.0178 \lambda_m N_m^\circ}{\lambda_g - \lambda_m} (e^{-\lambda_m t} - e^{-\lambda_g t}) + N_g^\circ e^{-\lambda_g t}$$

Decay during counts: $t: t_2 \rightarrow t_3$

$$\begin{cases} \Delta N_m = N_m(t_2) - N_m(t_3) \\ \Delta N_g = N_g(t_2) - N_g(t_3) \end{cases}$$

$$P_d = L$$

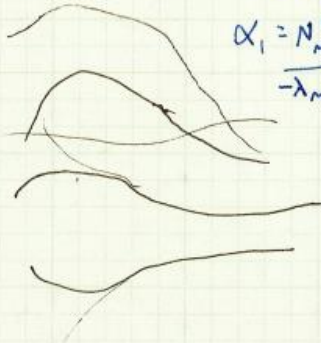
$$T_h = M$$

$$N_c(s) = \frac{N_m \lambda_m (e^{-\lambda_m s} - e^{-\lambda_c s})}{\lambda_c - \lambda_m} + N_c^* e^{-\lambda_c s}$$

$$sN_c(s) - N_c^* = \frac{N_m^* \lambda_m}{s + \lambda_m} - \lambda_c N_c(s) / s - A_{Pd} = A_{Pd}^* e^{-\lambda_{Pd} s} + \frac{\lambda_m^* \lambda_{Pd}}{\lambda_{Pd} - \lambda_m} (e^{-\lambda_m s} - e^{-\lambda_{Pd} s})$$

$$A = N\lambda$$

$$(s+\lambda_c) N_c(s) = \frac{N_m^* \lambda_m}{s + \lambda_m} + N_c^* = \frac{N_m^* \lambda_m + N_c^* (s + \lambda_m)}{(s + \lambda_m)(s + \lambda_c)} = \frac{\alpha_1}{s + \lambda_m} + \frac{\alpha_2}{s + \lambda_c}$$



$$\alpha_1 = \frac{N_m^* \lambda_m}{-\lambda_m + \lambda_c}$$

$$\alpha_2 = \frac{N_m^* \lambda_m + N_c^* (-\lambda_c + \lambda_m)}{-(\lambda_c + \lambda_m)}$$

$$R_m (\bar{s} - \bar{s}_n \lambda_m)$$

$$= R_m \left(\frac{s \lambda_m - s}{s(s + \lambda_m)} \right)$$

$$= R_m \left(\frac{\lambda_m}{s(s + \lambda_m)} \right)$$

$$\alpha_2 = \frac{N_m^* \lambda_m}{\lambda_m - \lambda_c} + N_c^*$$

$$R = \int \rho \Phi(E) \cdot \sigma(E) \cdot \rho dE \cdot dE$$

$$\frac{dN_c}{dt} = R_c + R_m R_m (1 - e^{-\lambda_m t}) - \lambda_c N_c$$

$$sN_c(s) - \alpha_1 = \frac{R_c}{s} + R_m \left(\frac{1}{s} - \frac{1}{s + \lambda_m} \right) - \lambda_c N_c(s)$$

$$N_c(s) (s + \lambda_c) = \frac{R_c}{s} + \frac{R_m}{s} - \frac{R_m}{s + \lambda_m} = \frac{R_c(s + \lambda_m) + R_m(s + \lambda_m) - R_m s}{s(s + \lambda_m)}$$

$$\alpha_2 = \frac{R_c(s + \lambda_m) + \lambda_m R_c + \lambda_m R_m}{\lambda_m (\lambda_m + \lambda_c)} = \frac{\lambda_m R_m}{\lambda_m - \lambda_c}$$

$$\alpha_3 = \frac{R_c(-\lambda_c) + \lambda_m R_c + \lambda_m R_m}{\lambda_c (\lambda_c - \lambda_m)} + \frac{\lambda_m R_m}{\lambda_c (\lambda_c - \lambda_m)}$$

$$= \frac{R_c s + \lambda_m R_c + R_m s - \lambda_m R_m - \lambda_c s}{s(s + \lambda_m)}$$

$$= \frac{R_c s + \lambda_m R_c + \lambda_m R_m}{s(s + \lambda_m)(s + \lambda_c)}$$

$$= \frac{\alpha_1}{s + \lambda_m} + \frac{\alpha_2}{s + \lambda_c}$$

$$\alpha_1 = \frac{\lambda_m R_c + \lambda_m R_m}{\lambda_m \lambda_c} = \frac{R_c + R_m}{\lambda_c} = \frac{R_c + R_m}{\lambda_c}$$

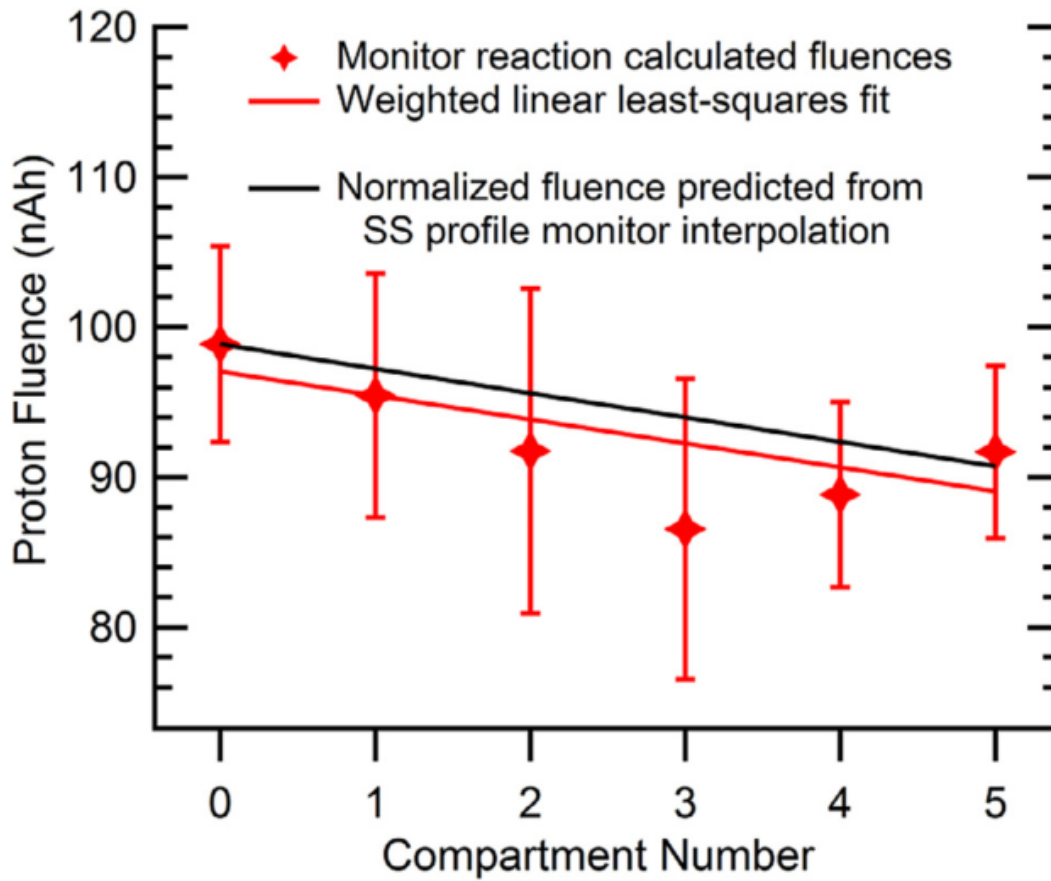


Fig. 5. Final fluence measurements as a function of target stack compartment number following monitor reaction derived proton fluence variance minimization. The red line represents a weighted linear line of regression indicating a drop in proton fluence of 7.2% as the beam travelled through the target stack. The black line is the estimated fluence loss determined by analysis of the stainless steel (SS) beam profile foils at the front and rear of the stack, normalized to the proton fluence measured in the first compartment.